SAND2013-7535C

Exceptional service in the national interest

Sandia National Laboratories

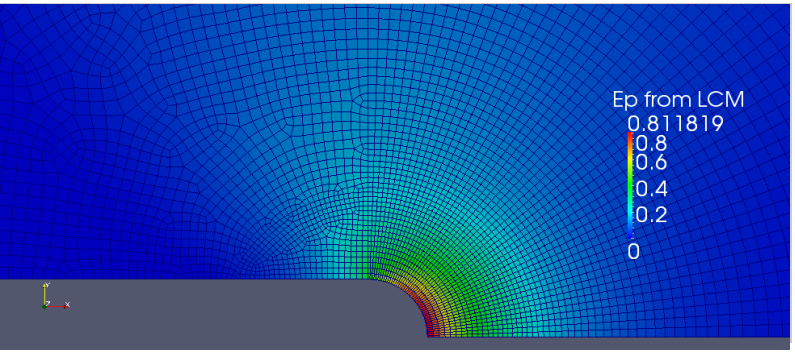

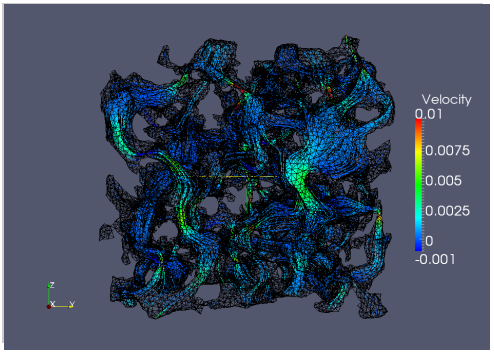

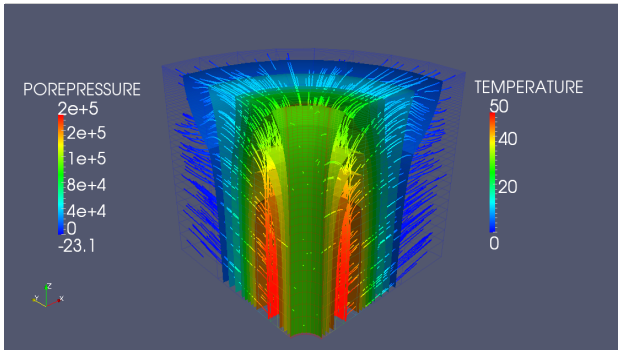

Computational Geomechanics across the pore, grain, specimen and field scales

Steve Sun[1]

[1]Senior Member of Technical Staff, Mechanics of Materials Department
Sandia National Laboratories, Livermore, California

U.S. DEPARTMENT OF ENERGY

National Nuclear Security Administration

Sandia National Laboratories is a multi-program laboratory managed and operated by Sandia Corporation, a wholly owned subsidiary of Lockheed Martin Corporation, for the U.S. Department of Energy's National Nuclear Security Administration under contract DE-AC04-94AL85000. SAND NO. 2011-XXXXP

Collaborators (current and past)

STONY BROOK UNIVERSITY

- James W Foulk III (Sandia, CA), localization element for hydrogen embrittlement
- Alejandro Mota (Sandia, CA), multiscale modeling, internal variable mapping
- Jakob T Ostien (Sandia, CA), finite strain FEM for thermo-hydro-mechanics
- Joseph E Bishop (Sandia, NM), mortar finite element method
- John W Rudnicki (Northwestern, IL), Mechanical and hydraulic properties of real and simulated compaction bands
- Jose E Andrade (Northwestern, IL; now at Caltech, CA), lattice Boltzmann/finite element hybrid simulations
- Matthew R Kuhn (University of Portland, OR), Shear band modeling with Discrete element method; granular physics
- Ronaldo I Borja (Stanford, CA), Monte-Carlo simulations for co-seismic deformations
- Teng-fong Wong (Stony-Brook University, NY; now at Chinese University of Hong Kong), Modeling and analysis with CT Images
- Peter Eichhubl (UT Austin), compaction band characterizations
- Yin Lu Young (Princeton University, NJ; now at University of Michigan, Ann Arbor, MI), Monte-Carlo simulation of sedimentation-consolidation process

Research Experience

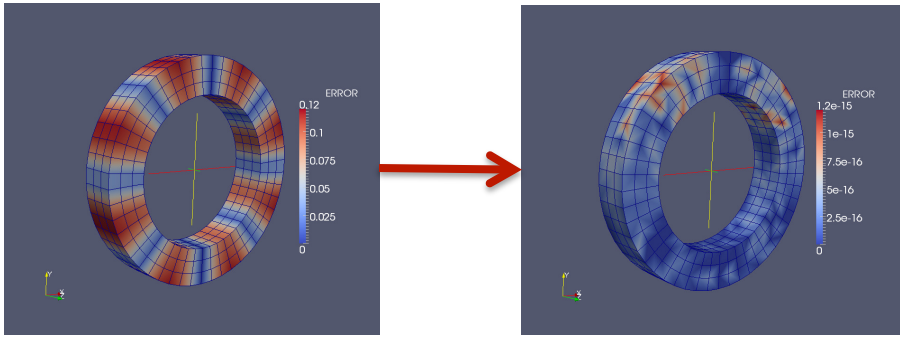

- Variational internal variable recovery with Lie algebra for adaptive finite element method
- Mota, Sun, Ostien, Foulk, Long, Computational Mechanics 2013

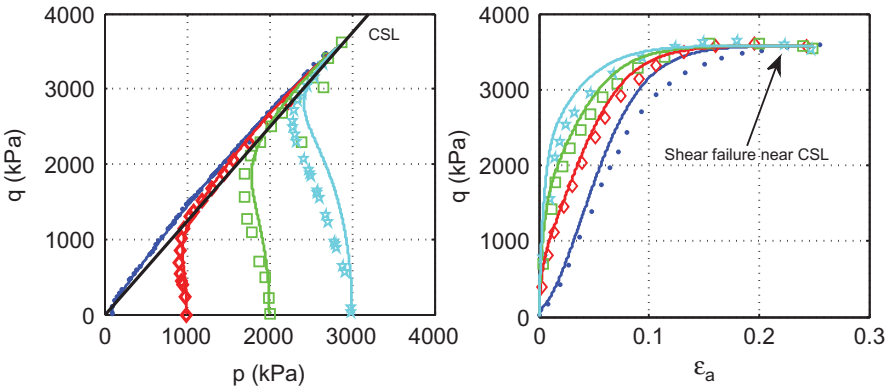

- Predicting liquefaction and shear localization with a critical state plasticity model
- Sun, Geomechanics and Geoengineering, 2013

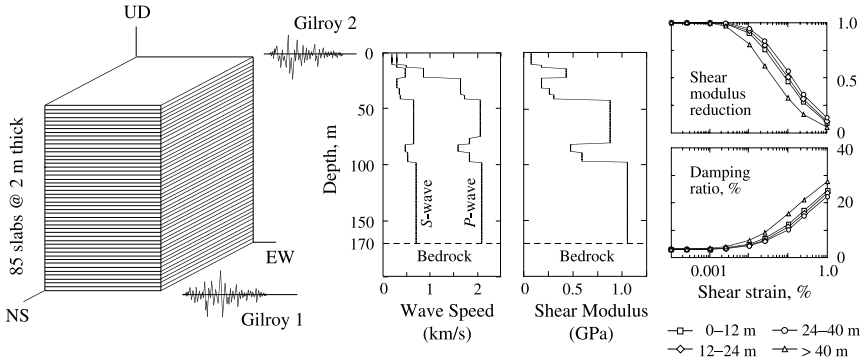

- Estimating co-seismic deformation of sediment during Loma Prieta earthuqake with Monte Carlos simulations
- Borja, Sun, Acta Geotechnica, 2007; Borja, Sun, Journal of Geophysical Research 2008

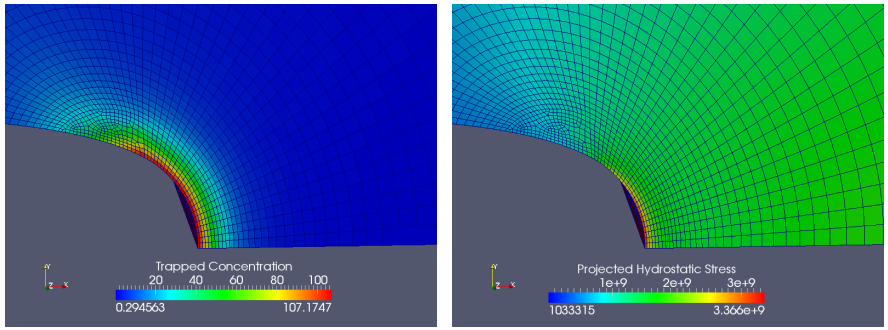

- Hydrogen embrittlement in stainless steel
- Foulk, Sun, Wagner, International Journal of Numerical Methods in Engineering, 2013

Computational Geomechanics Across the Pore, Grain, Specimen and Field scales

Sandia National Laboratories

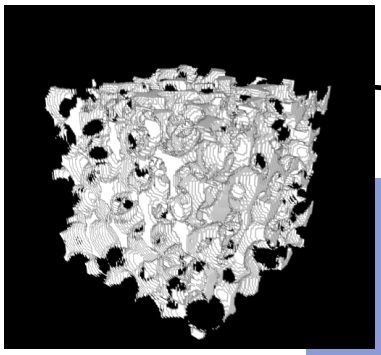

X-ray CT Image[3,4]

Level set scheme to obtain signed distance function, iso-surface and mesh

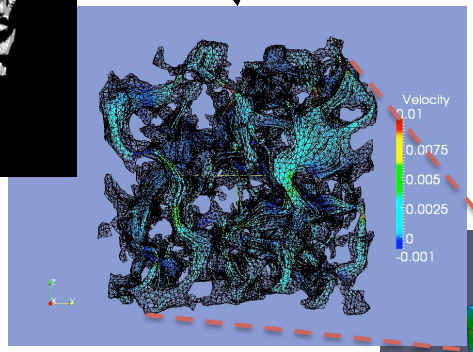

Pore-scale Calculation[8]

Up-scaling hydraulic and mechanical parameters by solving inverse problem

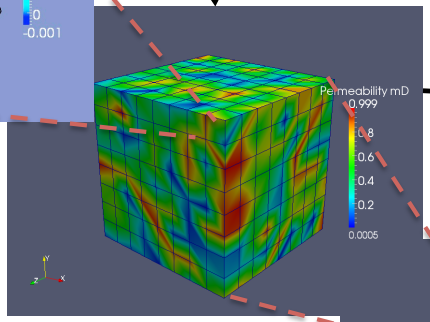

Meso-Scale homogenization[3,4]

Finite Element models incorporating Spatial Variability and length scale

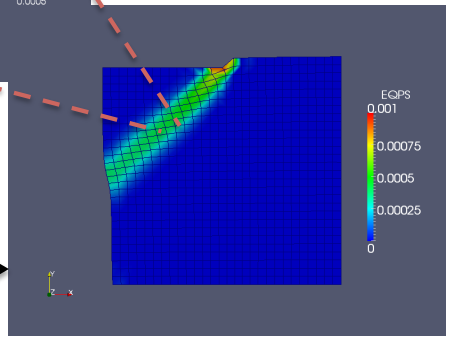

Field-scale Boundary Value Problem[1,2,5,6]

Create binary image from DEM assembly

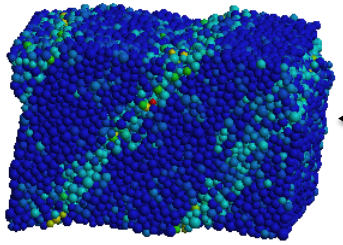

Grain Scale Discrete Element Simulation[7]

Arlequin domain coupling[9]

SCALE

1nm 1mm 1cm 1m

Structure of the Presentation

Sandia National Laboratories

- Motivations
- How to model large deformation thermo-hydro-mechanics at the field scale?
- How to use micromechanics models to predict the macroscopic mechanical and hydraulic responses?
- How to connect micro- and field- scale models with domain coupling methods?
- Conclusion and future Perspectives

Motivations

Sandia National Laboratories

Geothermal energy

Rainfall induced slope instability

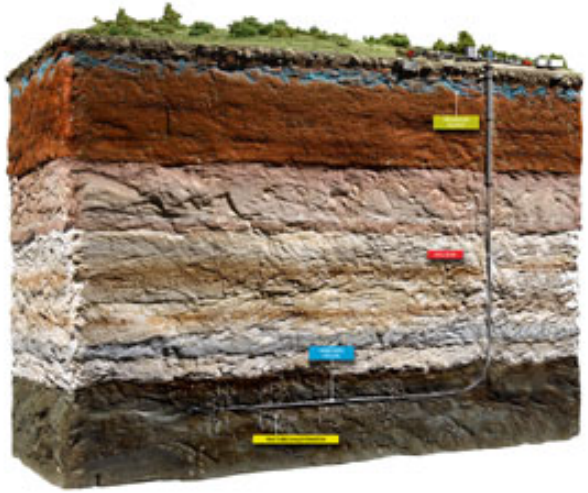

Hydraulic fracture (fracking)

Soil liquefaction

Thermo-hydro-mechanics modeling in the continuum scale

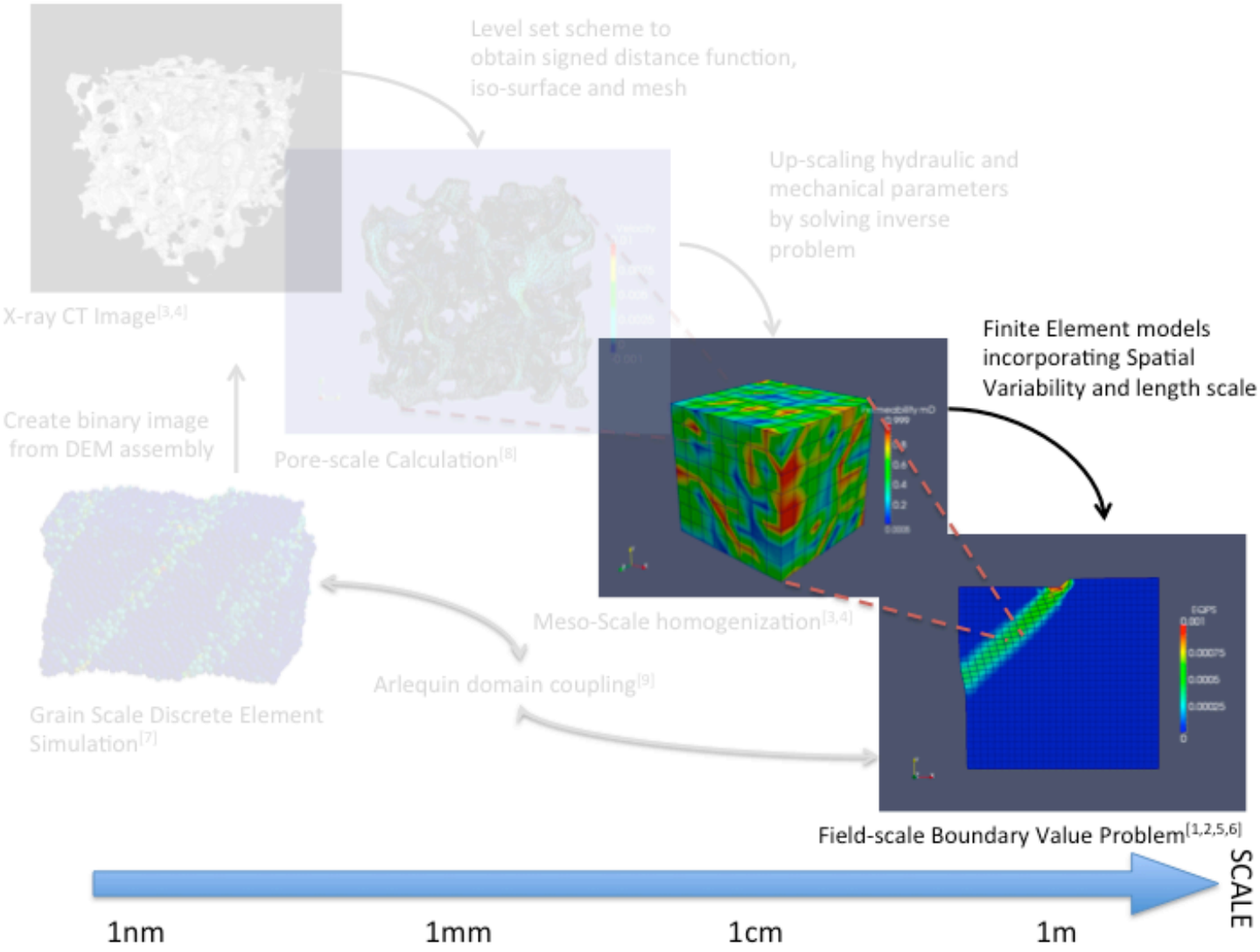

Kinematics of THM Problem at Finite Strain

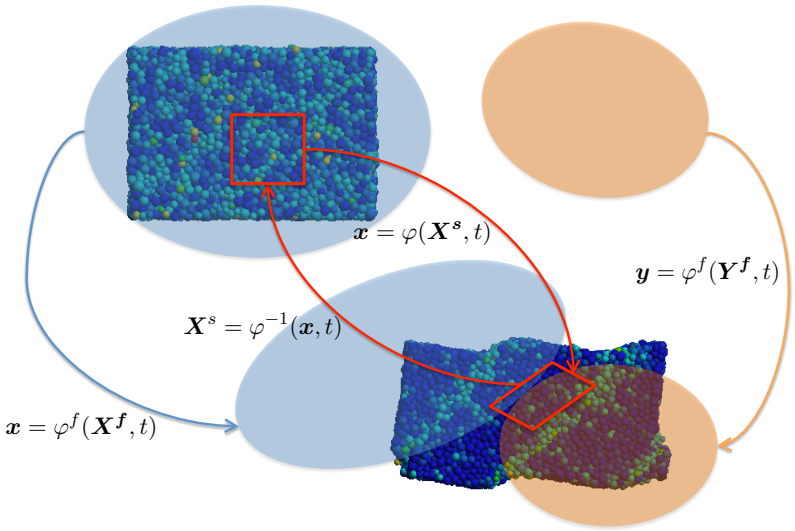

Trajectories of the solid and fluid constituent.

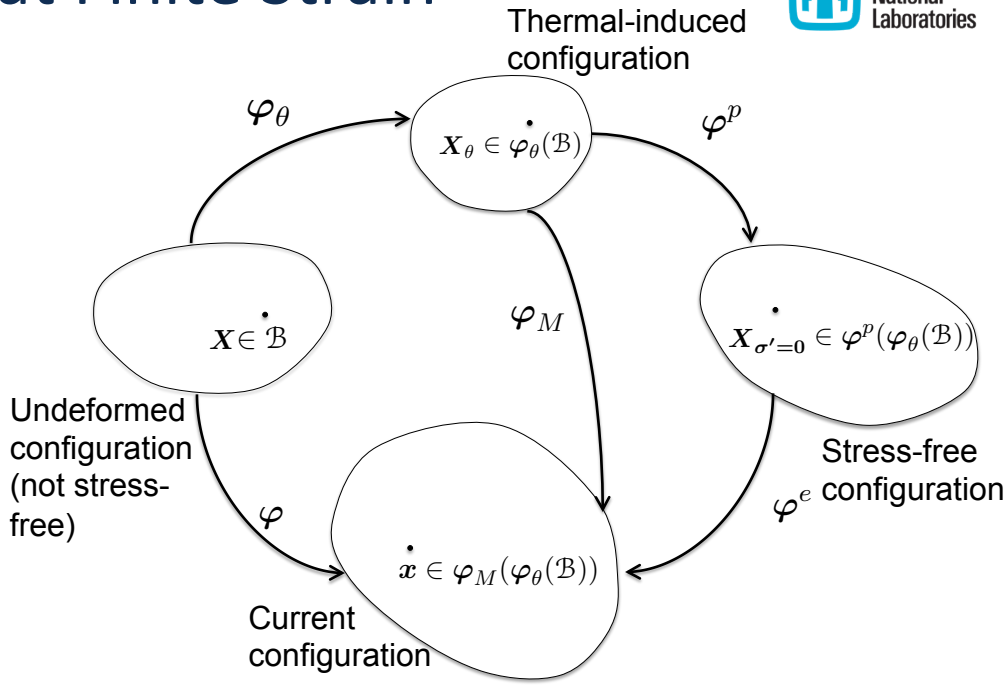

Multiplicative decomposition of the thermo-hydro-mechanics problem

Multiplicative decomposition of skeleton deformation gradient

$$\boldsymbol{F} = \frac{\partial \boldsymbol{\varphi}(\boldsymbol{X}, t)}{\partial \boldsymbol{X}} = \boldsymbol{F}_M \cdot \boldsymbol{F}_\theta \;;\; \boldsymbol{F}_\theta = \frac{\partial \boldsymbol{\varphi}_\theta(\boldsymbol{X}, t)}{\partial \boldsymbol{X}} \;; \boldsymbol{F}_M = \frac{\partial \boldsymbol{\varphi}_M(\boldsymbol{X}_\theta, t)}{\partial \boldsymbol{X}_\theta}$$

Isotropic tensor

Concept of Effective Stress

$$\boldsymbol{\sigma} = \boldsymbol{\sigma'} - Bp^{\mathrm{f}}\boldsymbol{I}, \qquad \boldsymbol{P}(\boldsymbol{F}, \boldsymbol{z}, p^f, \theta) = \boldsymbol{P'}(\boldsymbol{F}, \boldsymbol{z}, \theta) - JBp^f \boldsymbol{F}^{-T}$$

$$B = 1 - \frac{K}{K_{\mathrm{s}}} \qquad \boldsymbol{P}(\boldsymbol{F}_M, \boldsymbol{z}, p^f) = \boldsymbol{P'}(\boldsymbol{F}_M, \boldsymbol{z}) - JBp^f \boldsymbol{F}^{-T},$$

Strong Form of THM Problem at Finite Strain

Sandia National Laboratories

❑ Balance of Linear Momentum

$$\nabla^{\boldsymbol{X}} \cdot \boldsymbol{P} + J(\rho^s + \rho^f)\boldsymbol{G} = \boldsymbol{0}$$

where $\boldsymbol{P}(\boldsymbol{F}_M, \boldsymbol{z}, p^f) = \boldsymbol{P'}(\boldsymbol{F}_M, \boldsymbol{z}) - JBp^f \boldsymbol{F}^{-T},$

- $\boldsymbol{P}$: Total Stress
- $\boldsymbol{P'}$: Effective Stress
- p^f: 1st PK pore pressure

❑ Balance of Mass

$$\left(\frac{B}{J} - 3\alpha_{\mathrm{s}}(\theta - \theta_o)\right)\dot{J} + \frac{1}{M}\dot{p^{\mathrm{f}}} - 3\alpha^{\mathrm{m}}\dot{\theta} + \frac{1}{\rho_f}\nabla^{\boldsymbol{X}} \cdot \boldsymbol{W} = 0.$$

where

$\boldsymbol{W} = J\boldsymbol{F}^{-1} \cdot \boldsymbol{w}.$ (Piola's Transform) and $\boldsymbol{w} = \rho_{\mathrm{f}}\boldsymbol{k} \cdot \left[-\nabla^{\boldsymbol{x}} p^{\mathrm{f}} + \rho_{\mathrm{f}}(\boldsymbol{G} - \boldsymbol{a}^{\mathrm{f}}) \right] - \rho_{\mathrm{f}} s_T \nabla^{\boldsymbol{x}} \theta,$

- $-\nabla^{\boldsymbol{x}} p^{\mathrm{f}} + \rho_{\mathrm{f}}(\boldsymbol{G} - \boldsymbol{a}^{\mathrm{f}})$: Darcian Flow
- $\rho_{\mathrm{f}} s_T \nabla^{\boldsymbol{x}} \theta$: Soret Effect (neglected here)

❑ Balance of Energy

$$c_{\boldsymbol{F}}\dot{\theta} = [D_{\mathrm{mech}} - H_\theta] + [-\nabla^{\boldsymbol{X}} \cdot \boldsymbol{Q}_\theta - \frac{\Phi^{\mathrm{f}} c_{\boldsymbol{F}^{\mathrm{f}}}}{\rho_{\mathrm{f}}} \boldsymbol{W} \cdot \boldsymbol{F}^{-T} \nabla^{\boldsymbol{X}} \theta + R_\theta],$$

- D_{mech}: Dissipation
- $-\nabla^{\boldsymbol{X}} \cdot \boldsymbol{Q}_\theta$: Heat Flux
- $\frac{\Phi^{\mathrm{f}} c_{\boldsymbol{F}^{\mathrm{f}}}}{\rho_{\mathrm{f}}} \boldsymbol{W} \cdot \boldsymbol{F}^{-T} \nabla^{\boldsymbol{X}} \theta$: Convection
- R_θ: Heat source

where

$H_\theta = H_\theta^{\mathrm{s}} + H_\theta^{\mathrm{f}},$ (Total Structural Heating) and

$$H_\theta^{\mathrm{s}} = -\theta \frac{\partial}{\partial \theta} \boldsymbol{P'} : \dot{\boldsymbol{F}} = -3K\alpha_{sk}\theta \frac{\dot{J}}{J}$$

Solid Structural Heating (depending on which constitutive law being used)

$$H_\theta^{\mathrm{f}} = -\theta \frac{\partial}{\partial \theta} 3\alpha^{\mathrm{m}}(\theta - \theta_o)\dot{p^{\mathrm{f}}} = -3\alpha^{\mathrm{m}}\theta\dot{p^{\mathrm{f}}}.$$

Fluid contribution

Remarks on Estimating Effective Thermal Conductivity from Microstructures

- Volume averaging effective thermal conductivity

$$\boldsymbol{k}_\theta = \phi^{\mathrm{f}} \boldsymbol{k}_\theta^{\mathrm{f}} + (1 - \phi^{\mathrm{f}}) \boldsymbol{k}_\theta^{\mathrm{s}}$$

(cf. Preisig & Prevost, IJGGC 2011)

- Homogenized effective conductivity via Eshelby equivalent inclusion method (for spherical inclusions)

$$\boldsymbol{k}_\theta = \left(k_\theta^f + \frac{\phi^{\mathrm{f}}(k_\theta^{\mathrm{s}} - k_\theta^{\mathrm{f}}) k_\theta^{\mathrm{f}}}{(k_\theta^{\mathrm{s}} - k_\theta^{\mathrm{f}})\phi^{\mathrm{f}} + k_\theta^{\mathrm{f}}} \right) \boldsymbol{I}$$

(cf. Zhou & Meschke, IJNAMG 2013)

Important Note: In general, the temperature of the pore-fluid and solid skeleton are not the same in the REV, until after sufficient diffusion takes place. This difference is neglected in current formulation.

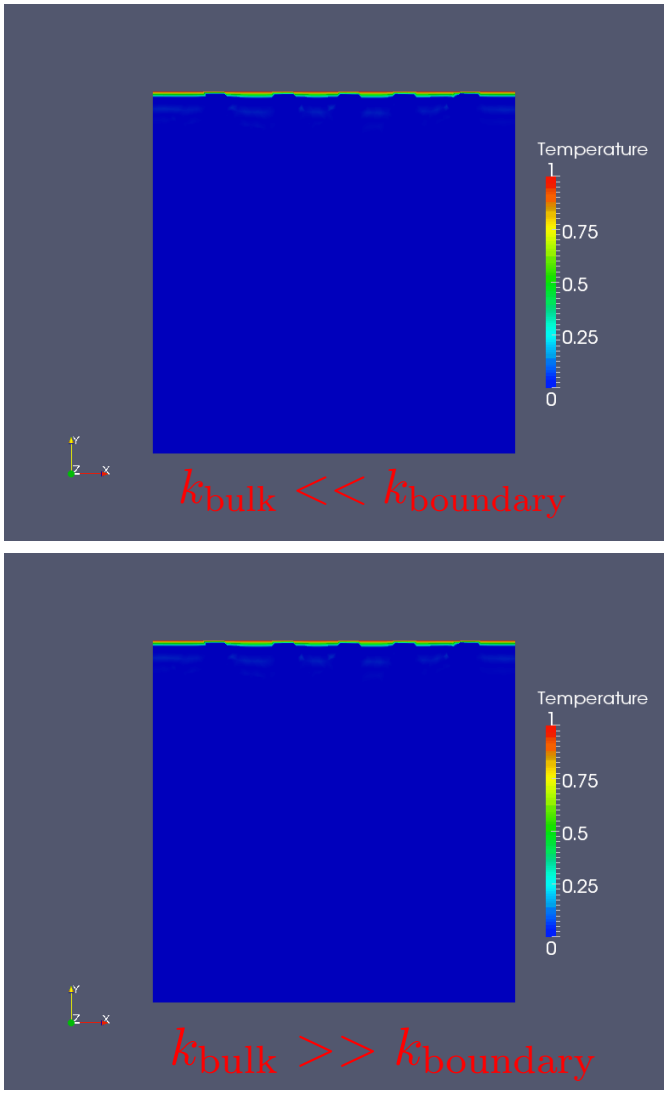

Solution of transient heat equation of two-phase materials

Stabilization of Two-fold Saddle Point Problem for Equal-order THM Finite Element Model

Sandia National Laboratories

❑ Combined Inf-sup Condition (not satisfied)

$$\sup_{\boldsymbol{w}^h \in V_{\boldsymbol{u}}{}^h} \frac{\int_{\mathcal{B}} \left(p^{\mathrm{f}h} B + 3\theta K \alpha_{\mathrm{sk}}\right) \nabla^{\boldsymbol{x}} \cdot \boldsymbol{w}^h \, d\mathrm{V}}{||\boldsymbol{w}^h||_{\boldsymbol{V}_{\boldsymbol{u}}^{\boldsymbol{h}}}} \geq C_o \left(||p^{\mathrm{f}h}||_{V_p^h} + ||\theta^h||_{V_\theta^h} \right)$$

❑ Combined Weak Inf-sup Condition (still satisfied)

$$\sup_{\boldsymbol{v}^h \in \boldsymbol{V}_{\boldsymbol{u}}^{\boldsymbol{h}}, \boldsymbol{v} \neq \boldsymbol{0}} \frac{\int_{\mathcal{B}} \left(p^{\mathrm{f}h} B + 3K \alpha_{\mathrm{sk}} \theta^h\right) \nabla^{\boldsymbol{x}} \cdot \boldsymbol{v}^h \, d\mathrm{V}}{||\boldsymbol{v}^h||_1} \geq C_1 \left(||p^{\mathrm{f}h}||_{V_{p^{\mathrm{f}}}^h} + ||\theta^h||_{V_\theta^h} \right)$$

$$- C_2 h \left(||\nabla^{\boldsymbol{x}} p^{\mathrm{f}h}||_{V_{p^{\mathrm{f}}}^h} + ||\nabla^{\boldsymbol{x}} \theta^h||_{V_\theta^h} \right)$$

❑ Projection-based Stabilization

$$\hat{H}^{\mathrm{stab}}(\psi, p_{n+1}^{\mathrm{f}h}, \theta_{n+1}^h) = \sum_{K \in \mathcal{B}} \int_K C(\psi - \Pi\psi) B \left(p_{n+1}^{\mathrm{f}h} - p_n^{\mathrm{f}h} - \Pi(p_{n+1}^{\mathrm{f}h} - p_n^{\mathrm{f}h}) \right) d\mathrm{V}$$

$$+ \sum_{K \in \mathcal{B}} \int_K C(\psi - \Pi\psi)(3\alpha^m) \left(\theta_{n+1}^h - \theta_n^h - \Pi(\theta_{n+1}^h - \theta_n^h) \right) d\mathrm{V} \, .$$

- Stabilization parameter
- Interpolated temperature changes
- Projected element-wise constant temperature changes

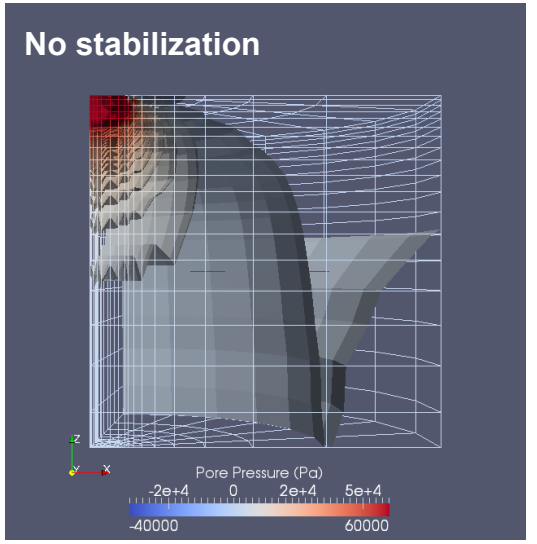

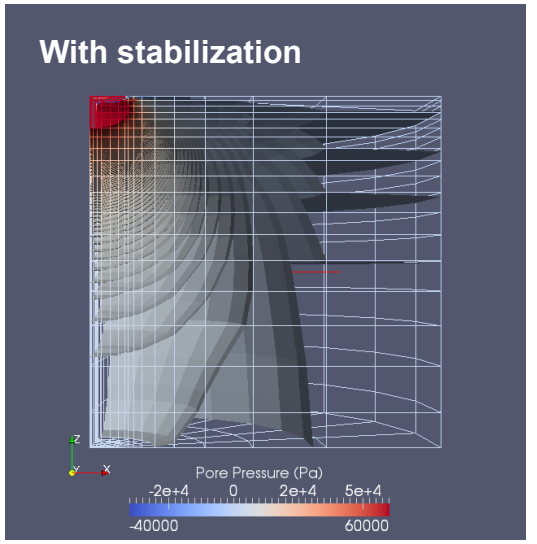

For isothermal small strain poromechanics, see White and Borja, 2009

Combined F-bar Formulation

Sandia National Laboratories

- Isochoric-volumetric split (Hughes 1975, Simo 1975)

$$\boldsymbol{F} = \boldsymbol{F}_{\text{vol}} \cdot \boldsymbol{F}_{\text{iso}}$$

- Replacing volumetric split with assumed term

$$\overline{\boldsymbol{F}} = \bar{J}^{1/3}\boldsymbol{F}_{\text{iso}} = \bar{J}^{1/3} J^{-1/3}\boldsymbol{F}$$

Modified det(F) — Original det(F)

Relaxing too much, we get instabilities
Relaxing too little, we get the volumetric locking

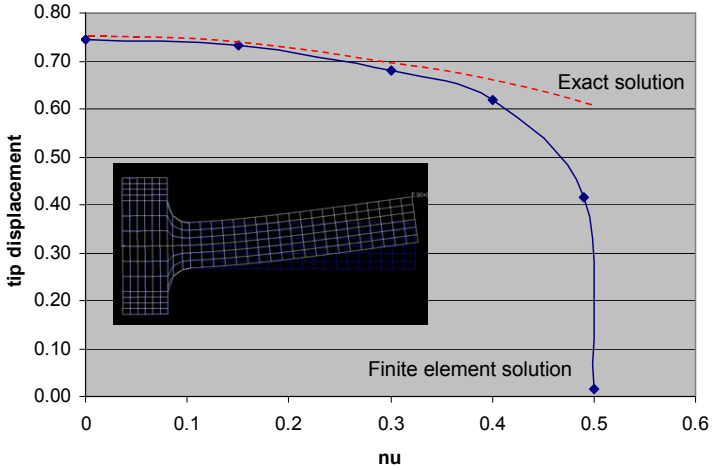

Standard F leads to Volumetric Locking

- Combined F-bar approach

$$\widetilde{\boldsymbol{F}} = \alpha\boldsymbol{F} + (1-\alpha)\overline{\boldsymbol{F}}.$$ ← Invalid operation

- Current Approach via Lie algebra

$$\widetilde{J} = \exp\left(\frac{1-\beta}{\mathrm{V}_{\mathcal{B}^e}}\int_{\mathcal{B}^e}\log J \,\mathrm{dV} + \beta \log J\right).$$

$$\widetilde{J}_M = \exp\left(\log\widetilde{J} - 3\left(\frac{1-\beta}{\mathrm{V}_{\mathcal{B}^e}}\int_{\mathcal{B}^e}\alpha_{sk}(\theta-\theta_o)\,\mathrm{dV} + \beta\alpha_{sk}(\theta-\theta_o)\right)\right)$$

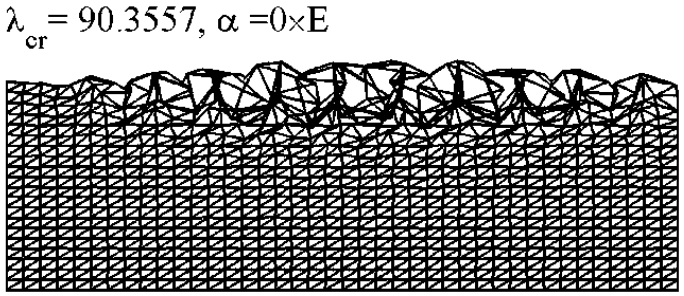

Pure F-bar leads to instability
(Brocardo, Micheloni, Krysl, IJNME, 2009)

Thermo-hydro-mechanical Responses of Porous Sphere in Thermal Reservoir

- Material
  - Neo-Hookean
  - Kozeny-Carman Permeability
  - Homogenized Thermal Conductivity
  - Very low Pore-fluid diffusivity
  - High thermal diffusivity
- Boundary Condition
  - Temperature at outer surface =5^{o}C
  - Initial Temperature = 0^{o}C
  - Globally Undrained
- Analytical Solution is available for linear THM problem (see Belotserkovets & Prevost 2011, Selvadurai and Suvorov 2013)

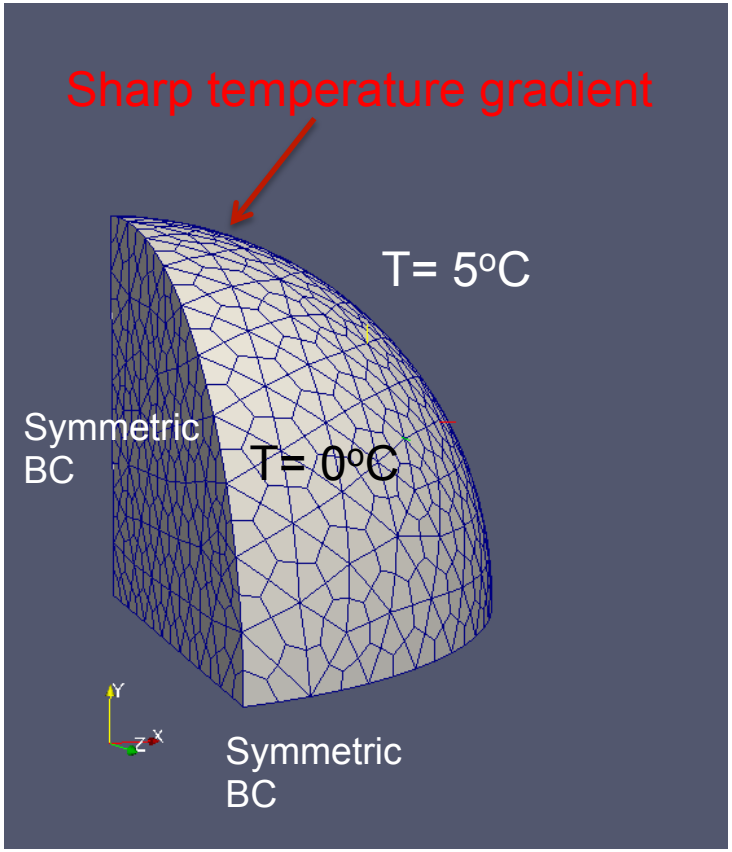

Thermo-hydro-mechanical Responses of Porous Sphere in Thermal Reservoir

Sandia National Laboratories

X Under-diffusion with spurious patterns

✓ Diffusion with estimated optimal stabilization

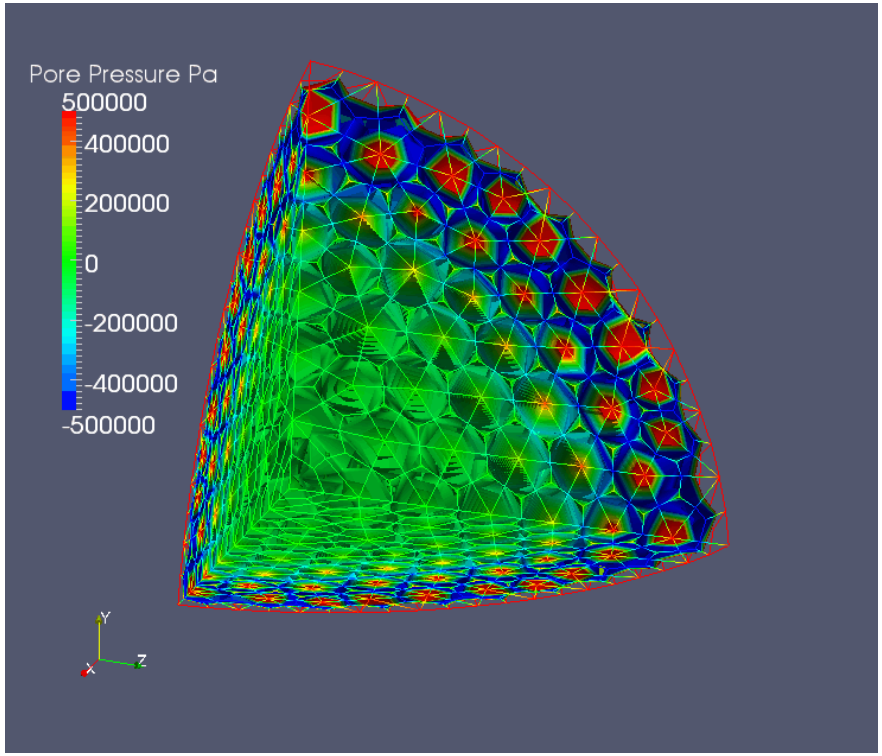

Pore Pressure computed with standard Galerkin FEM

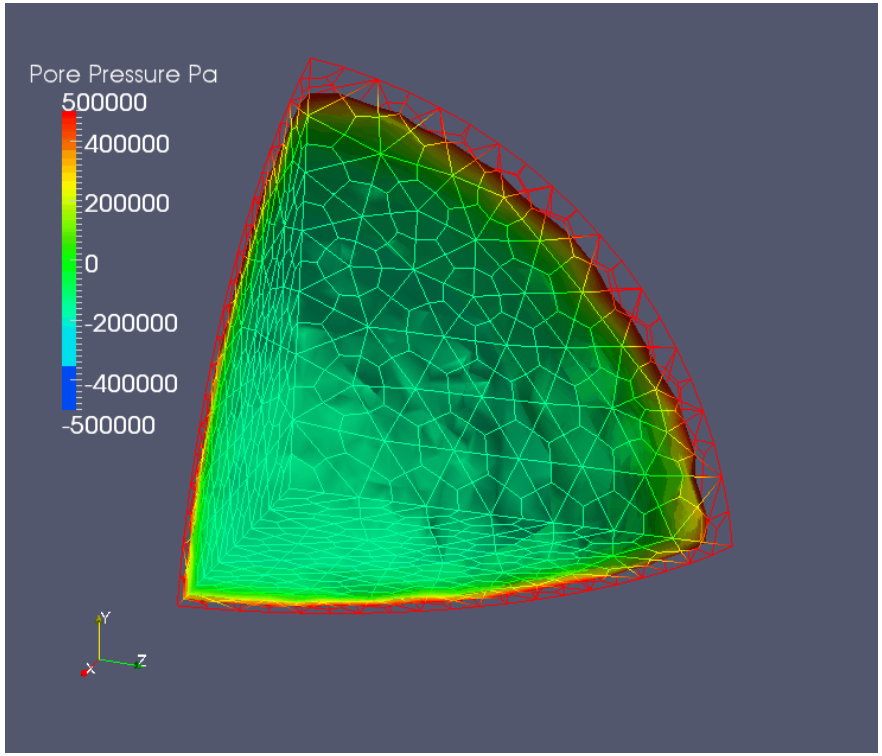

Pore Pressure computed with Stabilized FEM

Note: we do not impose shape pore pressure gradient.

Thermo-hydro-mechanical Responses of Porous Sphere in Thermal Reservoir

Sandia National Laboratories

X Under-diffusion with spurious patterns

✓ Diffusion with estimated optimal stabilization

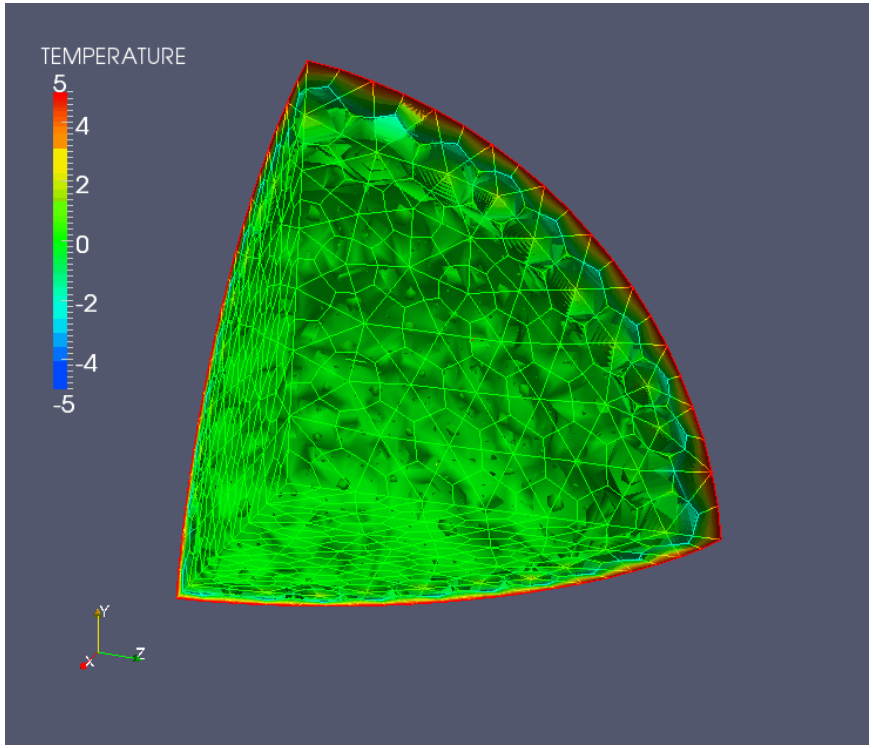

Temperature computed with standard Galerkin FEM

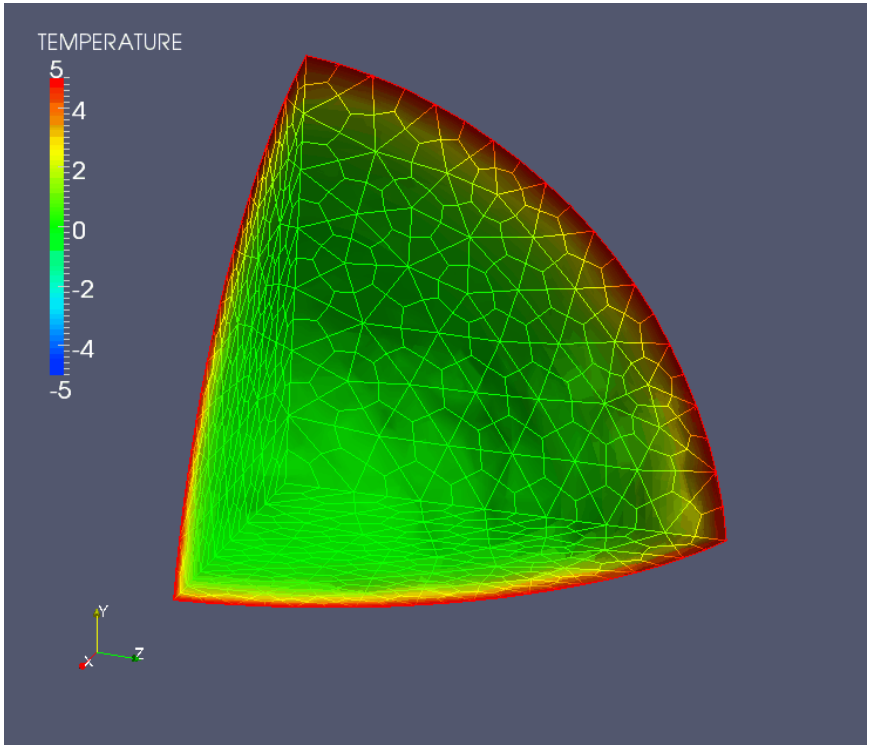

Temperature computed with Stabilized FEM

Generalized Mandel-Cryer Effect for THM Spherical problems

Sandia National Laboratories

✓ Solution with estimated optimal stabilization

X Over-diffused solution (Constant stabilization parameter C=200000)

Temperature Time History of the centroid

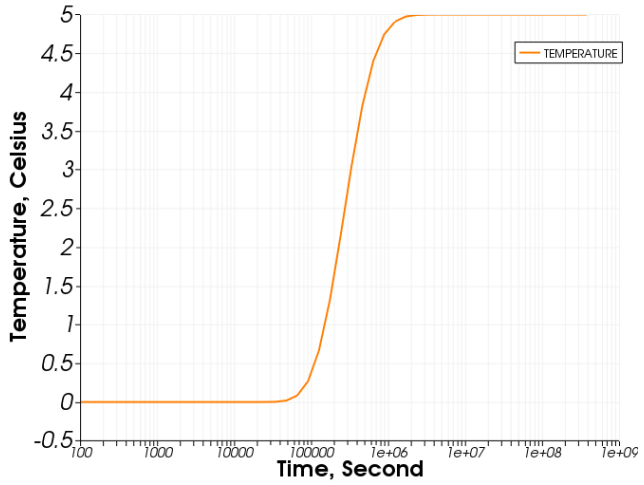

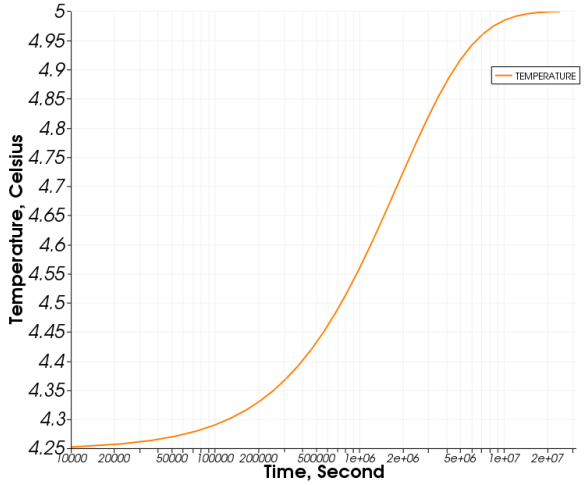

Pore pressure of Time History of the centroid

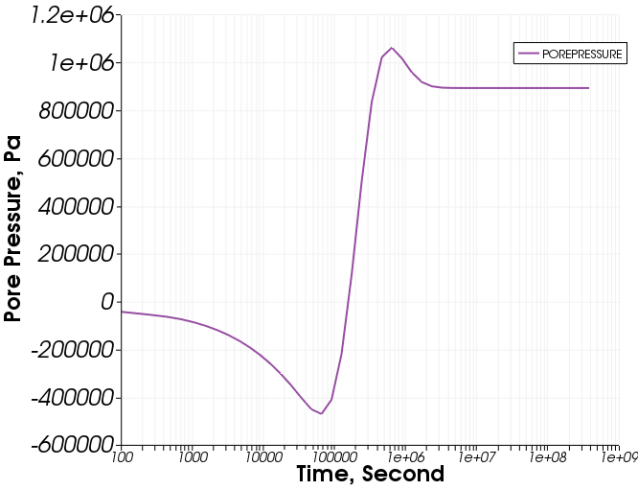

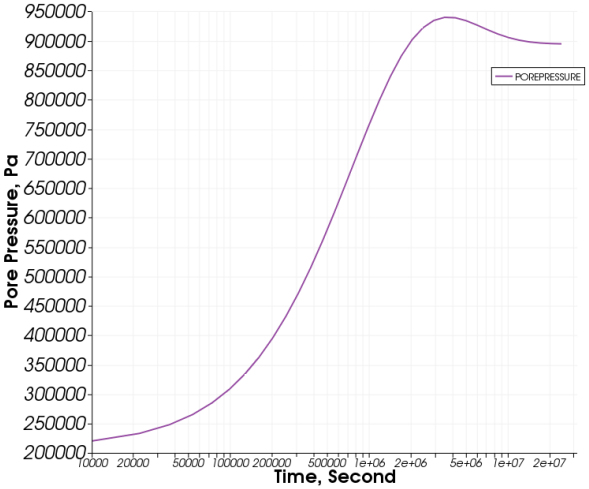

Optimal Stabilization Parameter Estimation

1D poromechanics governing equation

$$c\frac{\partial^2 \hat{p}}{\partial x^2} = \frac{\partial \hat{p}}{\partial t}, \qquad c = \frac{k}{\mu}\frac{M'H}{H+\nu\beta M'}; M' = \frac{M(K+4G/3)}{K+4G/3+B^2M}$$

Three node stencil (standard Galerkin method)

$$-\hat{p}_{A-1} + 2\hat{p}_A - \hat{p}_{A-1} + \frac{h^2}{6\vartheta c\Delta t}(\hat{p}_{A-1} + 4\hat{p}_A + \hat{p}_{A+1}) = 0$$

Three node stencil (Stabilized Galerkin method)

$$-\hat{p}_{A-1} + 2\hat{p}_A - \hat{p}_{A-1} + \frac{h^2}{12\vartheta c\Delta t}[(2-\gamma)\hat{p}_{A-1} + (8+2\gamma)\hat{p}_A + (2-\gamma)\hat{p}_{A+1}] = 0$$

Growth/decay rate

$$\cosh\frac{h}{(\sqrt{\vartheta c\Delta t})^h} = \frac{(1+h^2/\vartheta c\Delta t)(4+\gamma)/6}{(1-h^2/\vartheta c\Delta t)(2-\gamma)/12}$$

To have real growth/decay rate, we need

$$\gamma > 2 - 12\frac{\vartheta c\Delta t}{h^2} > 0$$

$$\gamma = (2 - 6\frac{\vartheta c\Delta t}{h^2})\left(\frac{1}{2} + \frac{1}{2}\tanh(2 - 12\frac{\vartheta c\Delta t}{h^2})\right)$$

Safety factor

Turn off stabilization without introducing switch

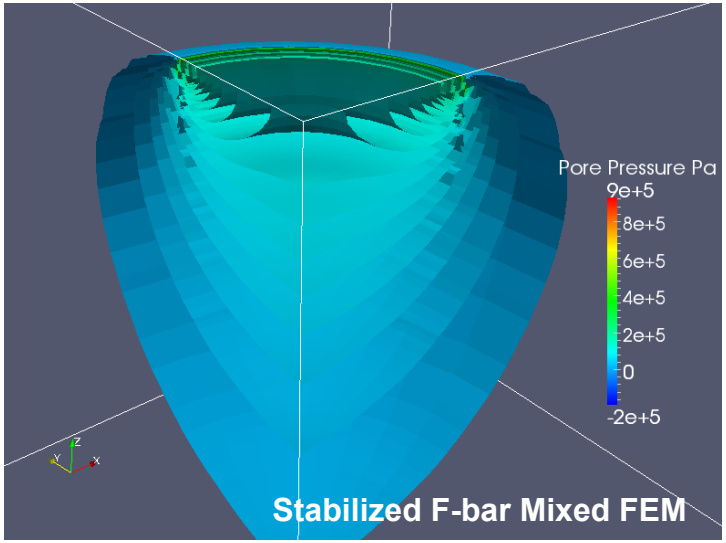

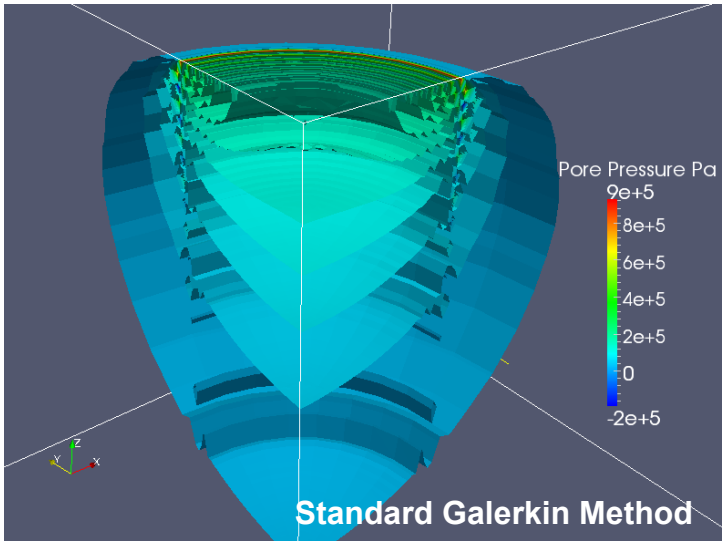

Unconfined Compression Test of Cold Thermo-sensitive Porous Media at Room Temperature

- Material
  - J2 perfect plasticity
  - Kozeny-Carman permeability
  - Homogenized thermal conductivity
  - Pore-fluid diffusivity < thermal diffusivity
- Boundary Condition
  - Temperature at surface =12^{o}C
  - Initial temperature = 0^{o}C
  - Globally undrained
  - Unconfined side surface
  - Prescribed displacement on the top and bottom
  - Under constant rate, apply 16.67% vertical strain in 10 hours

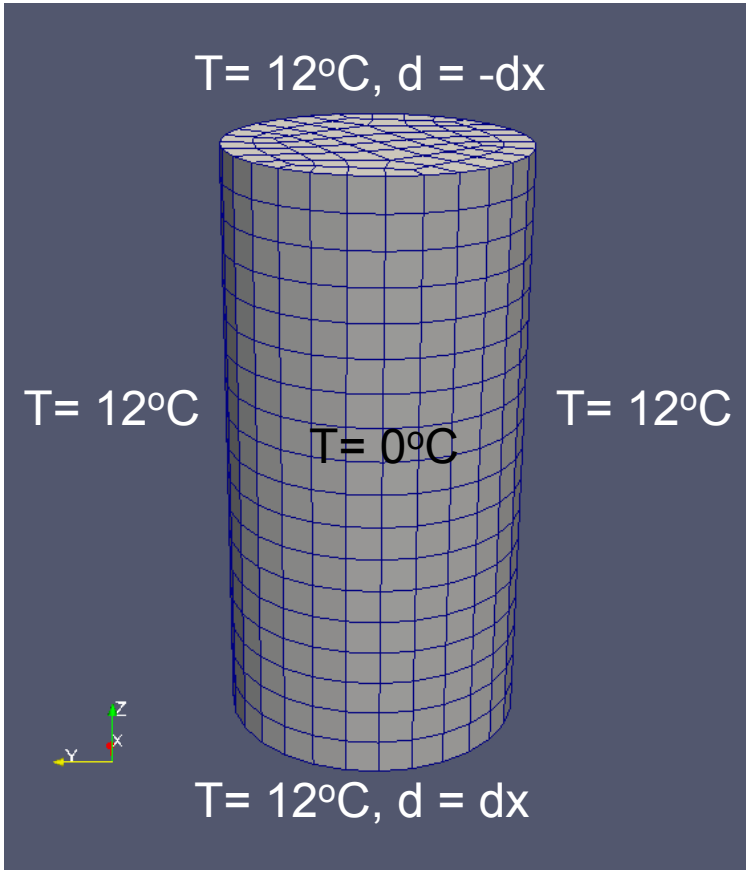

Coupling effects of Multiphysical Responses in Geometrically Nonlinear Regime

Sandia National Laboratories

- Temperature & equivalent plastic strain

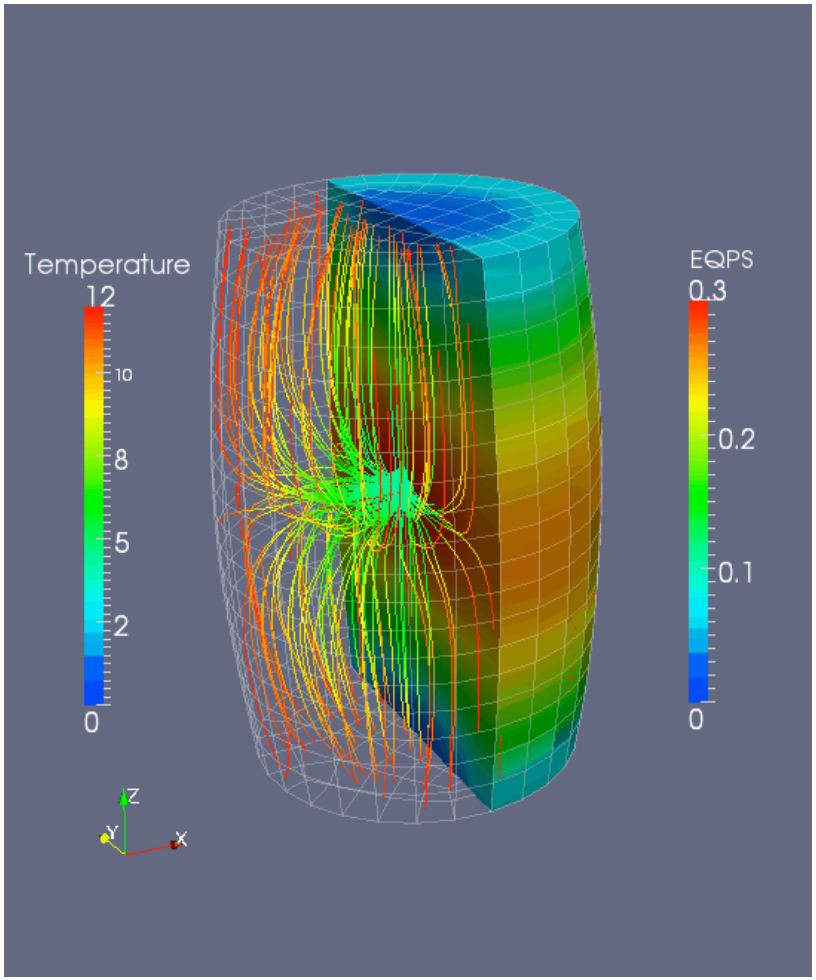

- Pore Pressure

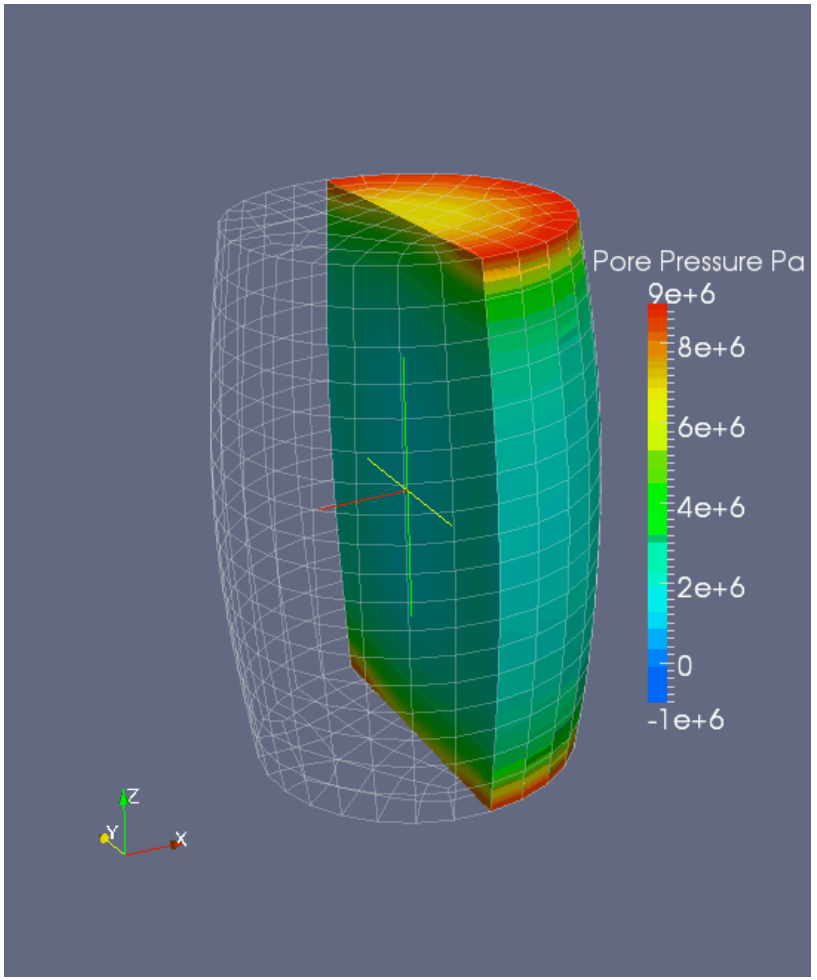

Why localization elements?

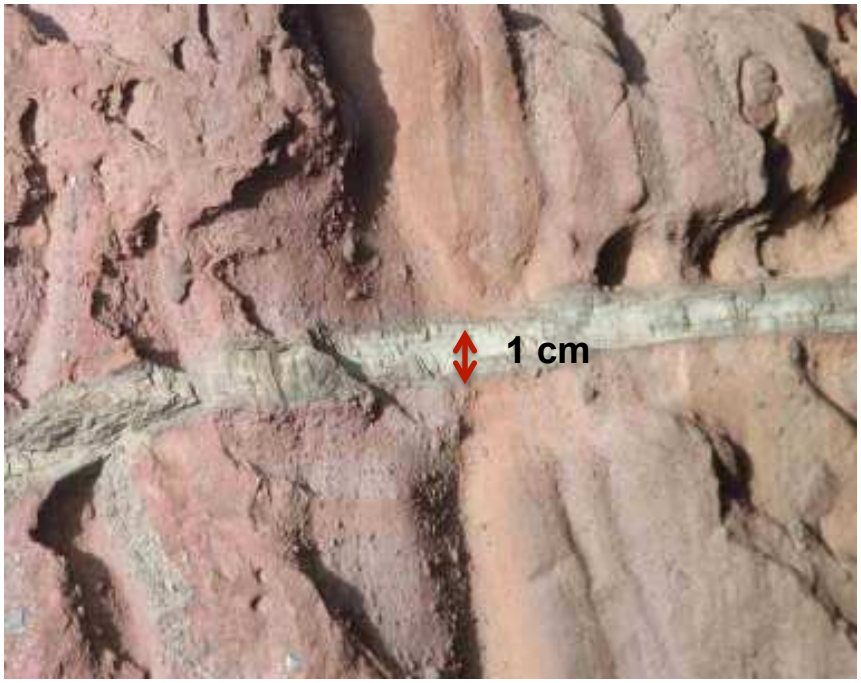

Figure from Hirschberger, Sukumar and Steinmann, Philosophical Magazine, 2008

- Model surface, rock joint and bulk materials without the need to discretize them in the same mesh.

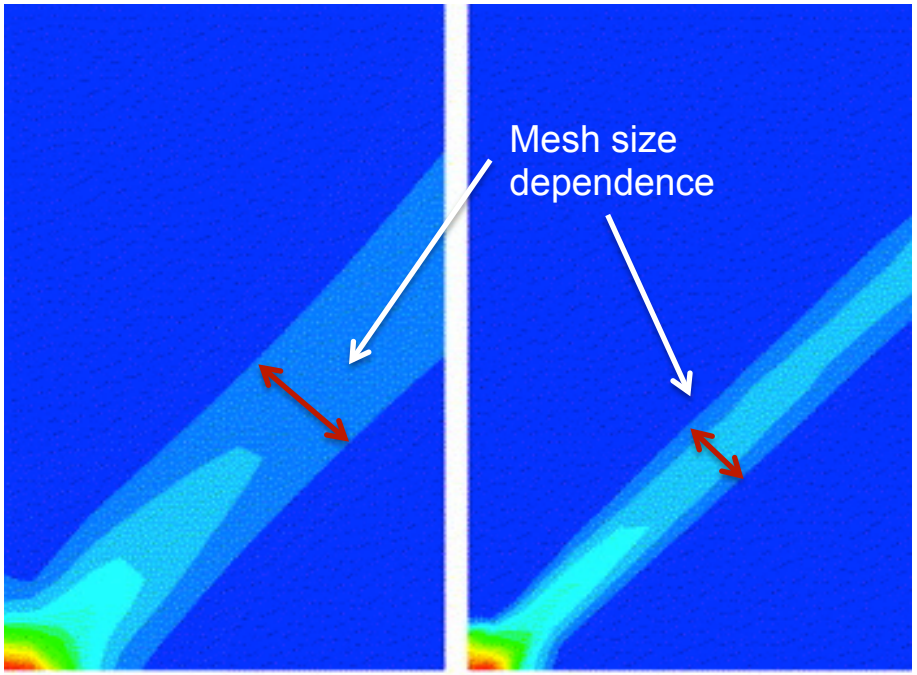

Figure from Khoei et al, Communications in Nonlinear Science and Numerical Simulation 2005

- Cure mesh dependence by introducing length scale.

Formulation of the localization element

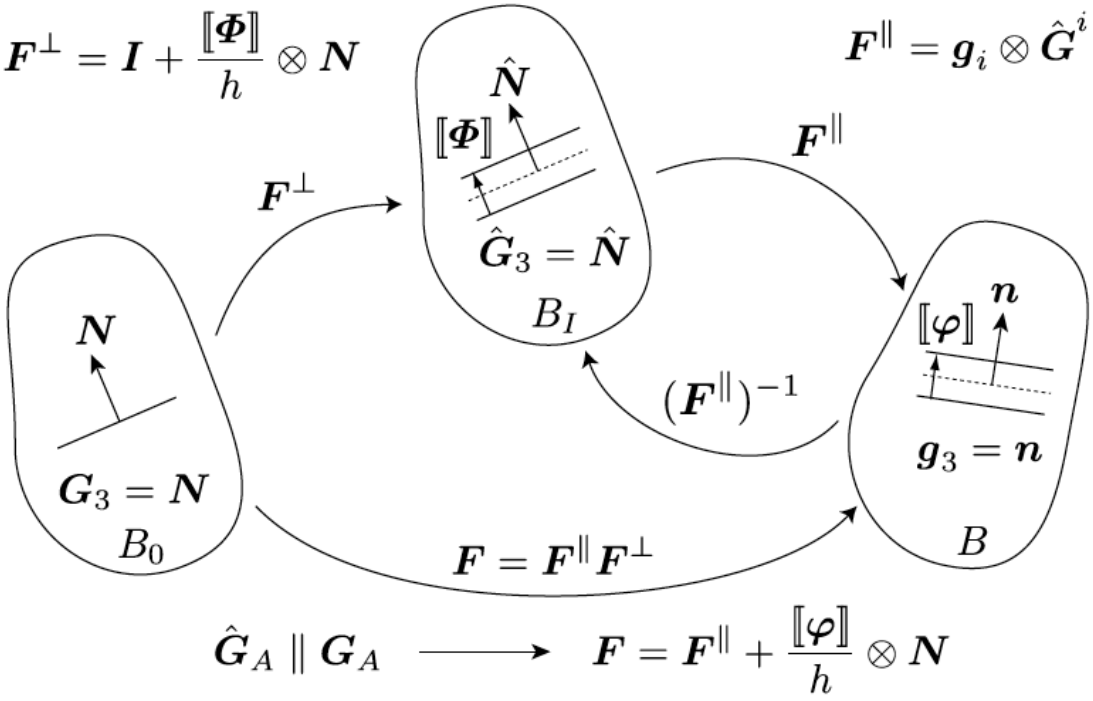

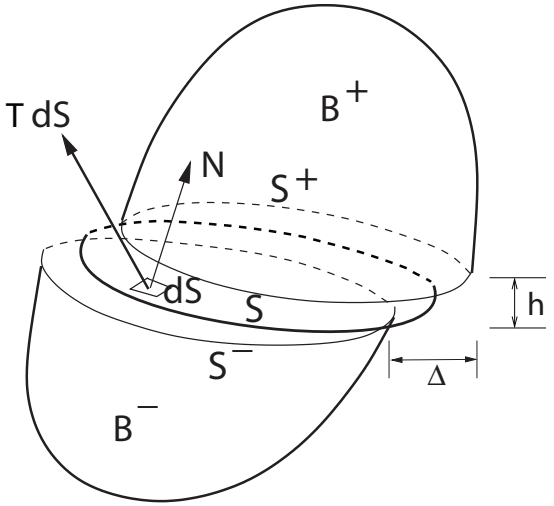

From Yang, Mota Ortiz, 2006; Foulk et al 2013

Deformation power of the solid skeleton

$$P^D = \sum_{\pm} \int_{B_0^{\pm}} \boldsymbol{P} \cdot \dot{\boldsymbol{F}}\, dV + \int_{S_0} \boldsymbol{P} \cdot \dot{\boldsymbol{F}} h\, dS$$

$$= \sum_{\pm} \int_{B_0^{\pm}} \boldsymbol{P} \cdot \dot{\boldsymbol{F}}\, dV + \int_{S_0} \boldsymbol{P} \cdot \left[\dot{\boldsymbol{F}}^{\parallel} h + [\![\dot{\varphi}]\!] \otimes \boldsymbol{N} \right] dS$$

$$= \sum_{\pm} \int_{B_0^{\pm}} \boldsymbol{P} \cdot \dot{\boldsymbol{F}}\, dV + \int_{S_0} \left[h\boldsymbol{P} \cdot \dot{\boldsymbol{F}}^{\parallel} + \boldsymbol{T} \cdot [\![\dot{\varphi}]\!] \right] dS$$

$$\mathbf{F} = \mathbf{F}^{\parallel}\mathbf{F}^{\perp}$$

deformation of mid-surface membrane

homogenized displacement jump

Globally undrained Simple Shear Test of Fully saturated media with flow barrier in the surface element (Pore Pressure)

Sandia National Laboratories

Without sealed rock joint

With sealed rock joint

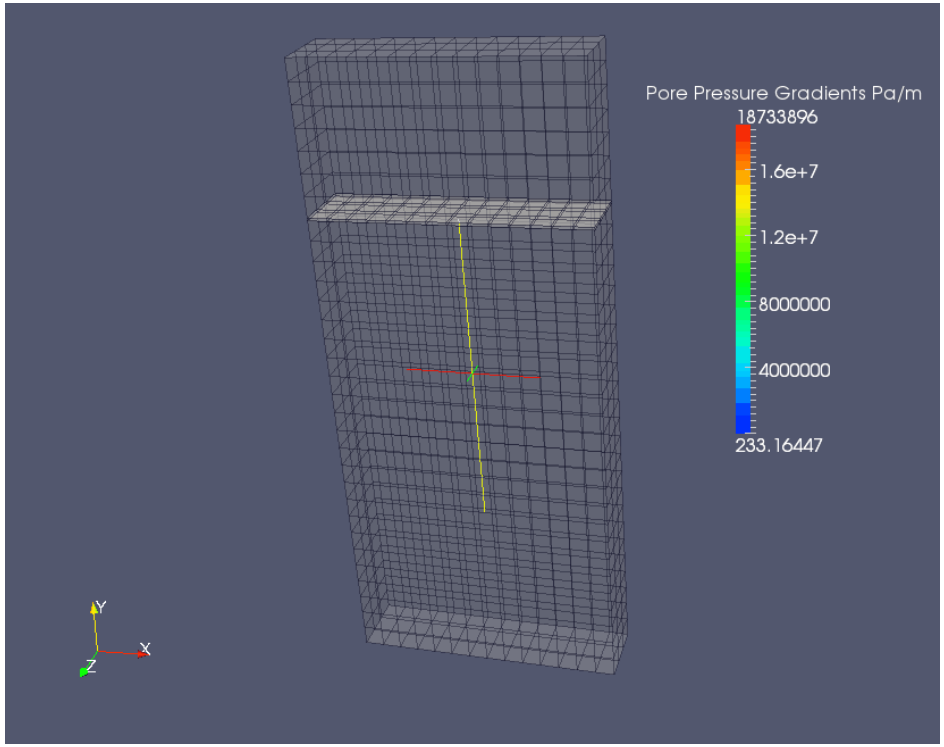

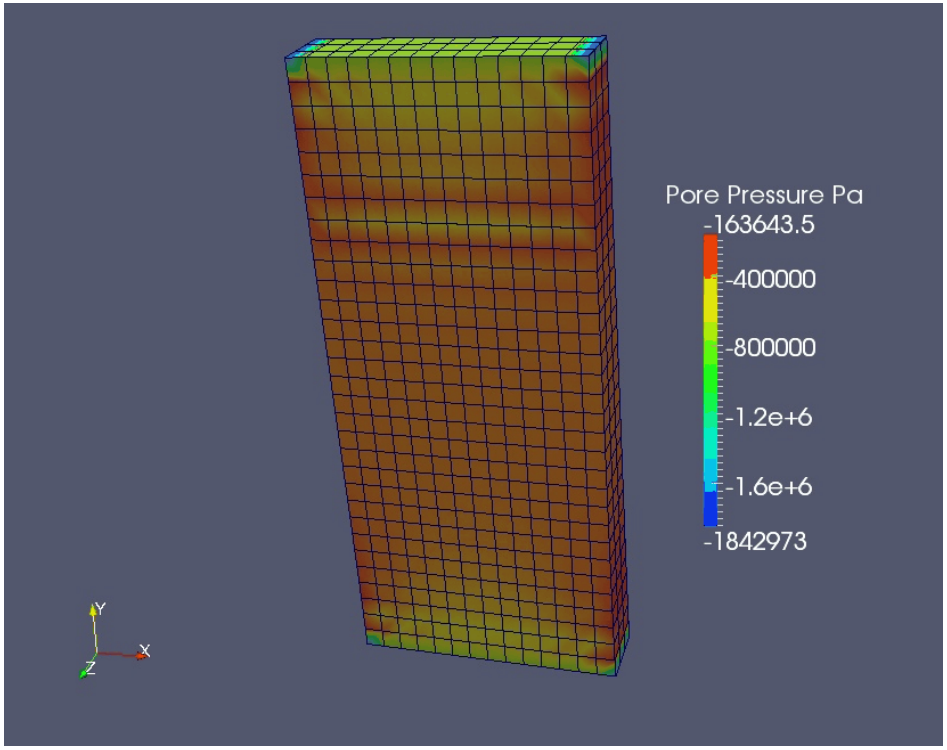

- In geometrical nonlinear regime, pore-fluid flow is significantly influenced by geometrical changes.
- Capturing localized hydraulic features triggered by deformation is important to analyze overall reservoir properties.

Conclusion and Future Perspective

Sandia National Laboratories

- For the 1st time, A fully coupled, finite deformation, stabilization thermo-hydro-mechanics finite element model is implemented.
- This model preserves Mandel-Cryer effect, and is able to eliminate spurious oscillation due to the lack of inf-sup condition.
- Thermo-poro-plasticity model is extended and tested.
- Localization element is introduced as localization limiter to cure mesh dependence.
- Unsaturated flow will be further tested against analytical solutions and classical problems in the literatures.

Connecting micro-structural attributes and macroscopic mechanical and hydraulic responses

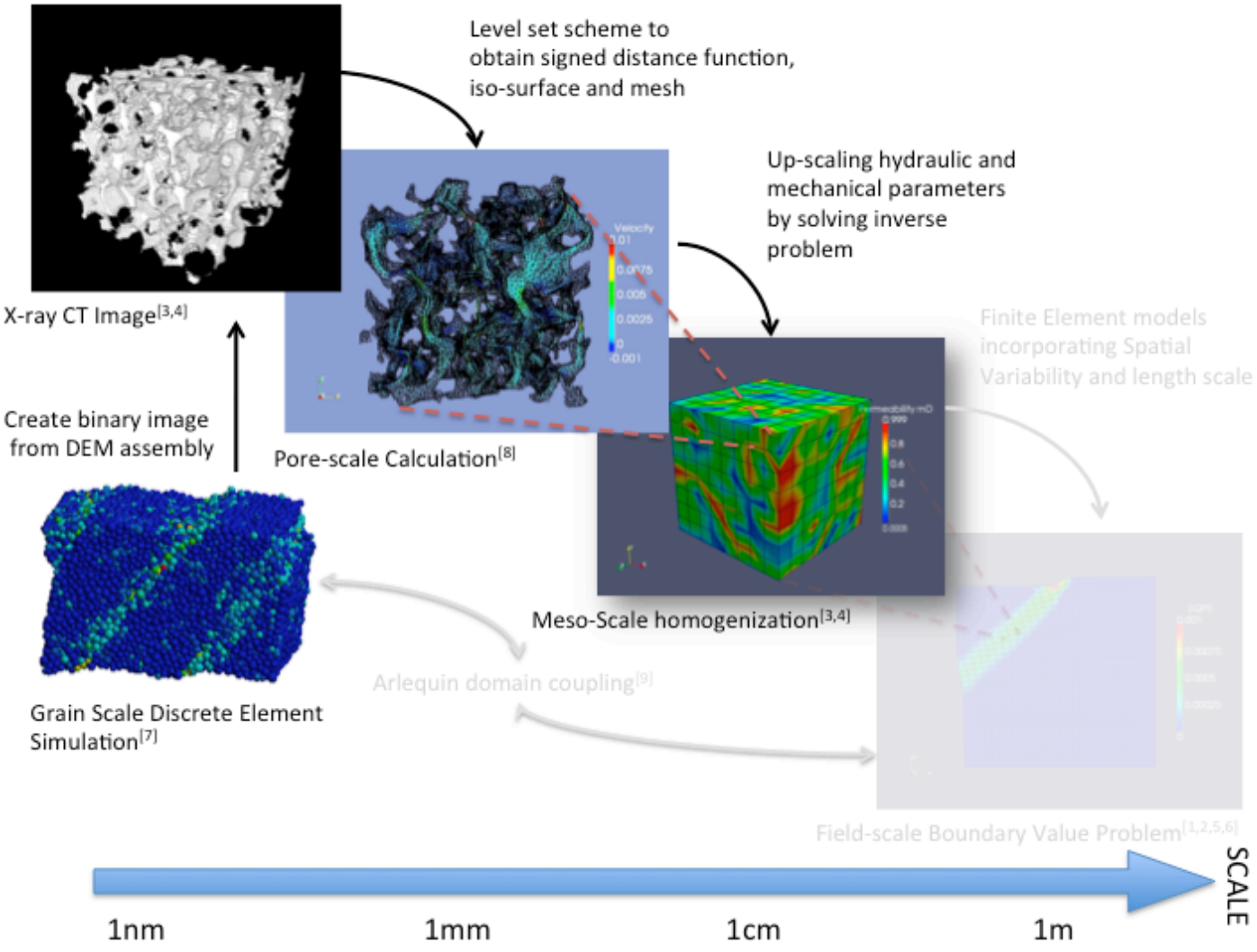

State-of-art on Analyzing Stress Induced Permeability Changes on Granular Materials

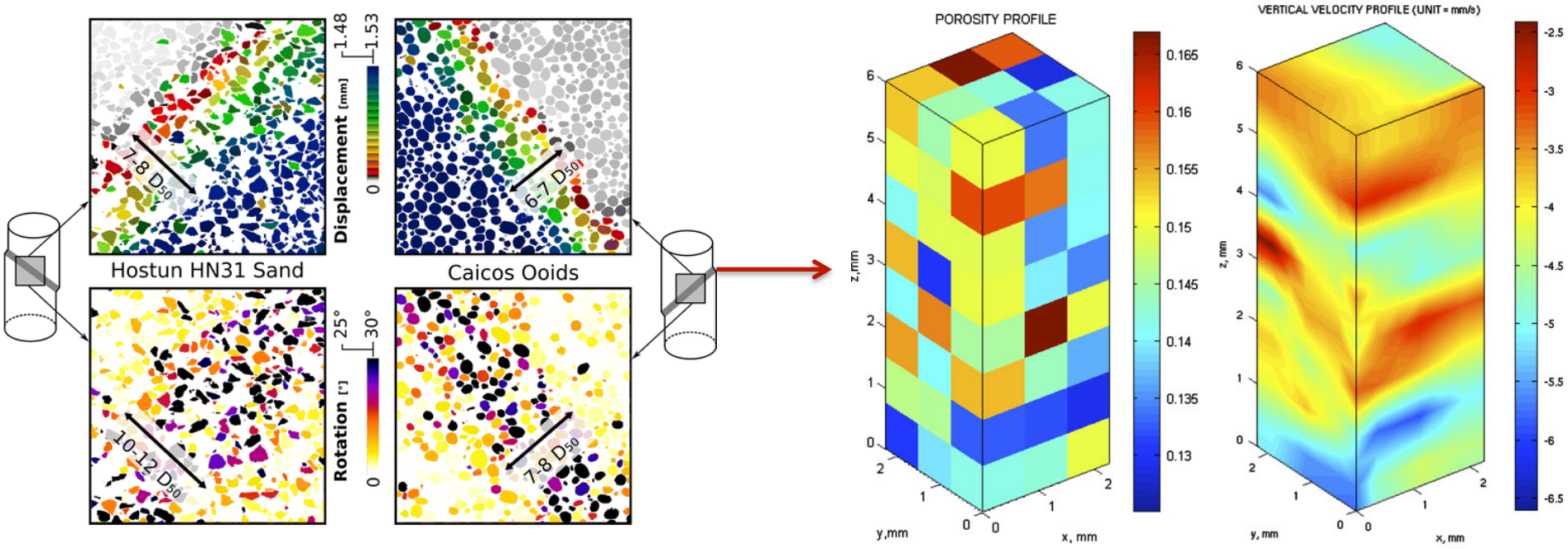

1. ID tracking approach performed on tomographic images
2. Obtain porosity profile
3. Compute permeability

Ando, Hall, Viggiani, Desrues, Besuelle, Acta Geotechnica, 2012

Sun, Andrade, Rudnicki, IJNME, 2011

Some problems with this approach….

1. Not repeatable for different stress path (It is impossible to prepare two identical granular assemblies in lab)

2. Technically, volumetric digital image correlation during mechanical test is difficult and very rare (Hall et al 2011).

3. Permeability changes due to changes of pore geometry (shape) is lost if porosity dependent empirical relation (i.e., Kozeny-Carman relation) is used to analyze pore-scale images.

Analyzing Microstructure Evolution of Shear Banding in Simple Shear Test

1. Run Discrete Element Simulation.
2. Extract 3D assembles inside and outside deformation bands
3. Analyze rotations, translations and damages of grains
4. Obtain macroscopic constitutive responses
5. Analyze pore geometry and estimate permeability with the multi-scale framework discussed before.

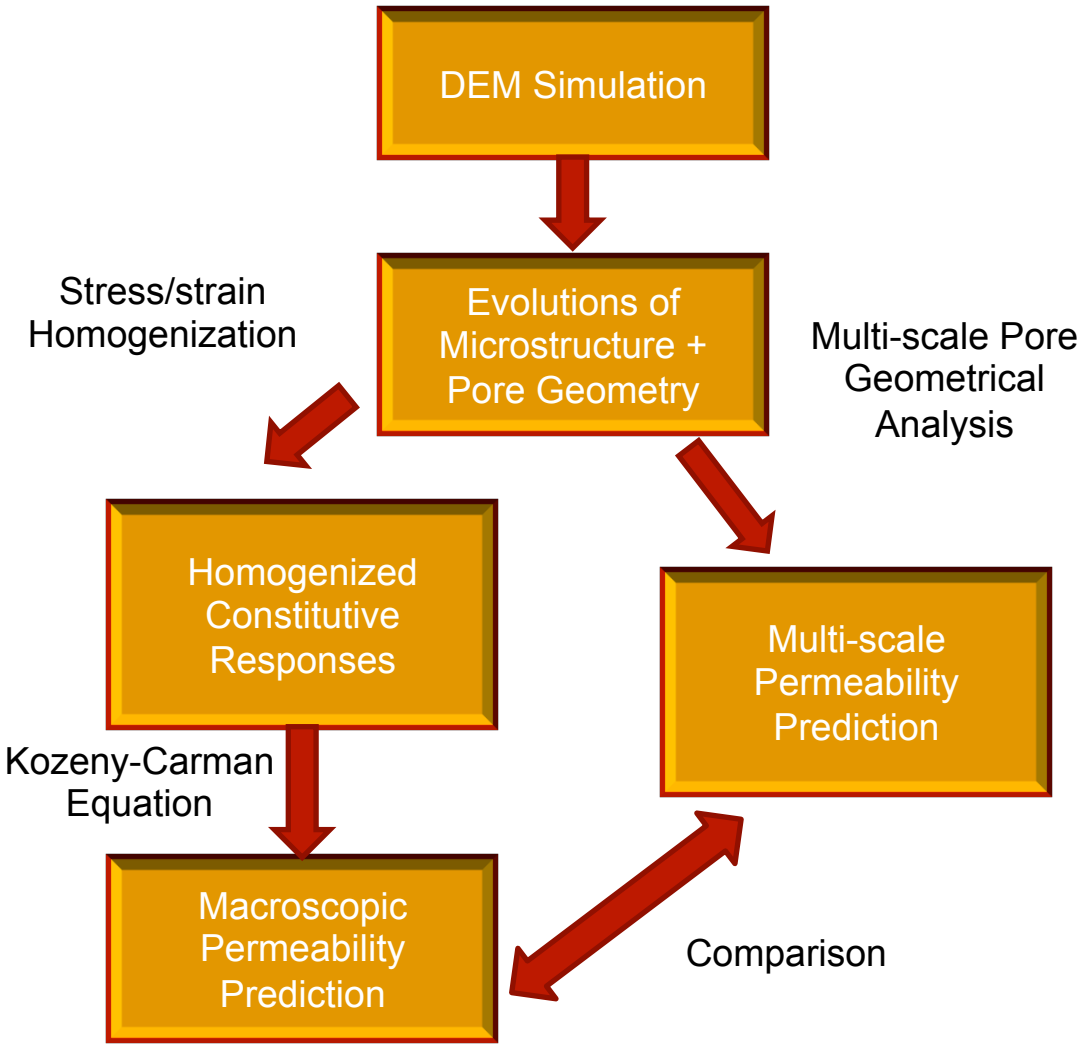

Discrete Element Simulation of Simple Shear Test

Balance of linear and angular momentum

$$m\ddot{u} + C^m \dot{u} + P(u) = F_{ext}$$

force balance

$$I \cdot \ddot{\omega} = M_{ext}$$

moment balance

Homogenized Cauchy stress and infinitesimal strain

$$\sigma_{ij} = \frac{1}{V_\Omega} \sum_{\alpha=1}^{N_c} f_i^\alpha l_j^\alpha ; \quad \varepsilon_{ij} = \frac{1}{2}(F_{ik}F_{kj} - I_{ij})$$

Hertz's contact model

$$df^n = k^n d\delta ; \quad k^n = \frac{\sqrt{2}G_g\sqrt{R^e}}{1-\nu}\delta^{1/2}$$

normal stiffness

$$df^t = k^s ds ; \quad k^s = \frac{2\sqrt{2}G_g\sqrt{R^e}}{2-\nu}\delta^{1/2}$$

tangential stiffness

$$R^e = \frac{2R_1R_2}{R_1+R_2}$$

effective radius

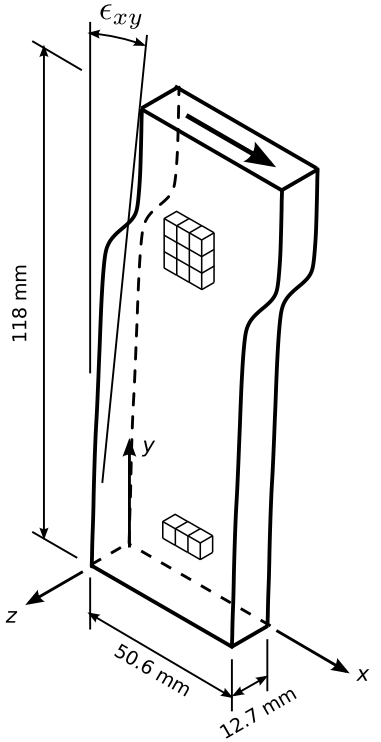

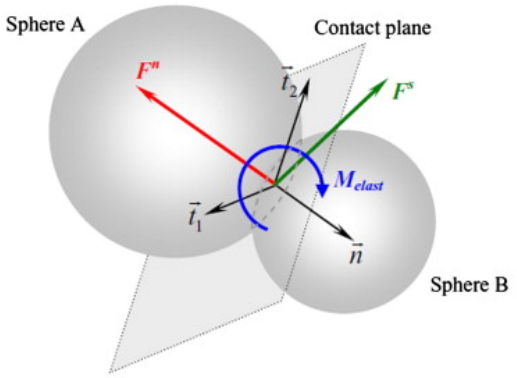

Rotation Magnitude of Grains Obtained From The Discrete Element Simulation of Simple Shear Test

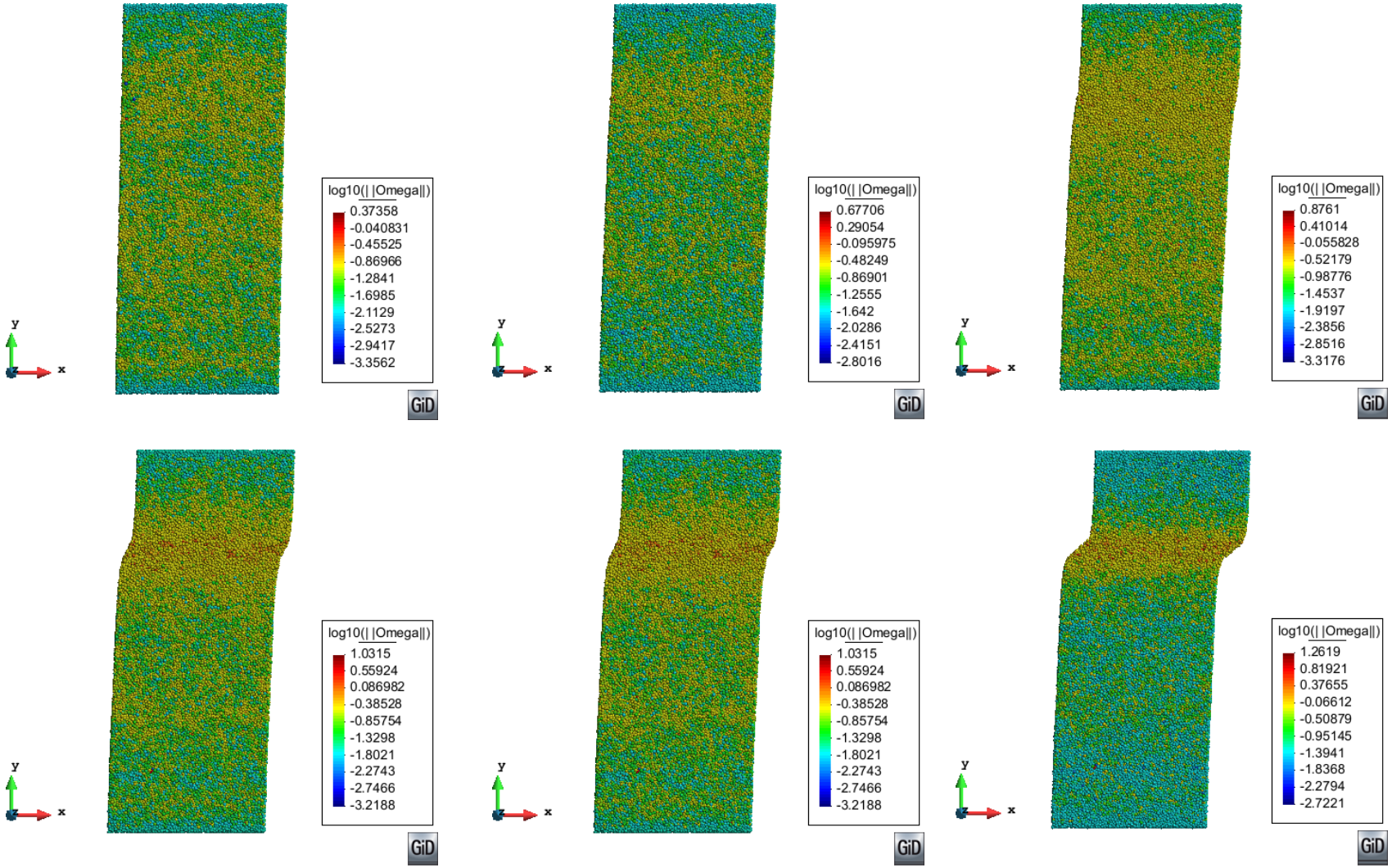

see W.C. Sun, M.R. Kuhn, J.W. Rudnicki, a multiscale DEM-LBM analysis on dilatant shear band, *Acta geotechnica, 2013*

Granular and Macroscopic Responses

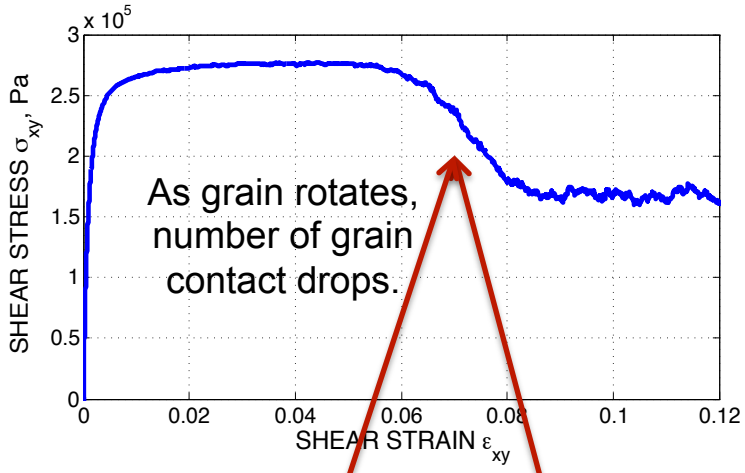

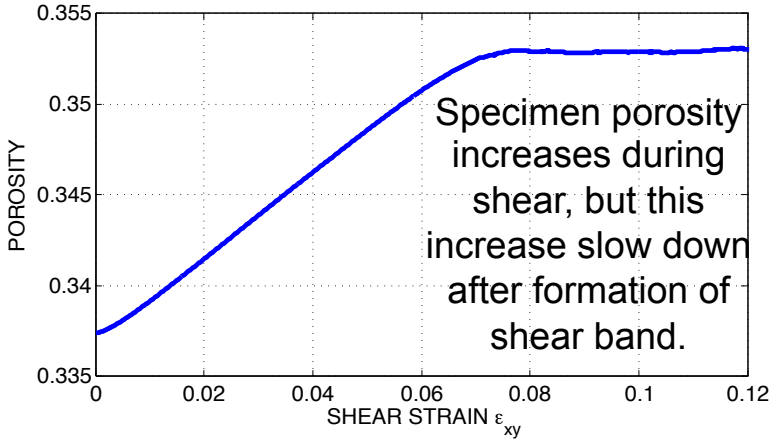

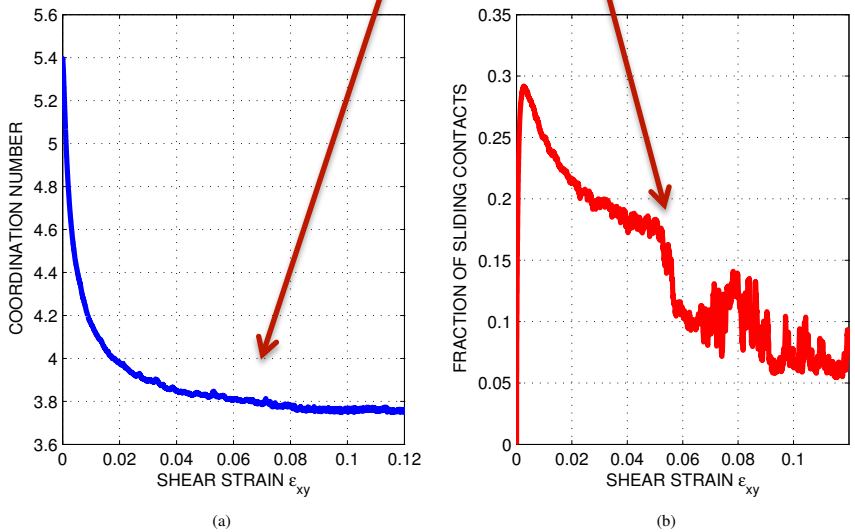

Number of grain contacts decreases as shear band develops.

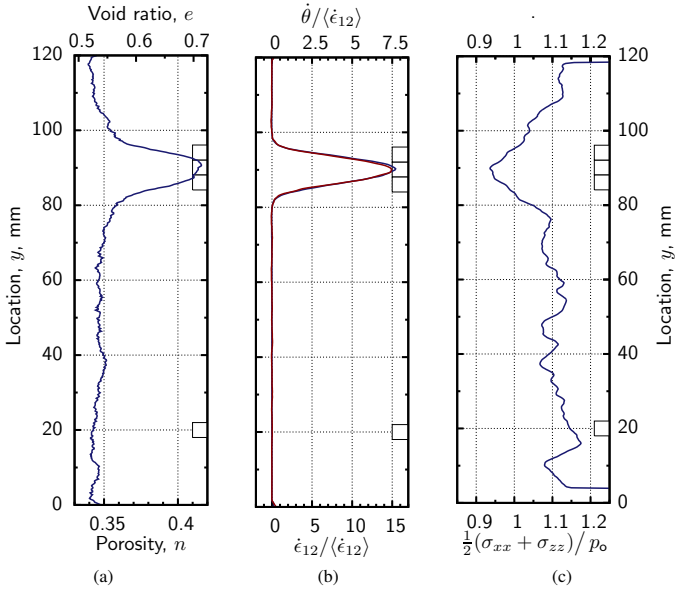

Locally, porosity increase is concentrated inside shear band.

Sandia National Laboratories

Question:

How does this granular motion affects pore geometry and hydraulic properties of deformation bands?

Obtain Pore Volume Binary Images from DEM Assemblies

Algorithm 1 Seed-fill (node, void-flag, solid-flag)

```
if the current node is not a void then
    return
else
    search the spherical particle closest to the current node
    Compute Euclidean distance between current node and the centroid of the closest spherical particle
    if Euclidean distance ≠ radius of the closest spherical particle then
        Perform Flood-fill (the west neighbor of the current node, void-flag, solid-flag)
        Perform Flood-fill (the east neighbor of the current node, void-flag, solid-flag)
        Perform Flood-fill (the north neighbor of the current node, void-flag, solid-flag)
        Perform Flood-fill (the south neighbor of the current node, void-flag, solid-flag)
        Perform Flood-fill (the upper neighbor of the current node, void-flag, solid-flag)
        Perform Flood-fill (the lower neighbor of the current node, void-flag, solid-flag)
    end if
end if
```

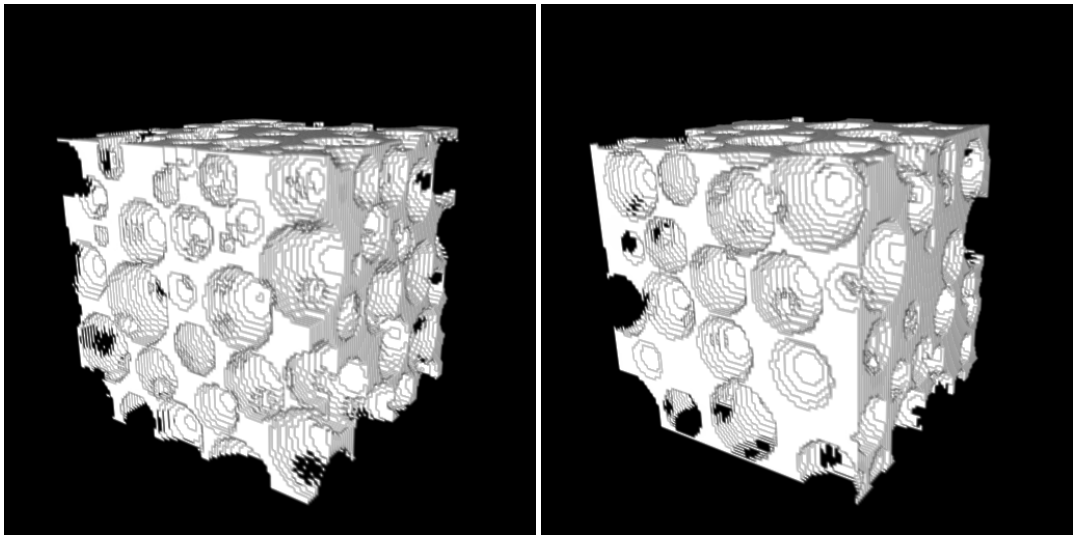

Binary images generated from DEM assemblies

Multi-scale Lattice Boltzmann/Finite Element Simulations

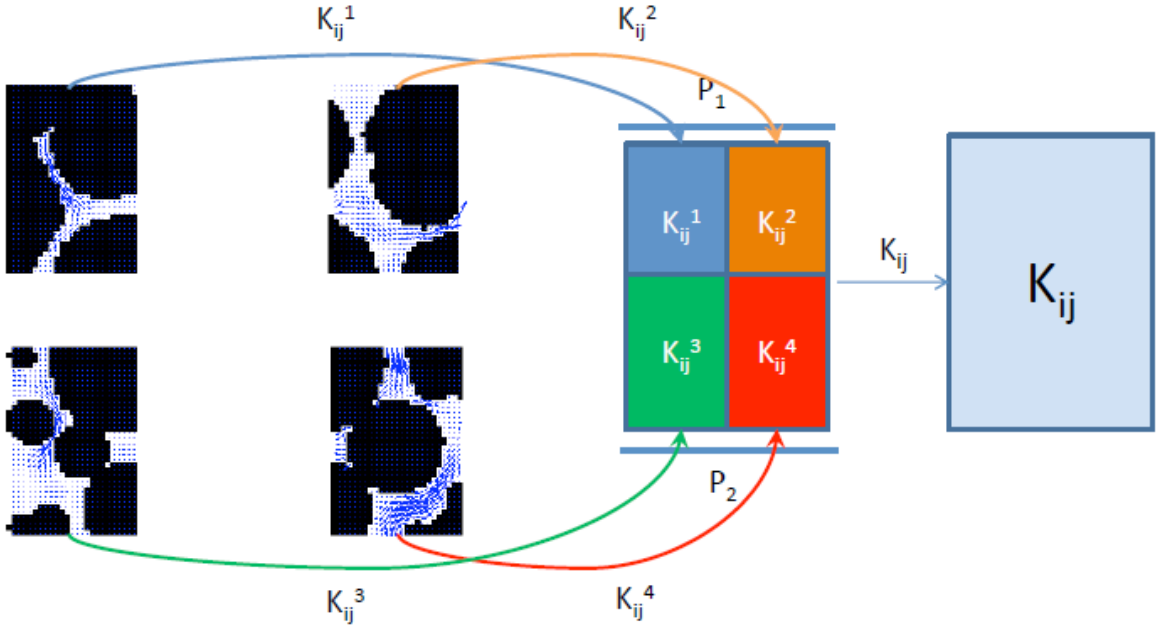

$$f_i(\mathbf{x}+\mathbf{e}_i, t+\Delta t) - f_i(\mathbf{x}, t) = -\frac{1}{\tau}(f_i(\mathbf{x}, t) - f_i^{\mathrm{eq}}(\mathbf{x}, t)),$$

$$f_i^{\mathrm{eq}} = w_i \rho\left(1 + \frac{3\boldsymbol{e}\cdot\boldsymbol{v}}{c^2} + \frac{9(\boldsymbol{e}\cdot\boldsymbol{v})^2}{2c^4} - \frac{3(\boldsymbol{v})^2}{2c^2}\right)$$

$$\boldsymbol{v} = \frac{1}{\rho}\sum_{i=1}^{\alpha} f_i \boldsymbol{e}_i, \quad p = c^2\rho, \quad \rho = \sum_{i=1}^{\alpha} f_i$$

$$\nabla^{\boldsymbol{x}} \cdot \boldsymbol{v}(\boldsymbol{x}) = 0$$

$$\boldsymbol{v}(\boldsymbol{x}) = -\frac{1}{\mu^v}\boldsymbol{k}(\boldsymbol{x}) \cdot \nabla^{\boldsymbol{x}} p(\boldsymbol{x})$$

See W.C Sun, J.E. Andrade, J.W. Rudnicki, A multiscale method for characterization of porous microstructures and their impact on macroscopic effective permeability, *International Journal of Numerical Methods in Engineering*, Vol. 88, No.12, 1260-1279, 2011.

Geometrical Changes of Pore Space Induced By Dilation Inside Shear Band

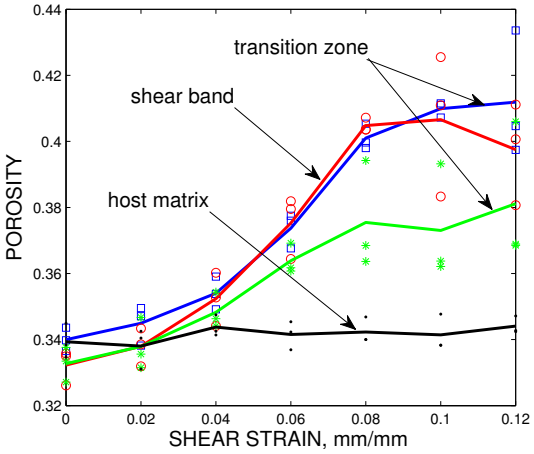

(a) Porosity

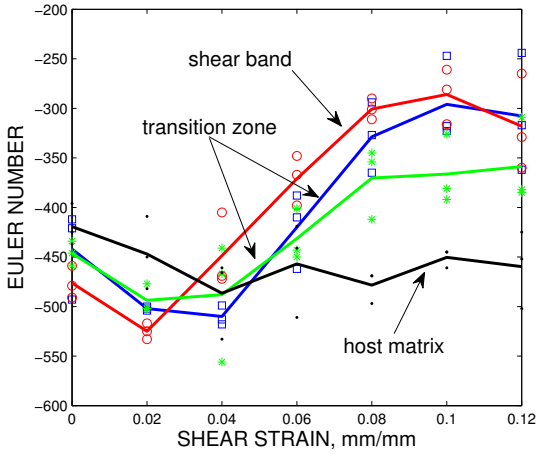

(b) Euler number

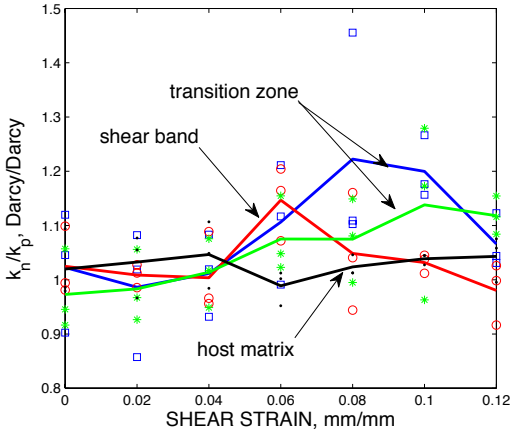

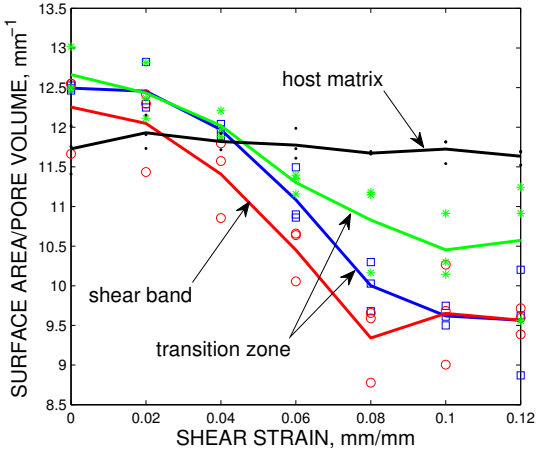

(c) Surface area/pore volume

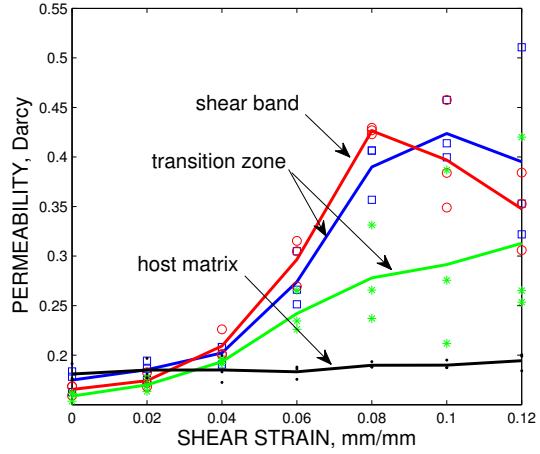

(d) Permeability

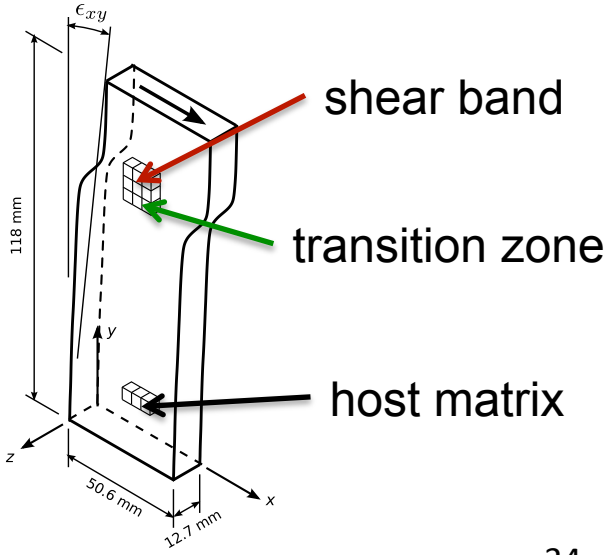

Locating Medial Axis of Flow Path via Level Set

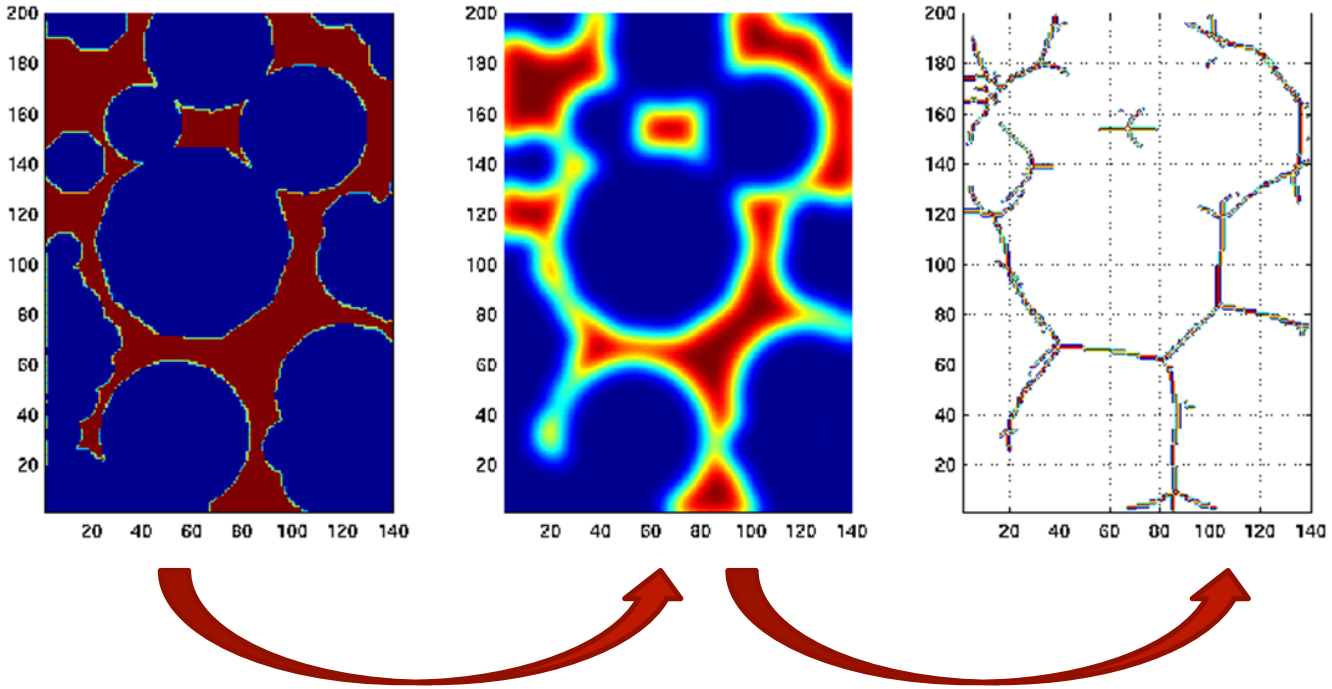

Convert binary image into level set via semi-implicit scheme

Extract Local minimum of level set function

See W.C Sun, J.E. Andrade, J.W. Rudnicki, A multiscale method for characterization of porous microstructures and their impact on macroscopic effective permeability, *International Journal of Numerical Methods in Engineering*, Vol. 88, No.12, 1260-1279, 2011.

Pore Network and Weighed Graph

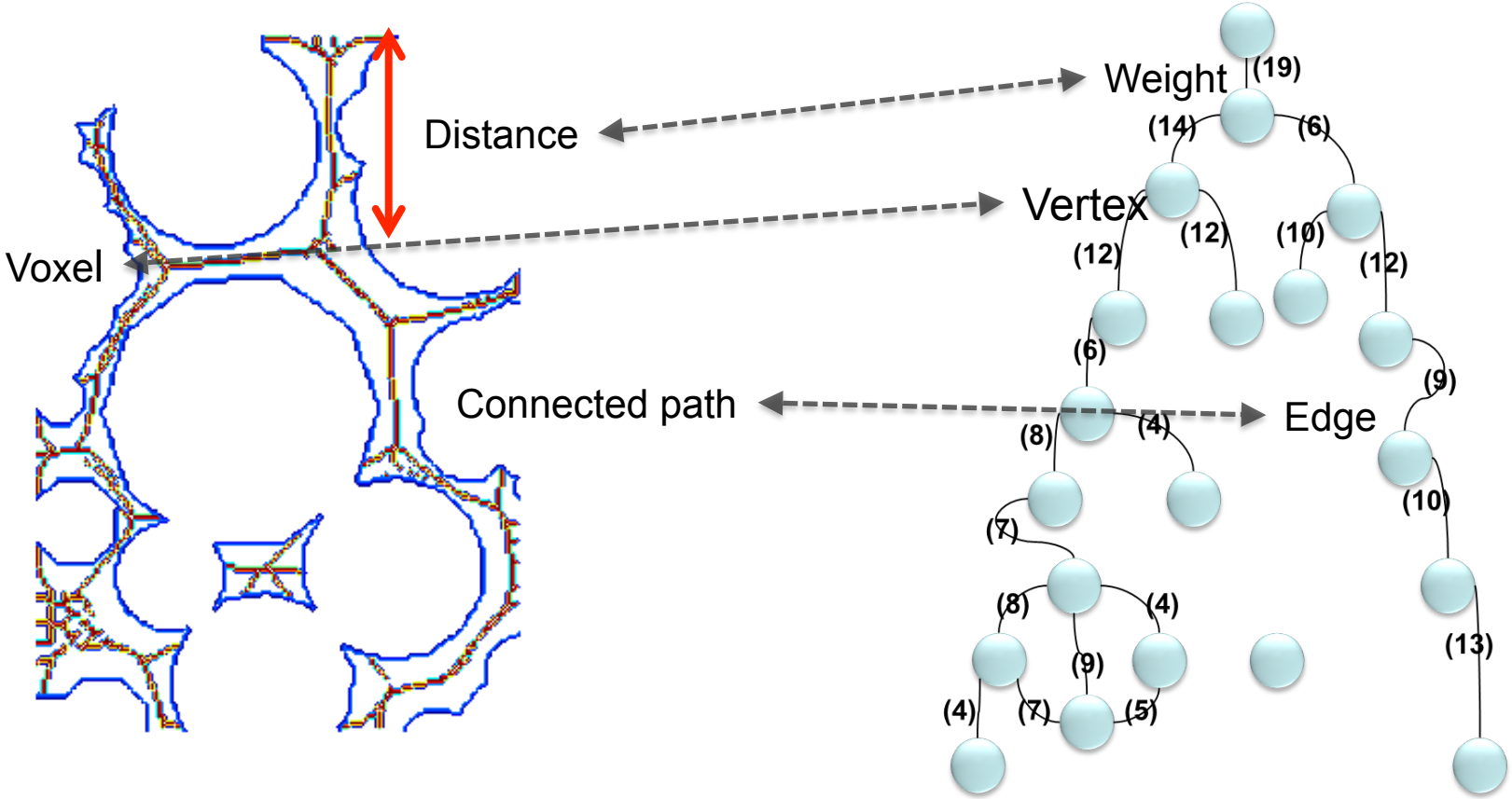

1. Use shortest path algorithm to determine tortuosity.
2. Use region growing method to distinguish connected and isolated pore space.

See W.C Sun, J.E. Andrade, J.W. Rudnicki, A multiscale method for characterization of porous microstructures and their impact on macroscopic effective permeability, *International Journal of Numerical Methods in Engineering*, Vol. 88, No.12, 1260-1279, 2011.

Shortest Flow Path Inside and Outside Compaction Bands (Aztec Sandstone)

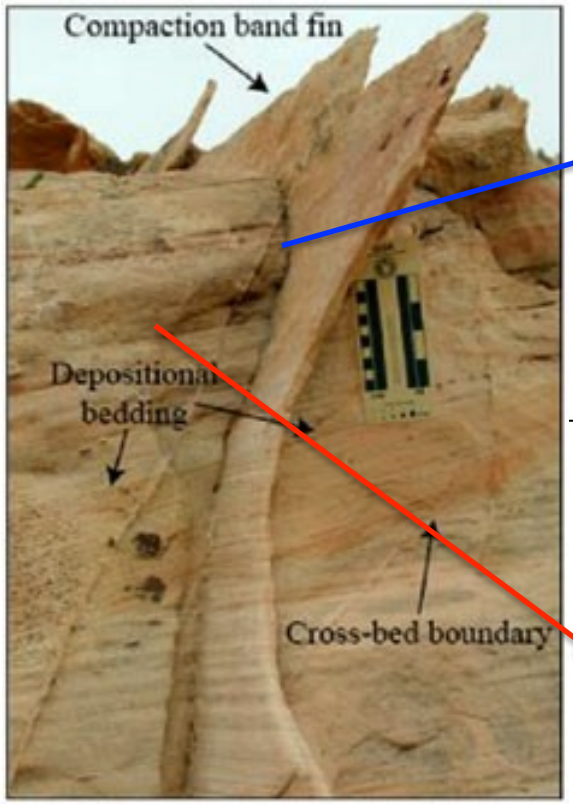

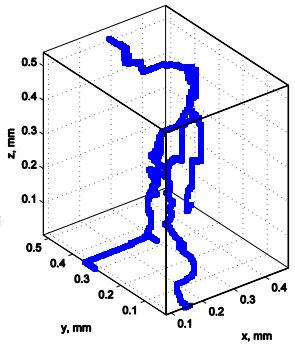

τ= 2.79
K= 3.4e-13 m^2

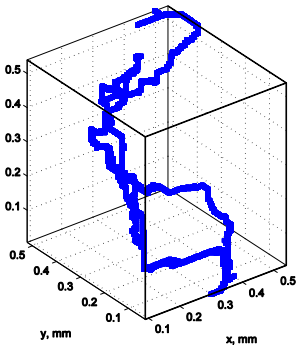

τ= 2.15
K= 5.3e-13 m^2

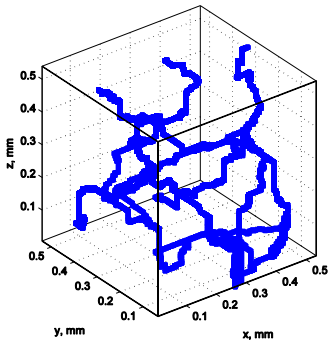

τ= 2.56
K= 4.4e-13 m^2

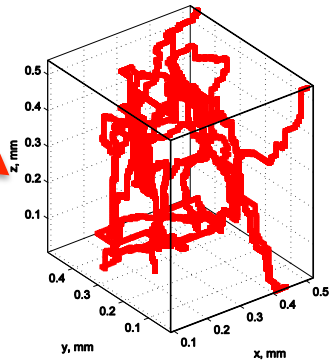

τ= 1.77
K= 1.3e-12 m^2

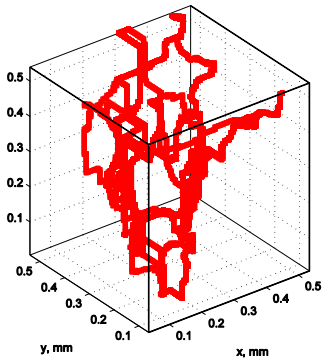

τ= 1.76
K= 1.2e-12 m^2

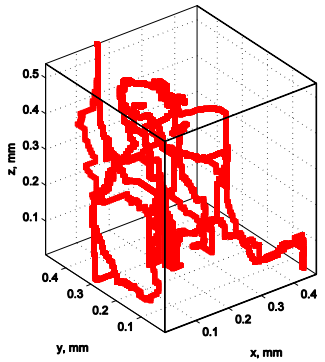

τ= 1.81
K= 1.3e-12 m^2

Occluded and Connected Pore Space in Shear Enhanced Compaction Bands

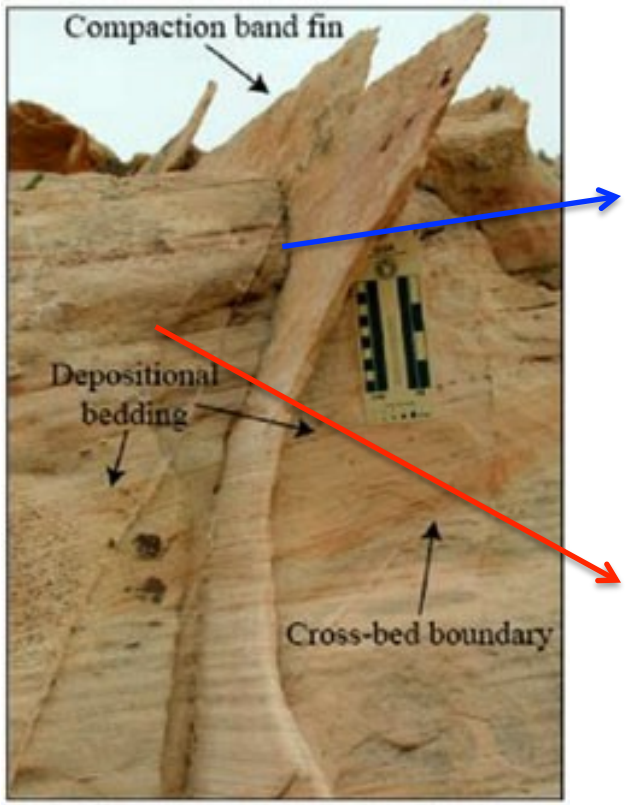

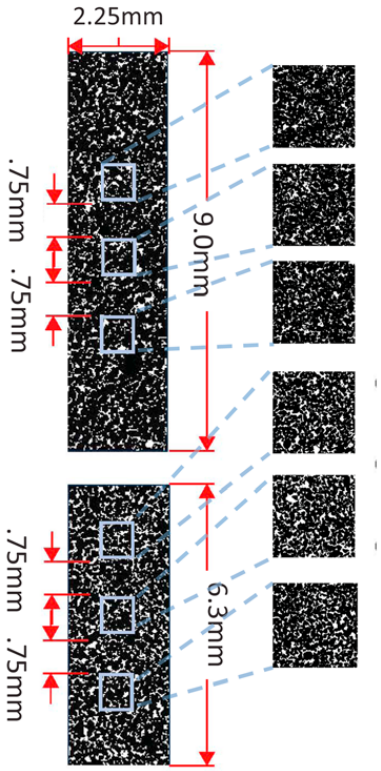

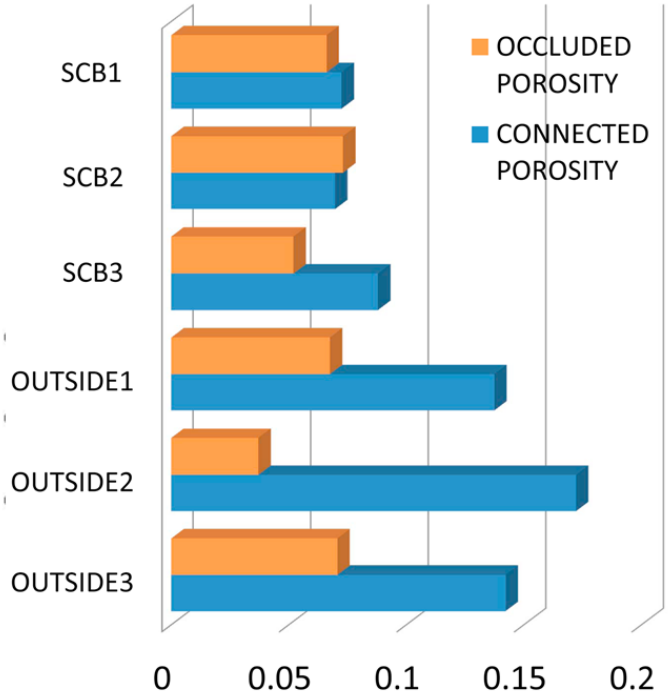

See W.C. Sun, J.W. Rudnicki, J.E. Andrade and P. Eichhubl, Connecting microstructural attributes and permeability from 3-D tomographic images of in situ compaction bands using multi-scale computation, *Geophysical Research Letter*, doi : 10.1029/2011GL047683, 2011.

Conclusion

Sandia National Laboratories

1. Multiscale geometrical analysis and flow simulation indicates that increased tortuosity, isolated pore space and reduction in porosity leads to the permeability reduction in compaction band in Aztec sandstone specimen.

2. Discrete element simulations suggest that increased porosity, more interconnected pore space (as indicated by the increased Euler number), and less tortuous flow paths (as indicated by the decrease in surface area/volume) leads to the permeability increase inside dilatant shear band

Concurrent Domain Coupling Method

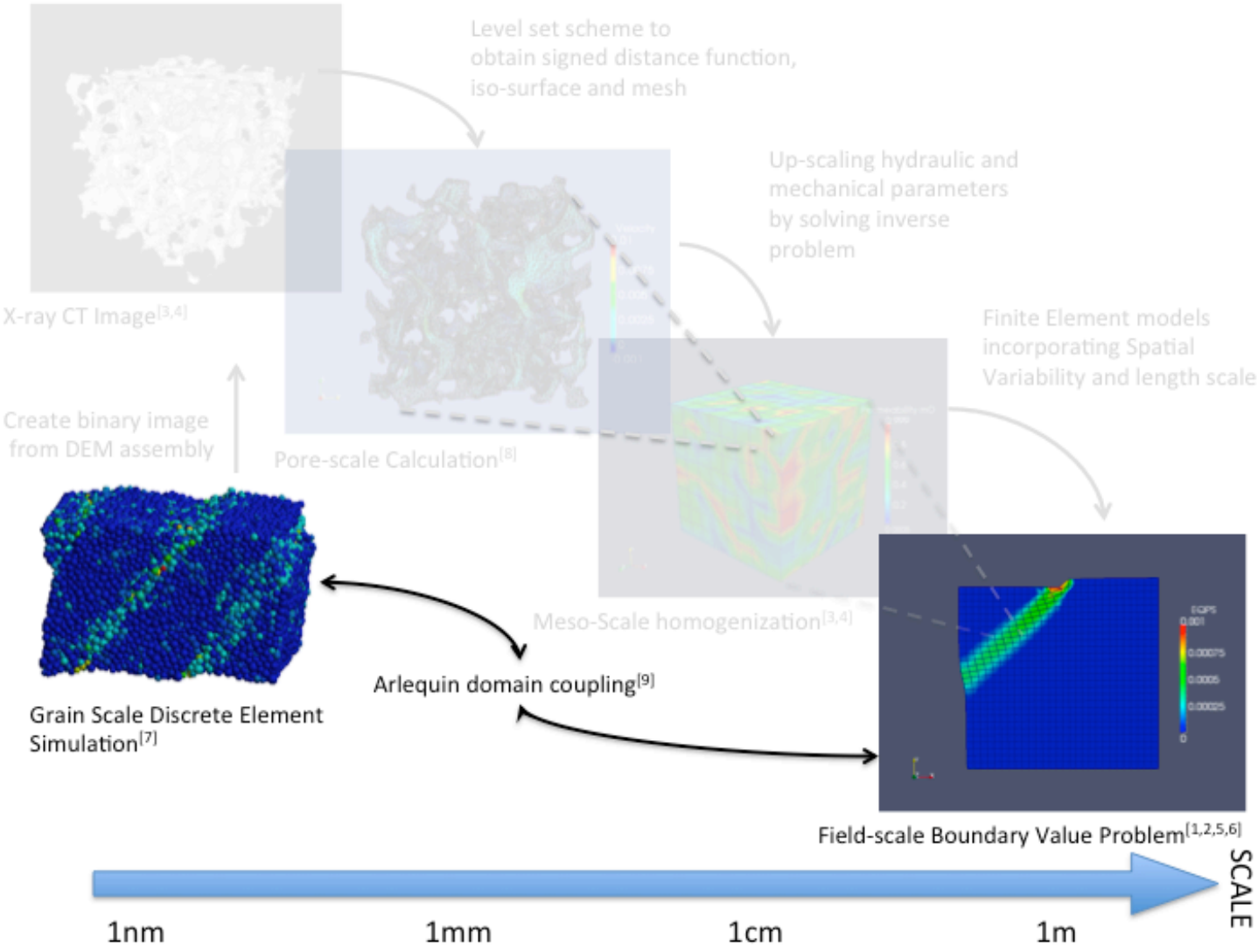

Overview of Domain overlapped method

- Background
  - Concurrently using different numerical methods/models designed for different scales
  - Very flexible : not limited to the type of material models (e.g. can coupled multiple model with different set of internal variables, multiple meshes)
- New Contribution
  1. Extension to large deformation problems (completed) and multiphysics problems (work-in-progress).
  2. Introduce coupling between local and nonlocal constitutive laws
  3. Introduce inf-sup tests to analyze stability of the energy blending domain overlapped method

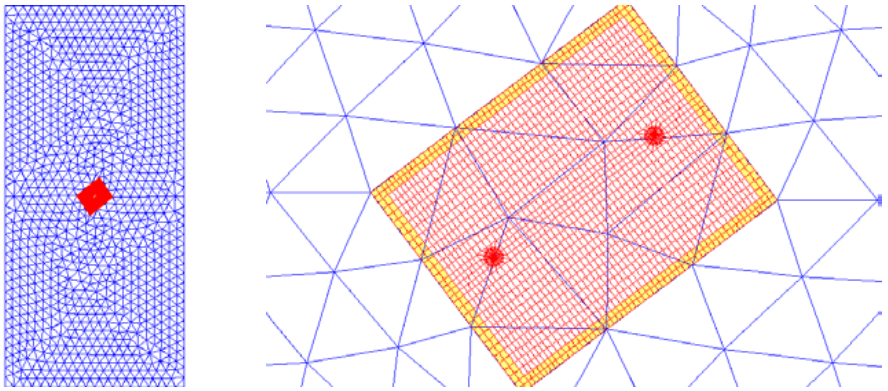

Figure from Hachmi Ben Dhia

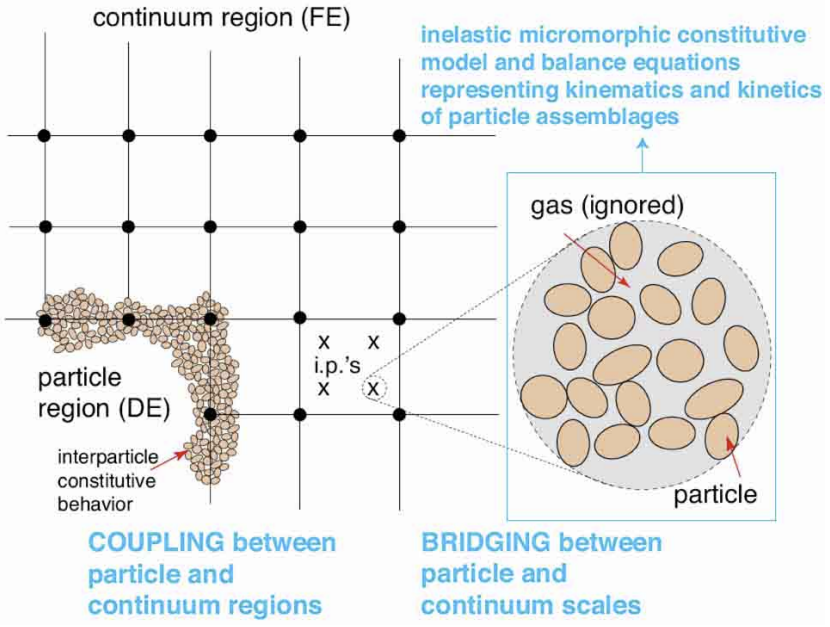

Figure from Richard A. Regueiro

Challenge

Surface Coupling

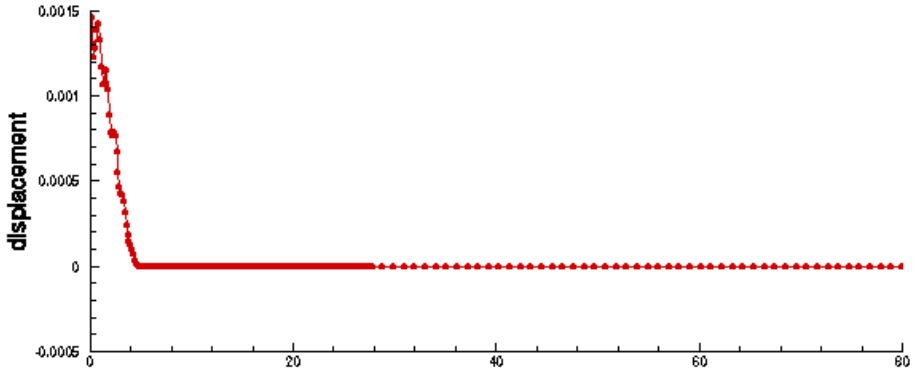

Domain Coupling

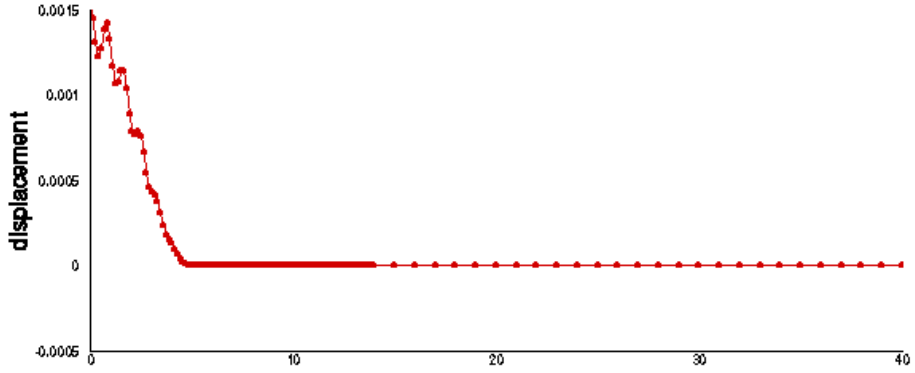

From Prof. Belytschko's webpage

Energy Partition – Method to Describe One Mechanical Response in One domain with Multiple Energy Functionals

Sandia National Laboratories

Partitioned Incremental Energy Functional

$$\Phi[\overline{\boldsymbol{\varphi}}, \widetilde{\boldsymbol{\varphi}}, \boldsymbol{\phi}] = \Phi^{\text{int}}[\overline{\boldsymbol{\varphi}}, \widetilde{\boldsymbol{\varphi}}] - \Phi^{\text{ext}}[\overline{\boldsymbol{\varphi}}, \widetilde{\boldsymbol{\varphi}}] + \Lambda[\overline{\boldsymbol{\varphi}}, \widetilde{\boldsymbol{\varphi}}, \boldsymbol{\phi}]$$

Partitioned internal energy | Partitioned external energy | Compatibility constraint energy

Partition of Unity for energy functional

$$\alpha(\boldsymbol{X}) = \beta(\boldsymbol{X}) = \begin{cases} 1 & \boldsymbol{X} \in \overline{\mathcal{B}} \setminus \mathcal{B}^c \\ 0 & \boldsymbol{X} \in \widetilde{\mathcal{B}} \setminus \mathcal{B}^c \end{cases}$$

$$\Phi^{\text{int}}[\overline{\boldsymbol{\varphi}}, \widetilde{\boldsymbol{\varphi}}] = \int_{\mathcal{B}} \alpha \overline{W}(\overline{\boldsymbol{F}}, \overline{\boldsymbol{Z}}) + (1-\alpha)\widetilde{W}(\widetilde{\boldsymbol{F}}, \widetilde{\boldsymbol{Z}})\, dV$$

$$\Phi^{\text{ext}}[\overline{\boldsymbol{\varphi}}, \widetilde{\boldsymbol{\varphi}}] = \int_{\mathcal{B}} \beta \overline{\boldsymbol{B}} \cdot \overline{\boldsymbol{\varphi}} + (1-\beta)\widetilde{\boldsymbol{B}} \cdot \widetilde{\boldsymbol{\varphi}} dV + \int_{\partial_T \mathcal{B}} \beta \overline{\boldsymbol{T}} \cdot \overline{\boldsymbol{\varphi}}\, dS + \int_{\partial_T \mathcal{B}} (1-\beta)\widetilde{\boldsymbol{T}} \cdot \widetilde{\boldsymbol{\varphi}}\, dS$$

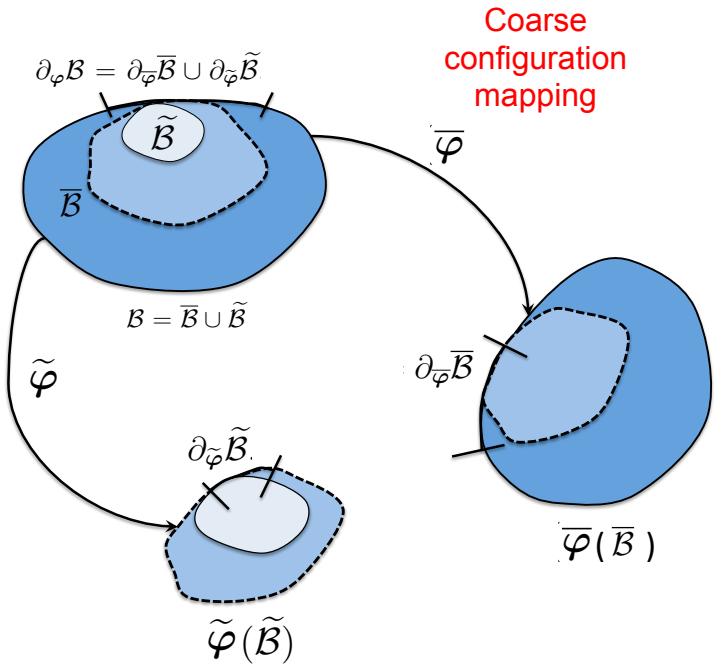

Partitioned Domains with overlapping region(s)

$$\Lambda[\overline{\boldsymbol{\varphi}}, \widetilde{\boldsymbol{\varphi}}, \boldsymbol{\phi}] = \int_{\mathcal{B}^c} \boldsymbol{\phi} \cdot (\overline{\boldsymbol{\varphi}} - \widetilde{\boldsymbol{\varphi}}) + \kappa l^2 \operatorname{Grad} \overline{\boldsymbol{\phi}} : (\operatorname{Grad} \overline{\boldsymbol{\varphi}} - \operatorname{Grad} \widetilde{\boldsymbol{\varphi}})\, dV$$

Minimizing displacement difference

Minimizing displacement gradient difference

Linearization System of Equations

- Incremental governing equation in matrix form

1. Tangent matrix not being positive definite
2. may have severe oscillation problems

$$\begin{bmatrix} \overline{\boldsymbol{K}}_{ab} & \boldsymbol{0}_{a\beta} & \overline{\boldsymbol{C}}_{ab} \\ \boldsymbol{0}_{b\alpha} & \widetilde{\boldsymbol{K}}_{\alpha\beta} & -\widetilde{\boldsymbol{C}}_{\alpha b} \\ \overline{\boldsymbol{C}}_{ba} & -\widetilde{\boldsymbol{C}}_{\beta a} & \boldsymbol{0}_{ab} \end{bmatrix} \begin{bmatrix} \Delta\overline{\boldsymbol{\varphi}}_b \\ \Delta\widetilde{\boldsymbol{\varphi}}_\beta \\ \Delta\boldsymbol{\phi}_b \end{bmatrix} = \begin{bmatrix} \overline{\boldsymbol{F}}_a \\ \widetilde{\boldsymbol{F}}_\alpha \\ \boldsymbol{0}_a \end{bmatrix}$$

- Tangent for implicit integration

Weighted coarse scale tangential stiffness matrix

$$\overline{\boldsymbol{K}}_{ab} := \int_{\mathcal{B}} \operatorname{Grad} N_a : \alpha\overline{\mathbb{C}} : \operatorname{Grad} N_b \; dV$$

Weighted fine scale tangential stiffness matrix

$$\widetilde{\boldsymbol{K}}_{\alpha\beta} := \int_{\mathcal{B}} \operatorname{Grad} N_\alpha : (1-\alpha)\widetilde{\mathbb{C}} : \operatorname{Grad} N_\beta \; dV$$

Coarse Coupling term

$$\overline{\boldsymbol{C}}_{ab} := \overline{\boldsymbol{C}}_{ba} = \int_{\mathcal{B}^c} N_a N_b \cdot + \kappa l^2 \operatorname{Grad} N_a : \operatorname{Grad} N_b \; dV$$

Fine Coupling term

$$\widetilde{\boldsymbol{C}}_{\alpha b} := \int_{\mathcal{B}^c} \lambda_\alpha N_b + \kappa l^2 \operatorname{Grad} \lambda_\alpha : \operatorname{Grad} N_b \; dV$$

L_2 coupling

H^1 coupling

Sandia National Laboratories

Question:

Can we cut cost by only regularizing constitutive law in fine domain?

Yes, if the fine and coarse energy functionals are blended "correctly".

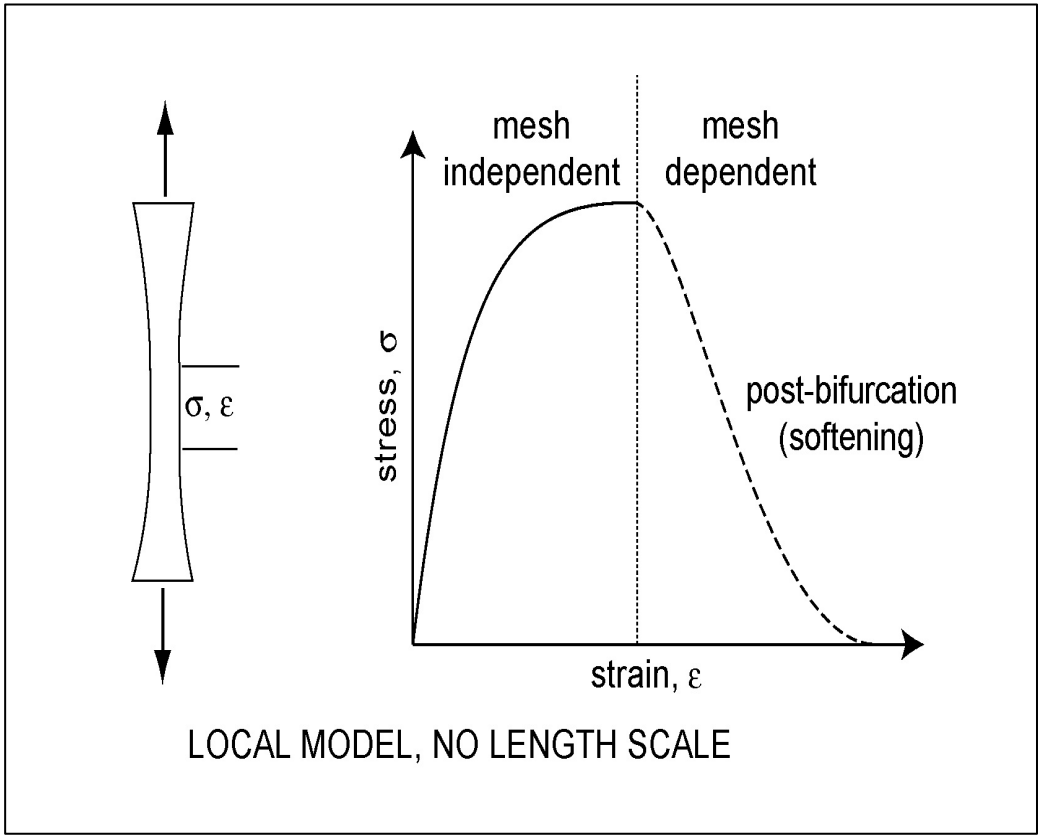

Figure from Bazant and Cedolin, 1991

Singular Bar Example

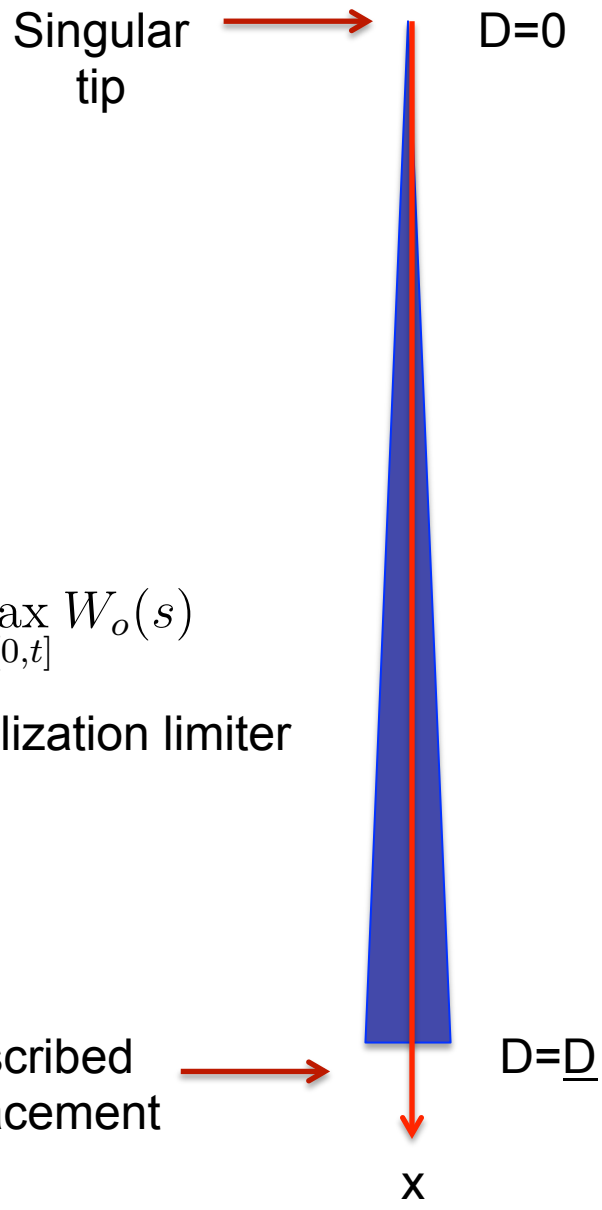

- Path dependent damage model

$$W(\boldsymbol{C},\zeta) = (1-\zeta)W_o(\boldsymbol{C})$$

- One dimensional simplification

$$W_o(\frac{d\varphi}{dX}) = \frac{1}{2}\bar{E}\Big((\frac{d\varphi}{dX})^{-2} + (\frac{d\varphi}{dX})^2 - 2\Big)$$

$$\zeta = \zeta(q) = \zeta_\infty[1-\exp(-q/\varsigma)] \quad q(t) = \max_{s\in[0,t]} W_o(s)$$

- Nonlocal internal variable (damage) as localization limiter

$$\bar{q} = \frac{1}{\mathrm{vol}(D)}\int_D q\ dV = \frac{1}{\mathrm{vol}(D)}\int_{L_D} qA(X)\ dX$$

Responses from Nonlocal/local Continuum Coupled Model

- With DOC method, only a small nonlocal domain is required to regularize the PDE. A large portion of the domain is modeled by simpler, cheaper constitutive law with coarser mesh to cut down computational cost.

Without regularization

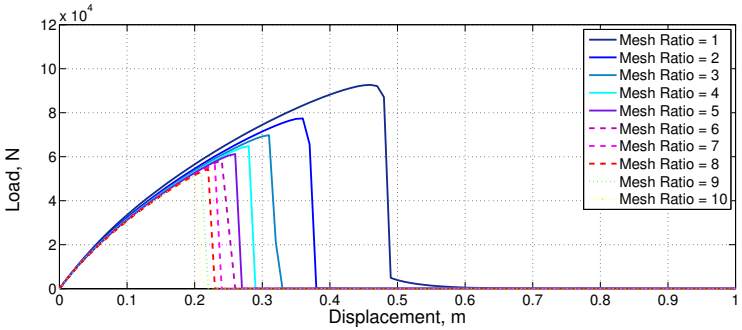

Mesh dependent

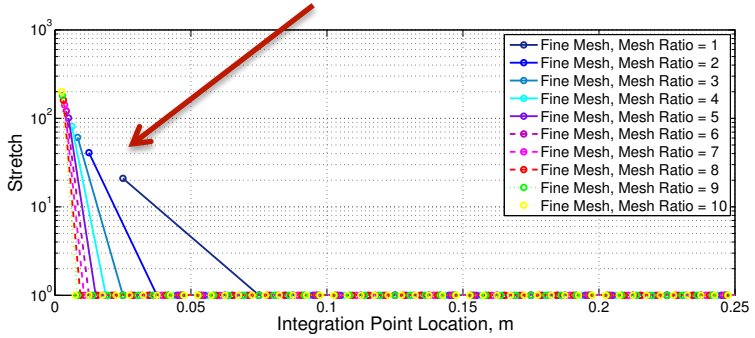

With regularization

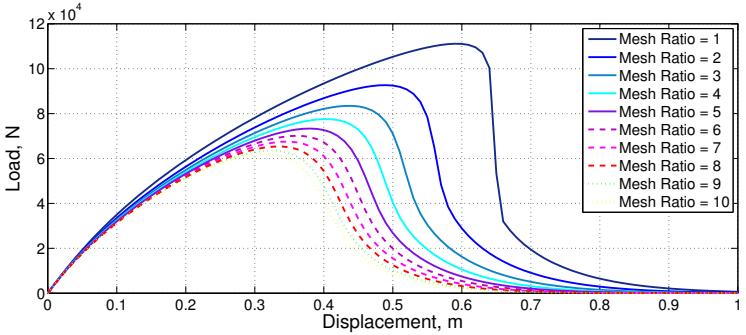

Converged solution

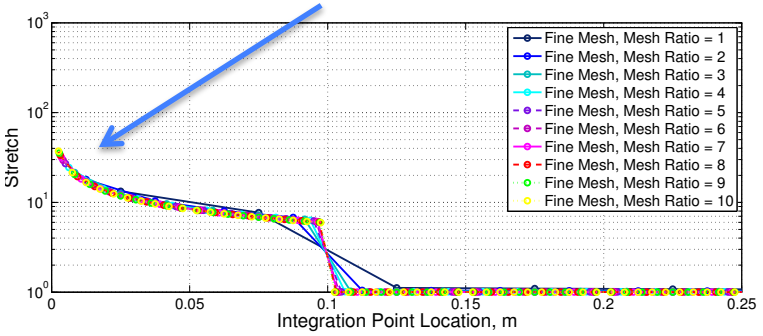

Load-displacement curve

Stretch vs. reference location

Sandia National Laboratories

Question:

Under what circumstance will the coupling method fails?

1D Patch Test (constant weighting function)

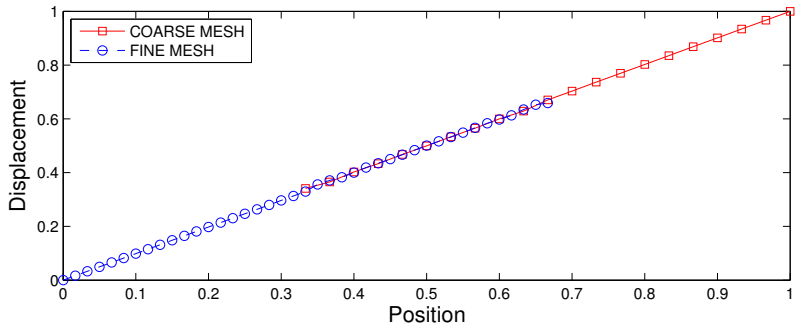

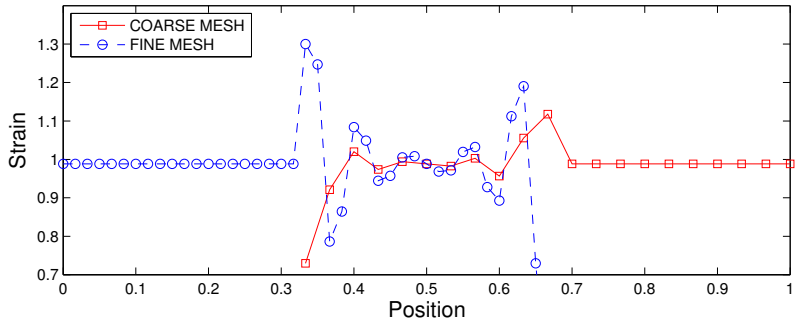

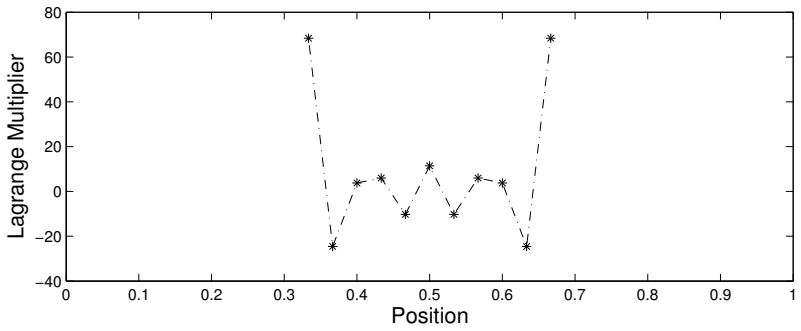

L_2 coupling

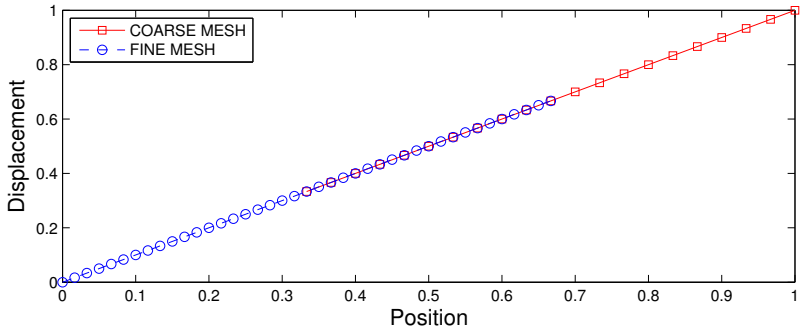

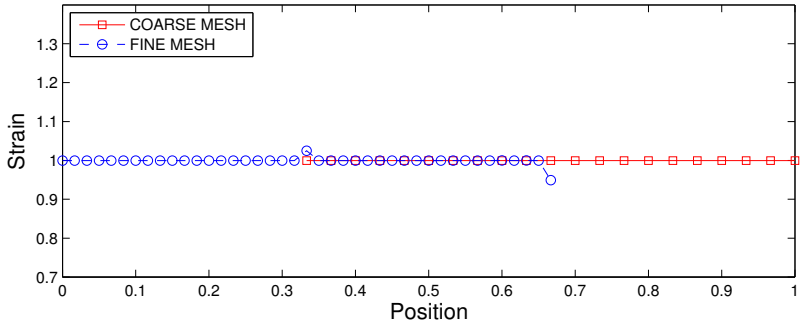

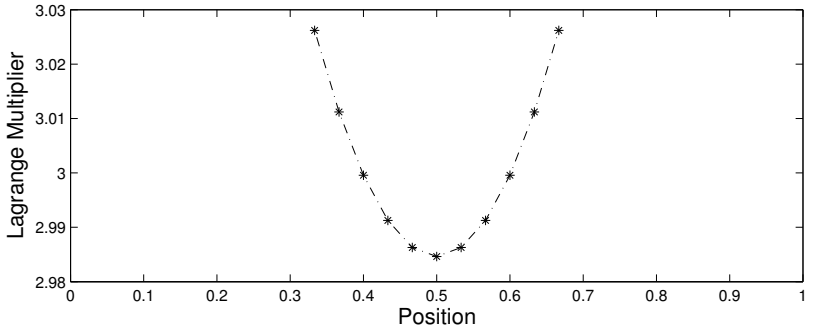

H^1 coupling

1D Patch Test (linear weighting function)

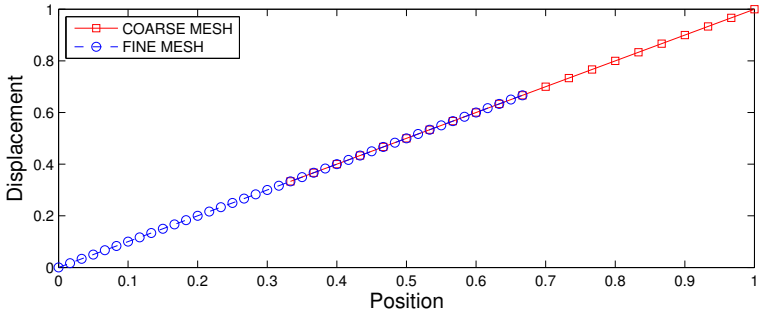

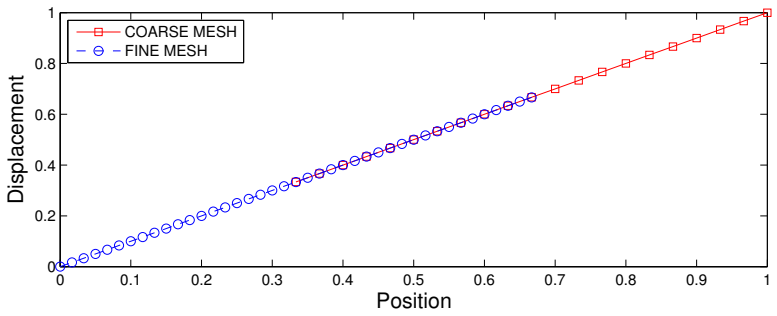

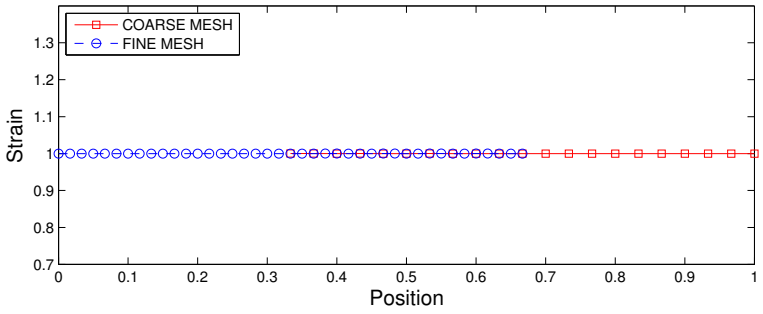

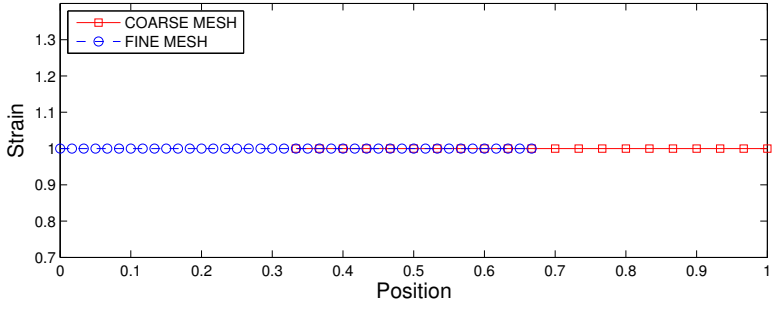

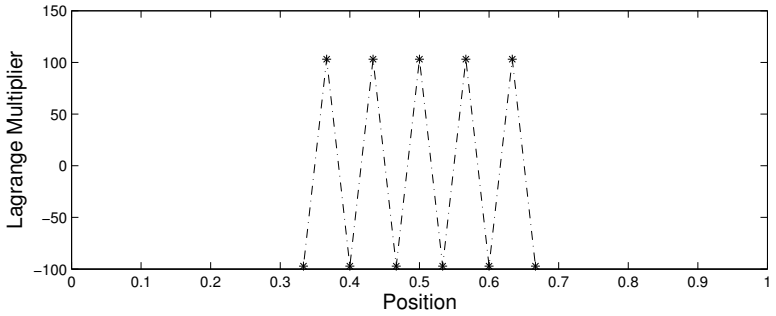

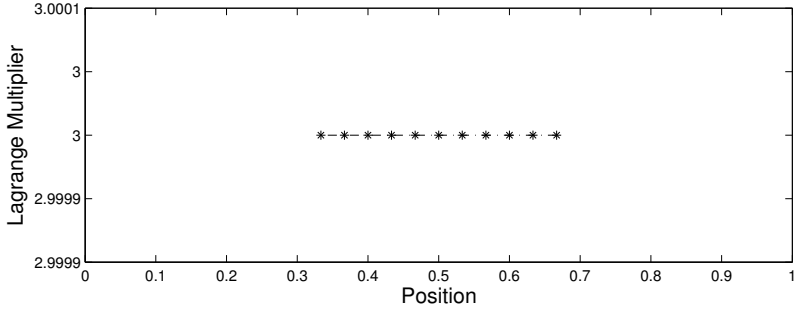

L_2 coupling

H^1 coupling

Sandia National Laboratories

Question:

What are the major factor(s) that leads to stable coupling?

How can we analyze the numerical stability?

Inf-sup Condition

- Static condensation may reduce the three-field equations to two subsystems, each with two solution fields

$$\begin{bmatrix} \overline{\boldsymbol{K}}_{ab} & \boldsymbol{0}_{a\beta} & \overline{\boldsymbol{C}}_{ab} \\ \boldsymbol{0}_{b\alpha} & \widetilde{\boldsymbol{K}}_{\alpha\beta} & -\widetilde{\boldsymbol{C}}_{\alpha b} \\ \overline{\boldsymbol{C}}_{ba} & -\widetilde{\boldsymbol{C}}_{\beta a} & \boldsymbol{0}_{ab} \end{bmatrix} \begin{bmatrix} \Delta\overline{\boldsymbol{\varphi}}_b \\ \Delta\widetilde{\boldsymbol{\varphi}}_\beta \\ \Delta\boldsymbol{\phi}_b \end{bmatrix} = \begin{bmatrix} \overline{\boldsymbol{F}}_a \\ \widetilde{\boldsymbol{F}}_\alpha \\ \boldsymbol{0}_a \end{bmatrix}$$

$$\begin{bmatrix} \widetilde{\boldsymbol{K}}_{\alpha\beta} & -\widetilde{\boldsymbol{C}}_{a\beta} \\ -\widetilde{\boldsymbol{C}}_{\beta a} & \overline{\boldsymbol{C}}_{am}\overline{\boldsymbol{K}}^{-1}_{mn}\overline{\boldsymbol{C}}_{nb} \end{bmatrix} \begin{bmatrix} \Delta\widetilde{\boldsymbol{\varphi}}_\beta \\ \Delta\boldsymbol{\phi}_b \end{bmatrix} = \begin{bmatrix} \widetilde{\boldsymbol{F}}_\alpha \\ -\overline{\boldsymbol{C}}_{am}\overline{\boldsymbol{K}}^{-1}_{mb}\overline{\boldsymbol{F}}_b \end{bmatrix}$$

$$\begin{bmatrix} \overline{\boldsymbol{K}}_{ab} & \overline{\boldsymbol{C}}_{ab} \\ \overline{\boldsymbol{C}}_{ba} & \widetilde{\boldsymbol{C}}_{a\alpha}\widetilde{\boldsymbol{K}}^{-1}_{\alpha\beta}\widetilde{\boldsymbol{C}}_{\beta b} \end{bmatrix} \begin{bmatrix} \Delta\overline{\boldsymbol{\varphi}}_b \\ \Delta\boldsymbol{\phi}_b \end{bmatrix} = \begin{bmatrix} \overline{\boldsymbol{F}}_a \\ \widetilde{\boldsymbol{C}}_{a\alpha}\widetilde{\boldsymbol{K}}^{-1}_{\alpha\beta}\widetilde{\boldsymbol{F}}_\beta \end{bmatrix}$$

- Inf-sup Condition can be used to test whether the spaces for the displacement increment and Lagrange multiplier are chosen correctly.

$$\inf_{\boldsymbol{\eta}\in V}\sup_{\overline{\boldsymbol{\xi}}\in\overline{U}} \frac{\int_{\mathcal{B}^c} \boldsymbol{\eta}\cdot\overline{\boldsymbol{\xi}} + \kappa l^2 \operatorname{Grad}\boldsymbol{\eta} : \operatorname{Grad}\overline{\boldsymbol{\xi}}\; dV}{||\overline{\boldsymbol{\xi}}||_{\overline{U}}||\boldsymbol{\eta}||_V} \geq \beta > 0$$

$$\inf_{\boldsymbol{\eta}\in V}\sup_{\widetilde{\boldsymbol{\xi}}\in\widetilde{U}} \frac{\int_{\mathcal{B}^c} \boldsymbol{\eta}\cdot\widetilde{\boldsymbol{\xi}} + \kappa l^2 \operatorname{Grad}\boldsymbol{\eta} : \operatorname{Grad}\widetilde{\boldsymbol{\xi}}\; dV}{||\widetilde{\boldsymbol{\xi}}||_{\widetilde{U}}||\boldsymbol{\eta}||_V} \geq \gamma > 0$$

Discrete Inf-sup Condition in Euclidean Space

- We can construct a one-to-one mapping from the function space to the Euclidean spaces such that the inf-sup condition (and the lack of) can be checked algebraically

$$\overline{\boldsymbol{v}} \equiv (\overline{v}_1, \overline{v}_2, ...\overline{v}_{N_{\overline{U}}}) \leftrightarrow \sum_{a=1}^{N_{\overline{U}}} \overline{v}_a N_a$$

$$\widetilde{\boldsymbol{v}} \equiv (\widetilde{v}_1, \widetilde{v}_2, ...\widetilde{v}_{N_{\widetilde{U}}}) \leftrightarrow \sum_{\alpha=1}^{N_{\widetilde{U}}} \widetilde{v}_\alpha \lambda_\alpha$$

$$\boldsymbol{\theta} \equiv (\theta_1, \overline{\theta}_{12}, ...\overline{\theta}_{N_V}) \leftrightarrow \sum_{a=1}^{N_V} \theta_a N_a$$

$$\inf_{\boldsymbol{\theta}\in\mathbb{R}^{N_V}} \sup_{\overline{v}\neq\mathbf{0}} \frac{\boldsymbol{\theta}_a \overline{\boldsymbol{C}}_{ab} \overline{\boldsymbol{v}}_b}{\left(\boldsymbol{\theta}_m \overline{\boldsymbol{Q}}_{mn} \boldsymbol{\theta}_n\right)^{1/2} \left(\overline{\boldsymbol{v}}_r \overline{\boldsymbol{K}}_{rs} \overline{\boldsymbol{v}}_s\right)^{1/2}} \geq \beta > 0$$

$$\inf_{\boldsymbol{\theta}\in\mathbb{R}^{N_V}} \sup_{\widetilde{v}\neq\mathbf{0}} \frac{\boldsymbol{\theta}_a \widetilde{\boldsymbol{C}}_{ab} \widetilde{\boldsymbol{v}}_b}{\left(\boldsymbol{\theta}_m \overline{\boldsymbol{Q}}_{mn} \boldsymbol{\theta}_n\right)^{1/2} \left(\widetilde{\boldsymbol{v}}_r \widetilde{\boldsymbol{K}}_{rs} \widetilde{\boldsymbol{v}}_s\right)^{1/2}} \geq \gamma > 0$$

$$(\overline{\boldsymbol{C}}_{am} \overline{\boldsymbol{K}}^{-1}_{mn} \overline{C}_{nb} - \overline{\lambda \boldsymbol{Q}}_{ab}) \boldsymbol{\theta}_b = \mathbf{0}$$

$$(\widetilde{\boldsymbol{C}}_{a\alpha} \widetilde{\boldsymbol{K}}^{-1}_{\alpha\beta} \widetilde{\boldsymbol{C}}_{\beta b} - \widetilde{\lambda} \overline{Q}_{ab}) \boldsymbol{\theta}_b = \mathbf{0}$$

Now, inf-sup condition is guaranteed if the smallest eigenvalue is larger than 0!

Inf-sup Tests on Foulk's Singular Bar (2008)

Sandia National Laboratories

Inf-sup Test 1

$$(\overline{\boldsymbol{C}}_{am}\overline{\boldsymbol{K}}^{-1}_{mn}\overline{C}_{nb} - \overline{\lambda\boldsymbol{Q}}_{ab})\boldsymbol{\theta}_b = \boldsymbol{0}$$

which is corresponding to

$$\begin{bmatrix} \overline{\boldsymbol{K}}_{ab} & \overline{\boldsymbol{C}}_{ab} \\ \overline{\boldsymbol{C}}_{ba} & \boldsymbol{C}'_{a\alpha}\boldsymbol{K}'^{-1}_{\alpha\beta}\boldsymbol{C}'_{\beta b} \end{bmatrix} \begin{bmatrix} \Delta\overline{\boldsymbol{\varphi}}_b \\ \Delta\boldsymbol{\phi}_b \end{bmatrix} = \begin{bmatrix} \overline{\boldsymbol{F}}_a \\ \boldsymbol{C}'_{a\alpha}\boldsymbol{K}'^{-1}_{\alpha\beta}\boldsymbol{F}'_{\beta} \end{bmatrix}$$

H1 Coupling

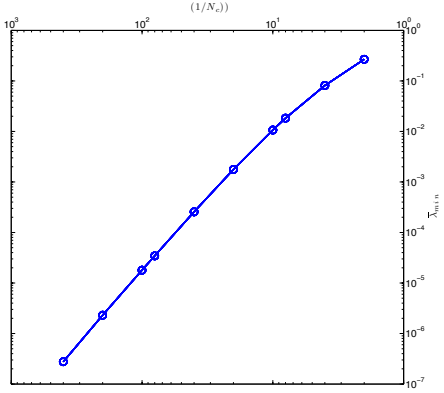

Inf-sup value = [10^{-7}, 1]

L2 Coupling

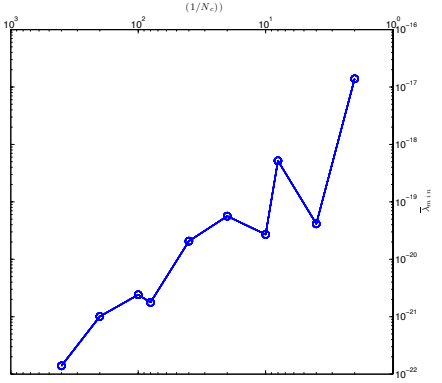

Inf-sup value = [10^{-16}, 10^{-22}]

Inf-sup Test 2

$$(\boldsymbol{C}'_{a\alpha}\boldsymbol{K}'^{-1}_{\alpha\beta}\boldsymbol{C}'_{\beta b} - \lambda'\overline{Q}_{ab})\boldsymbol{\theta}_b = \boldsymbol{0}$$

which is corresponding to

$$\begin{bmatrix} \boldsymbol{K}'_{\alpha\beta} & -\boldsymbol{C}'_{a\beta} \\ -\boldsymbol{C}'_{\beta a} & \overline{\boldsymbol{C}}_{am}\overline{\boldsymbol{K}}^{-1}_{mn}\overline{\boldsymbol{C}}_{nb} \end{bmatrix} \begin{bmatrix} \Delta\boldsymbol{\varphi}'_{\beta} \\ \Delta\boldsymbol{\phi}_b \end{bmatrix} = \begin{bmatrix} \boldsymbol{F}'_{\alpha} \\ -\overline{\boldsymbol{C}}_{am}\overline{\boldsymbol{K}}^{-1}_{mb}\overline{\boldsymbol{F}}_b \end{bmatrix}$$

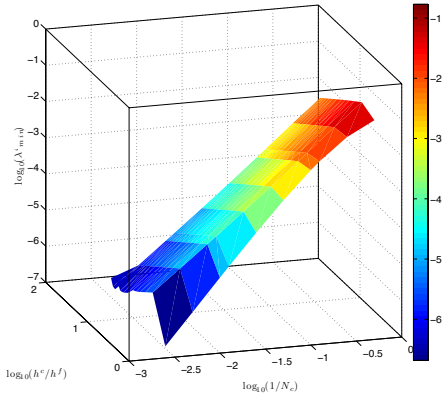

Inf-sup value = [10^{-7}, 1]

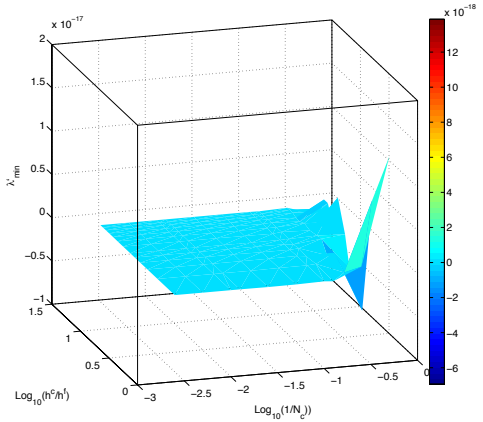

Inf-sup value = [10^{-18}, 10^{-17}]

Notice that the inf-sup values of both tests are very small for L2 coupling!

Conclusions

Sandia National Laboratories

1. If coarse and fine meshes are conformal, then no search algorithm is needed and hence the implementation becomes much simpler.
2. Numerical study demonstrates that H1 coupling eliminates spurious pattern exhibiting in L2 coupling. This finding is consistent with the inf-sup condition.
3. Localization limiter can be used in a small domain via DOC coupling to enhance computational efficiency.
4. Numerical examples seem to suggest that a more even partition (e.g. half and half) or higher order weighted partition in energy leads to more stable and compatible solutions in overlapped domain.

On-going Challenges

Sandia National Laboratories

1. How thermal and pore-fluid diffusion affects mechanical stability, strain localization and fracture process at various temporal scales (e.g. undrained vs. drained, isothermal vs. adiabatic)?
2. How to homogenize or properly take account of the couplings of various physical processes at different spatial scales (e.g. anisotropy of diffusivity induced by deformation, yield surface size changes by heat) ?
3. How to model fully coupled thermo-hydro-mechanical–chemical (THMC) effect (biodegradation, Calcite formation, dissolving solid, fate of fracking water)?
4. Will fluid injection mobilize existing fault systems?
5. Validations of numerical modeling? Comparisons with other THM code, centrifuge models, field studies (In Salah Project)?

Figure from Columbia University

Future Works / Wish List

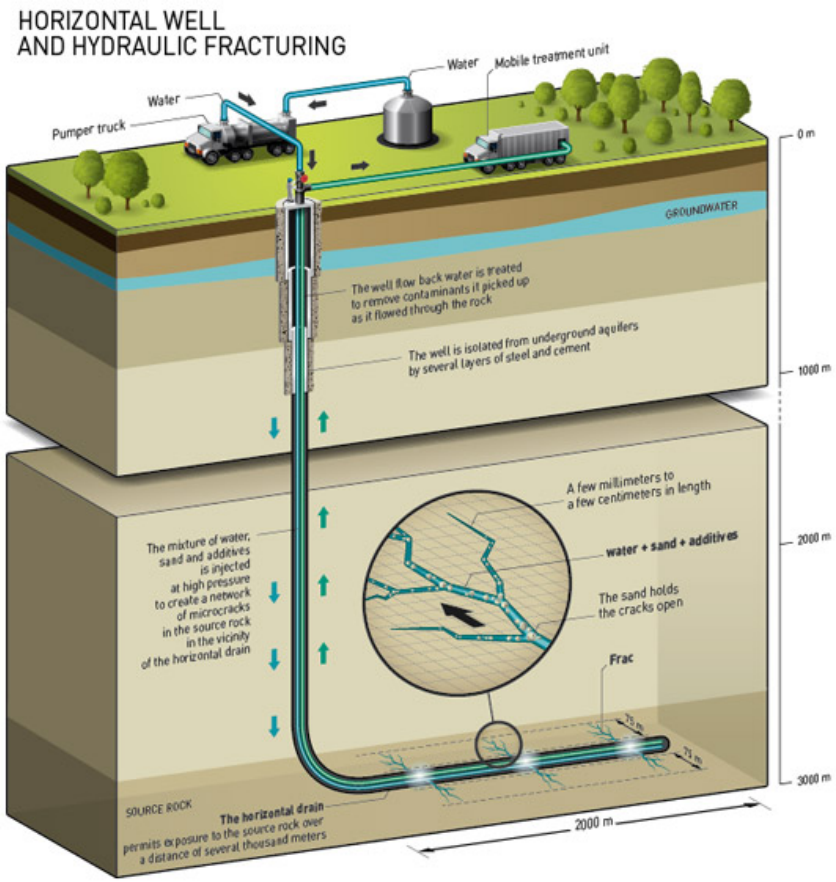

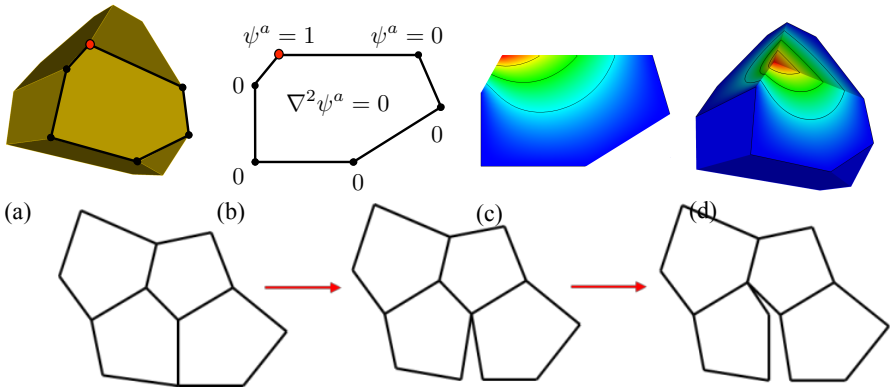

Usage of polyhedral finite element to eliminate mesh bias for fracture process (Bishop, IJNME, 2013)

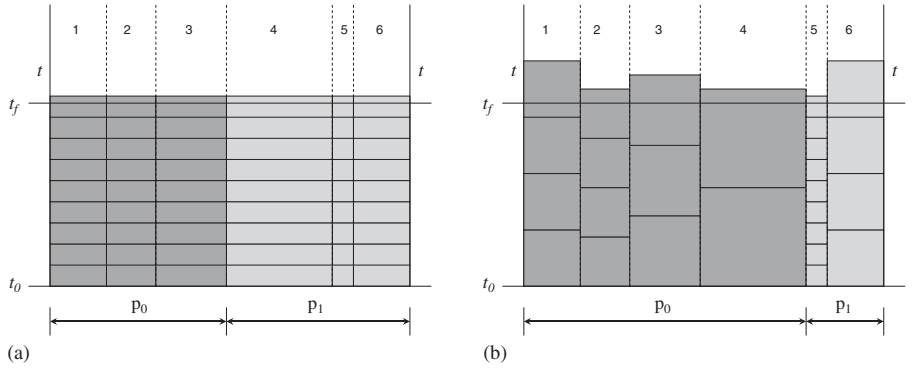

Enabling asynchronous variational integrator for domain coupling methods (Lew, Marsden, Ortiz and West, 2003)

- Hydraulic Fracture
- injection induced seismic event
- Numerical modeling of rainfall instability

Sandia National Laboratories

Thank you for your patience and time!

Bibliography

- **W.C. Sun**, J.T. Ostien and A.G. Salinger, a stabilized enhanced deformation gradient finite element formulation for strongly coupled poromechanical simulations at finite strain, doi:10.1002/nag.2161 *International Journal for Numerical and Analytical Methods in Geomechanics*, 2013.
- J.W. Foulk III, **W.C. Sun**, G. Wagner, C. San Marchi, B. Somerday, the evolution of hydrogen concentration in 21 Cr-6Ni-9Mn austenitic stainless steel, in preparation.
- A. Mota, **W.C. Sun**, J.T. Ostien, J.W. Foulk III and K.N., Long Lie-Group interpolation and variational recovery for internal variables, doi:10.1007/s00466-013-0876-1, *Computational Mechanics*.
- **W.C. Sun**, Y.L. Young, Influence of soil heterogeneity on finite strain sedimentation-consolidation phenomena, submitted to *International Journal for Numerical and Analytical Methods in Geomechanics*.
- **W.C. Sun**, M.R. Kuhn, J.W. Rudnicki, a multiscale DEM-LBM analysis on dilatant shear band, doi:10.1007/s11440-013-0210-2, *Acta geotechnica,* 2013.
- **W.C. Sun**, An unified method to predict diffuse and localized instabilities in sands, *Geomechanics and Geoengineering*, doi:0.1080/17486025.2012.695403, 2012
- **W.C. Sun**, J.W. Rudnicki, J.E. Andrade and P. Eichhubl, Connecting microstructural attributes and permeability from 3-D tomographic images of in situ compaction bands using multi-scale computation, *Geophysical Research Letter*, doi : 10.1029/2011GL047683, 2011.
- **W.C Sun**, J.E. Andrade, J.W. Rudnicki, A multiscale method for characterization of porous microstructures and their impact on macroscopic effective permeability, *International Journal of Numerical Methods in Engineering*, Vol. 88, No.12, 1260-1279, 2011.
- R.I. Borja and **W.C. Sun**, Co-seismic sediment deformation during the 1989 Loma Prieta Earthquake, *Journal of Geophysical Research*, Vol.113, B08314,doi:10.1029/2007JB005265, 2008.
- R.I. Borja and **W.C. Sun**, Estimating inelastic sediment deformation from local site response simulations, *Acta Geotechnica*, Vol. 2, Number 3, 2007, pp.183-195.

Bibliography (Cont')

- **W.C. Sun** and J.E. Andrade, Capturing the effective permeability of field compaction band using hybrid lattice Boltzmann/Finite element simulations, Proceedings of 9th World Congress of Computational Mechanics/APCOM 2010, Sydney, Australia, 2010.
- **W.C. Sun** and J.E. Andrade, Surface Slumping of Submarine Slope And Its Relation To Material Instability, Proceedings of 16th US National Congress on Theoretical and Applied Mechanics, University Park, Pennsylvania, 2010.
- **W.C. Sun** and J.E. Andrade, Diffuse bifurcations of porous media under partially drained conditions, Proceedings of International Workshop on Multiscale and Multiphysics Processes in Geomechanics, Stanford, California, 2010.
- N. Lenoir, J.E. Andrade, **W.C. Sun** and J.W. Rudnicki, In situ permeability measurement inside compaction bands using X-ray CT and lattice Boltzmann calculations, Proceedings of 3th International Workshop on X-ray CT for geomaterials, New Orleans, Louisiana, 2010.
- J.E. Andrade, and **W.C. Sun**, Predictive framework for simulation of instabilities in sands, Jornadas Geotecnicas Colombianas, Bogota, Colombia, 2009.

Sandia National Laboratories

Extra Slides

Hydraulic property changes due to formation of deformation bands

Sandia National Laboratories

Permeability

Compaction Band -flow barrier to fluid flow

Flow barriers trap fluid and improve efficiency of the storage

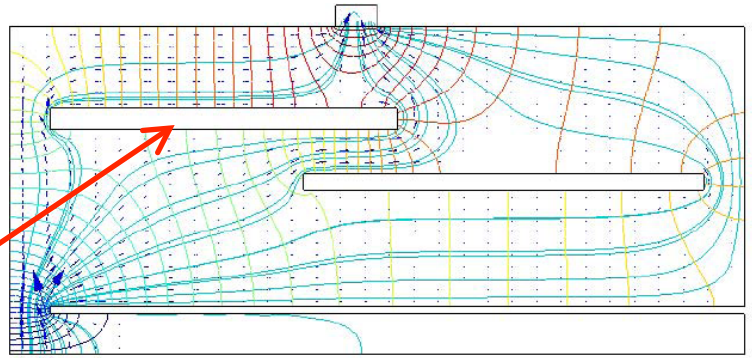

Uniform Compaction

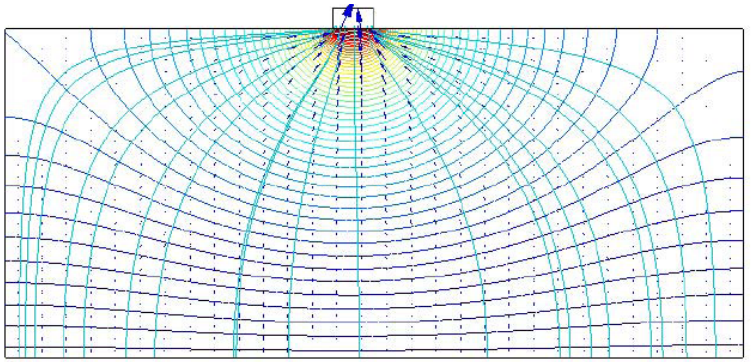

Dilatant Shear Band - flow conduits to fluid flow

Flow conduits may lead to leakage, which could be fatal.

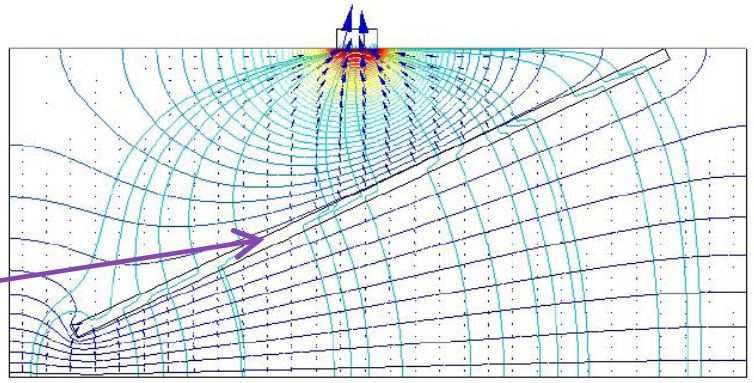

Relation between Level Set Function and Medial Axis

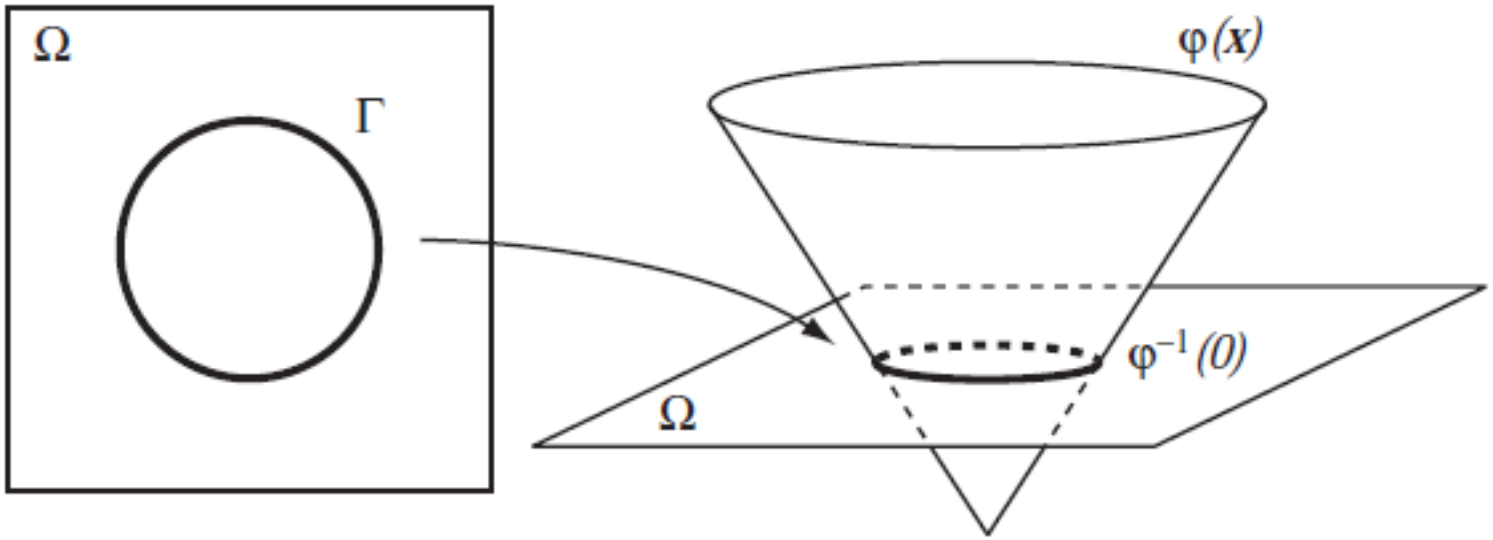

- Local minimum of the signed distance function φ are located at medial axis.
- Use level set scheme to obtain signed distance function

Skeletonization with Level Set

- Action functional (Li et al 2005)

$$\mathcal{E}(\phi) = \mu\mathcal{P}(\phi) + \lambda\mathcal{L}_g(\phi) + \nu\mathcal{A}_g(\phi)$$

Diffusion term to convert level set into signed distance function

- Governing equation

Fix level set value at the boundary

$$\frac{\partial\phi}{\partial t} = \mu[\Delta^x\phi - \nabla^x\cdot(\frac{\nabla^x\phi}{|\nabla^x\phi|})] + \lambda\delta(\phi)\nabla^x\cdot(g\frac{\nabla^x\phi}{|\nabla^x\phi|}) + \nu g\delta(\phi)$$

- Semi-Implicit Finite Difference Scheme

$$\frac{\phi^{n+1}-\phi^n}{t_{n+1}-t_n} = \mu\Delta^c\phi^{n+1} - \mu\nabla^c\cdot\frac{\nabla^c\phi}{||\nabla^c\phi||} + \lambda\delta(\phi^n)\nabla^c\cdot(g\frac{\nabla^c\phi}{||\nabla^c\phi||}) + \nu g\delta(\phi^n)$$

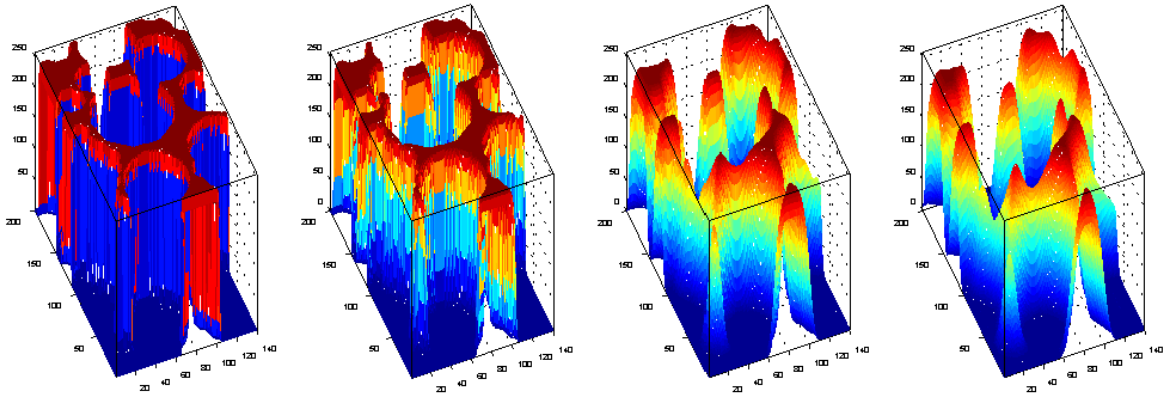

Medial Axis of Flow Paths

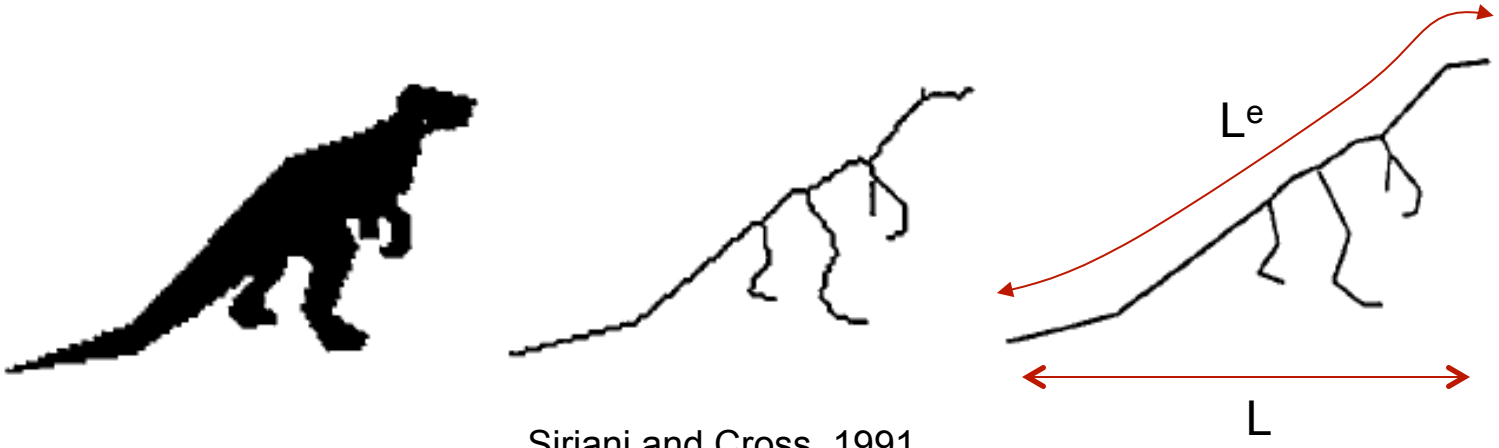

Sirjani and Cross, 1991

- Medial axis is the spine of a volume filling object
- Media axis is a union of curves that represent the topology and geometry of the volume

Locating Medial Axis of Flow Path via Level Set

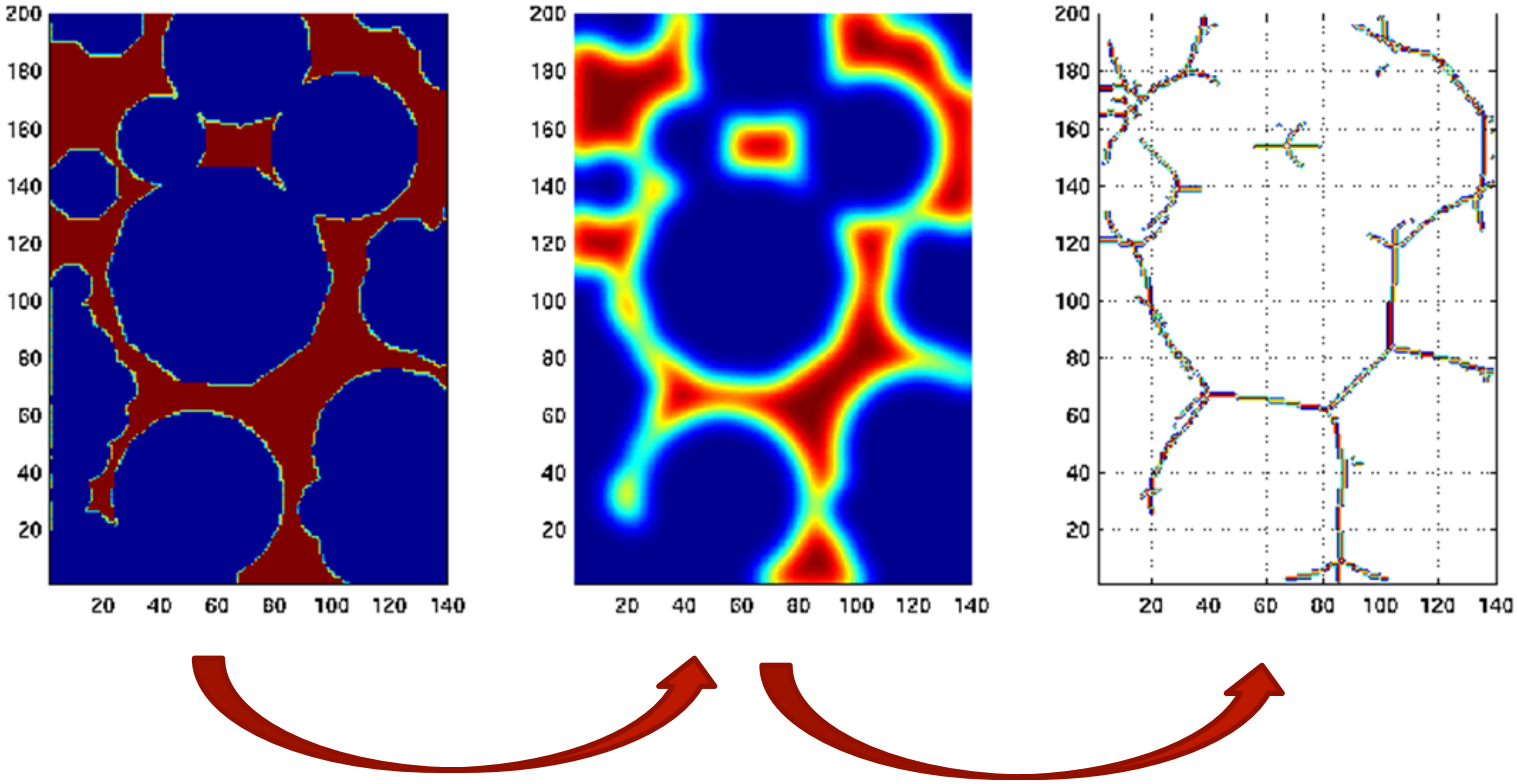

Convert binary image into level set via semi-implicit scheme

Extract Local minimum of level set function

Pore Network and Weighed Graph

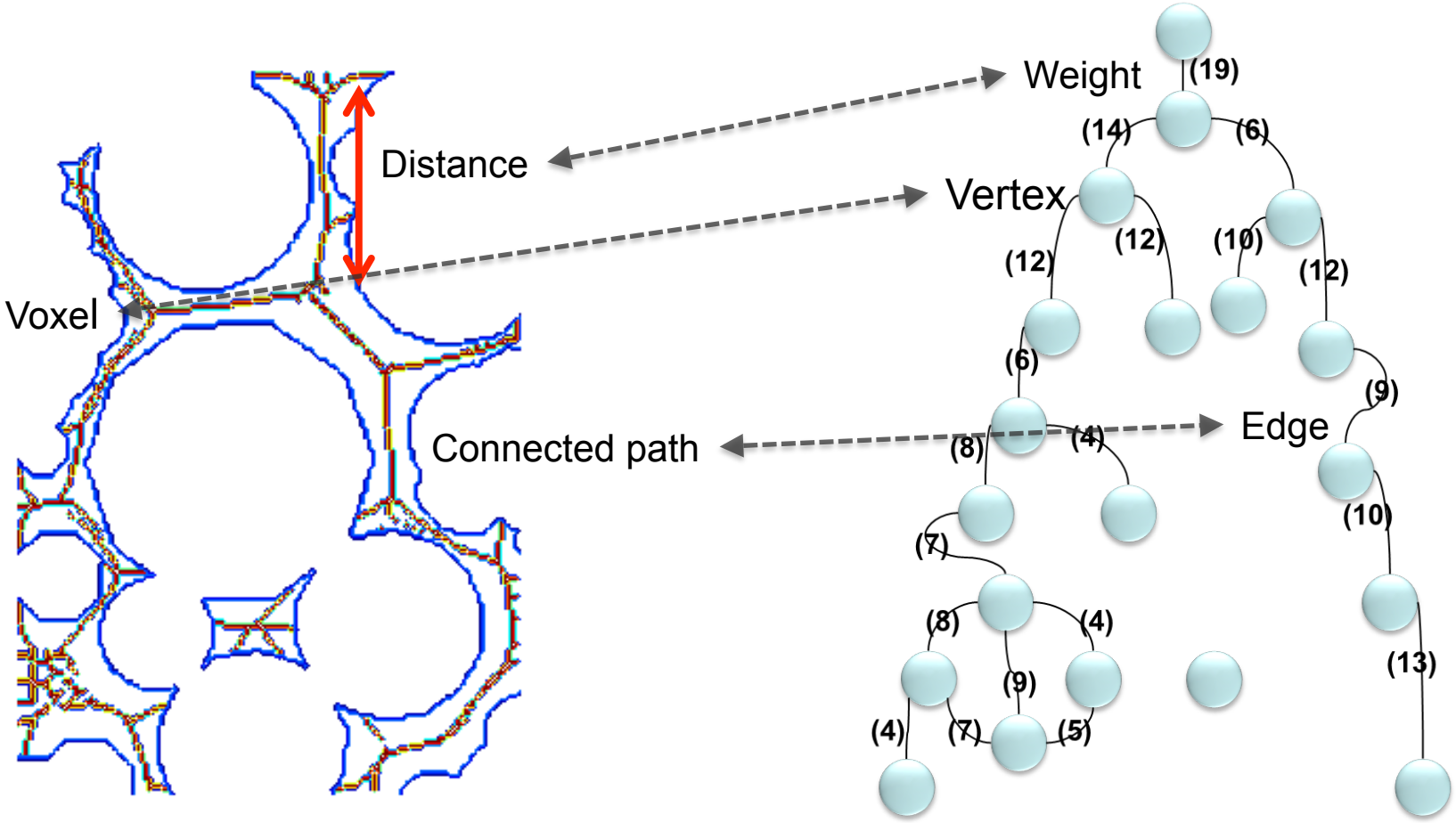

Shortest Path Searching Algorithm

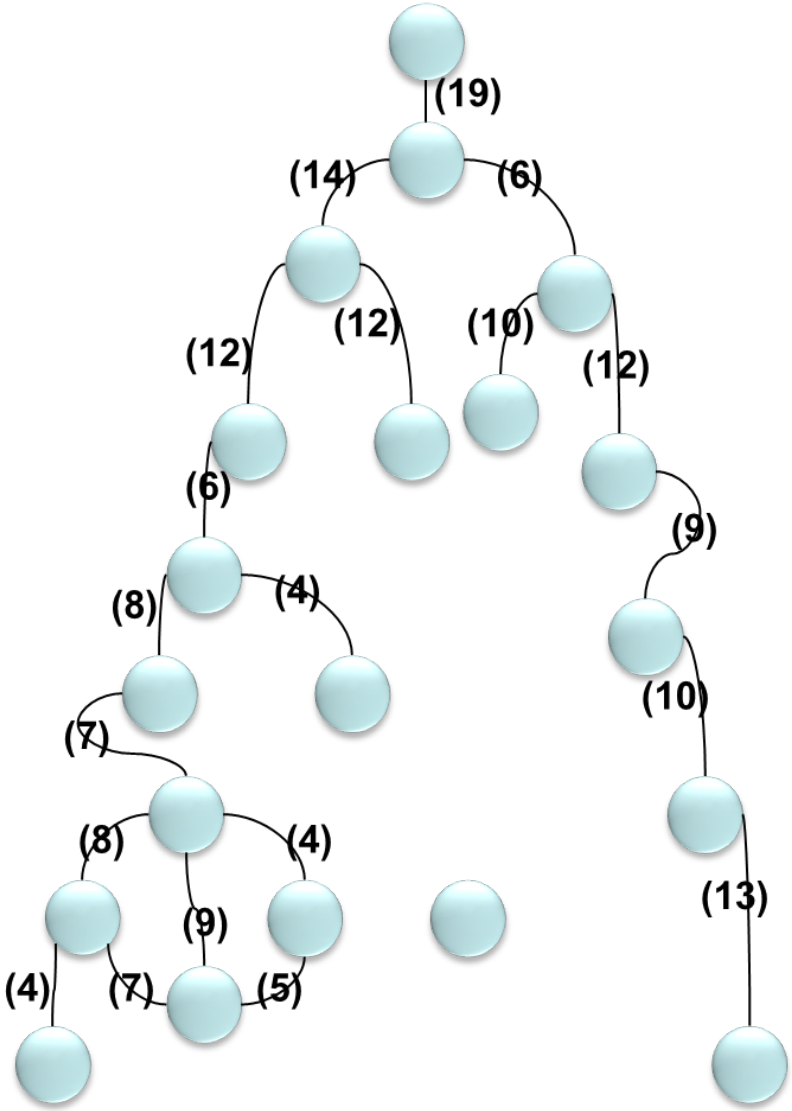

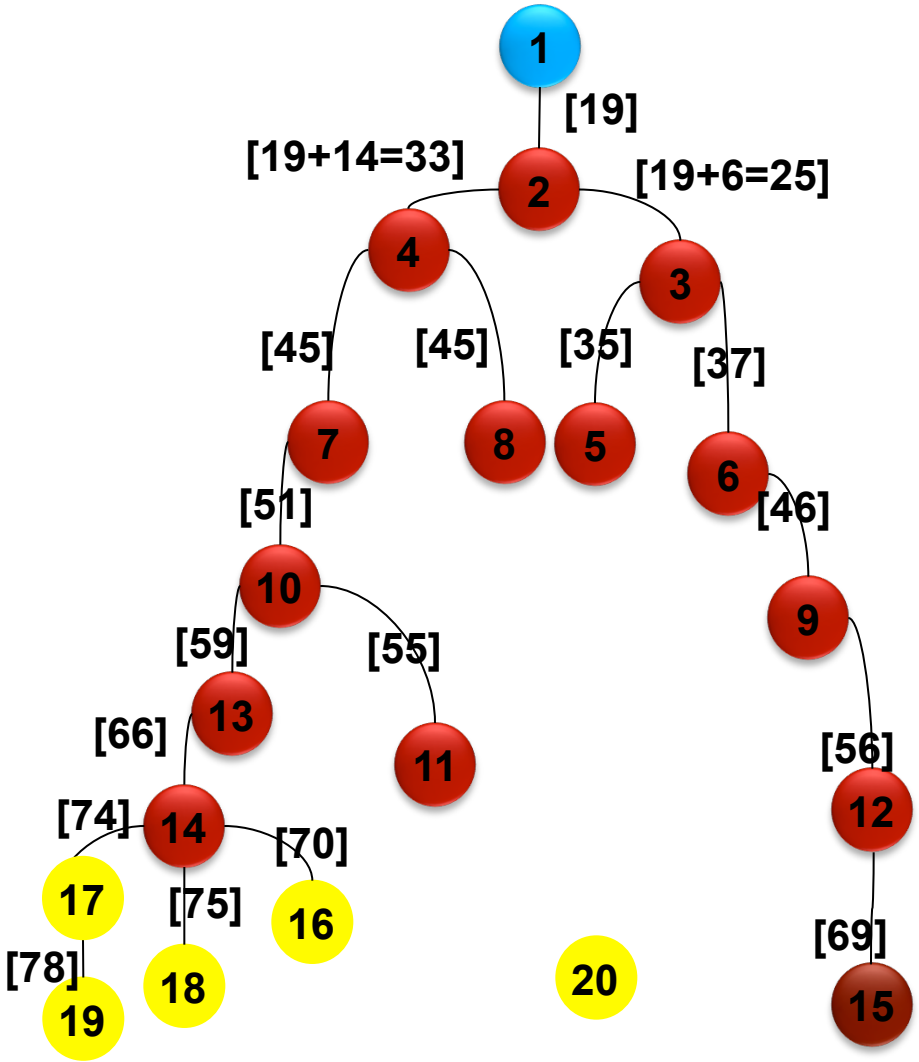

Determining Connectivity with Recursive Functions

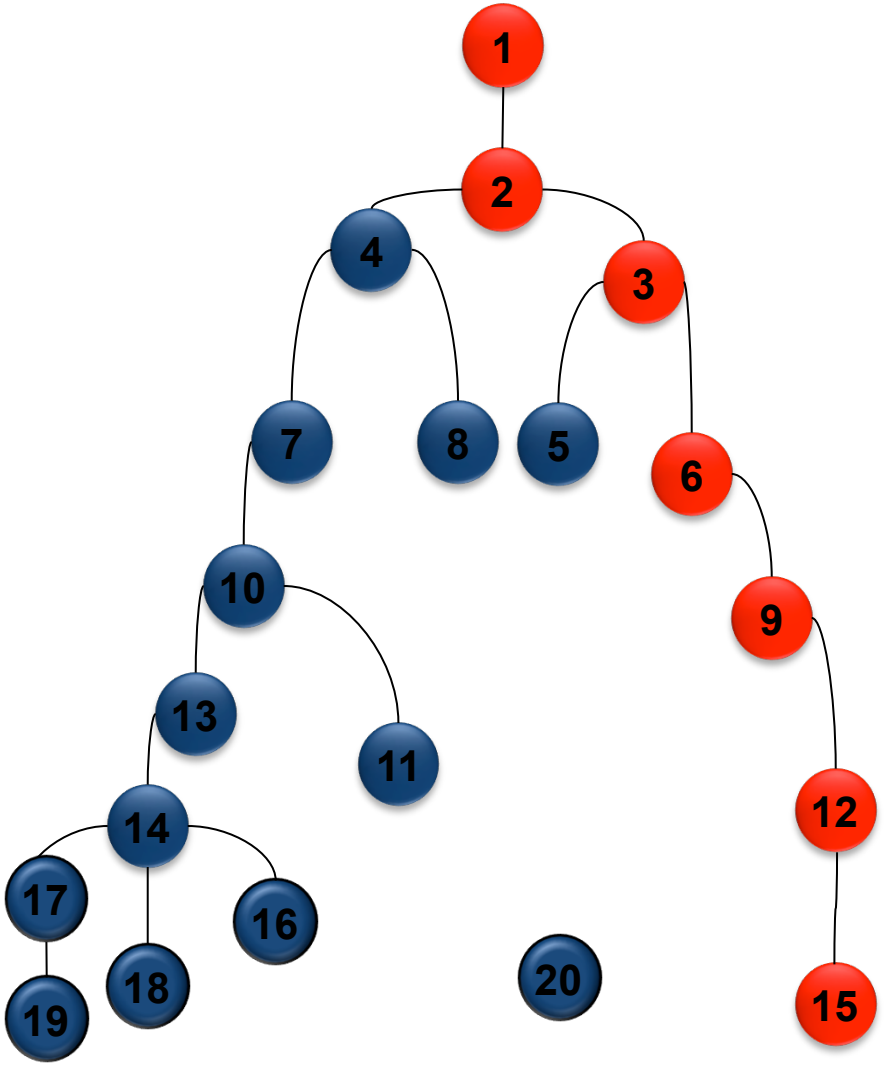

PROGRAM MAIN

1. Activate all vertices along the flow path as active nodes and mark them as visited vertices
2. While there exists at least one active node
3. call the recursive function MARKNEIGHBOR

EXIT

FUNCTION MARKNEIGHBOR

1. IF at least one neighbors of the active nodes has not yet been visited
    1. Activate the unvisited neighbor vertices
    2. Mark them as visited vertices.
    3. Deactivate the old active nodes with unvisited neighbor(s).
    4. Call the recursive function MARKNEIGHBOR
2. ELSE
    1. Deactivate the active nodes with no unvisited neighbor.
3. EXIT

EXIT

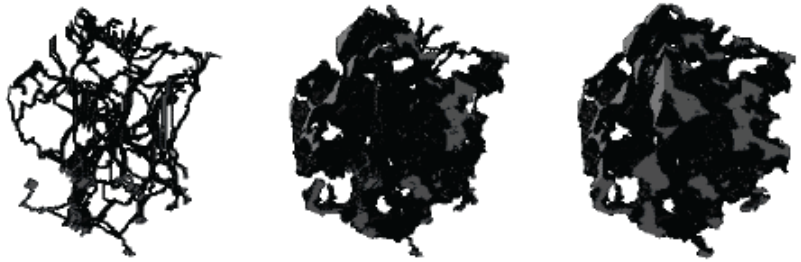

Partitions of Total and Connected Pores Space

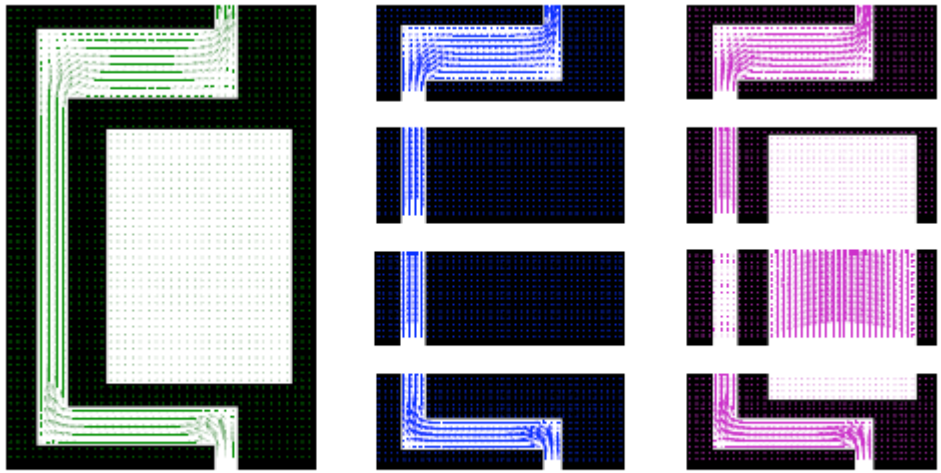

(a) (b) (c)

Case	1	2	3
Number of Unit Cell(s)	1	4	4
Occluded Pore Identified?	No	Yes	No
Local Permeability, u^2 (top)	N/A	0.011	0.011
Local Permeability, u^2 (2nd top)	N/A	0.015	0.0029
Local Permeability, u^2 (2nd bottom)	N/A	0.015	0.45
Local Permeability, u^2 (bottom)	N/A	0.014	0.014
Global Permeability, u^2	0.015	0.013	0.0078
Relative Error	0	12 %	48 %

Size of Representative Elementary Volume

- Pore- to unit cell up-scaling criterion (Energy Dissipation Rate)

$$D^{micro} = 2\mu^v \epsilon : \epsilon\,; \qquad \epsilon = \frac{1}{2}(\nabla^{\boldsymbol{x}} v + (\nabla^{\boldsymbol{x}} v)^T)$$

$$\frac{1}{\Omega^c}\int_{\Omega^c} D^{micro}\mathrm{d}\Omega^c = \nabla^{\boldsymbol{x}} p \cdot \boldsymbol{k}^{meso} \cdot \nabla^{\boldsymbol{x}} p$$

- Unit Cell- to specimen up-scaling criterion (Hill-Mandel Condition)

$$D^{macro} = \frac{1}{\Omega}\int_{\Omega} \nabla^{\boldsymbol{x}} p \cdot \boldsymbol{v}\ \mathrm{d}\Omega = \frac{1}{\Omega}\int_{\Omega} \nabla^{\boldsymbol{x}} p\ \mathrm{d}\Omega \cdot \frac{1}{\Omega}\int_{\Omega} \boldsymbol{v}\ \mathrm{d}\Omega$$

$$D^{macro} = \frac{1}{\Omega}\int_{\Omega} \frac{1}{\mu^v}\nabla^{\boldsymbol{x}} p \cdot \boldsymbol{k}^{meso} \cdot \nabla^{\boldsymbol{x}} p\ \mathrm{d}\Omega = \frac{k_{zz}^{marco}}{\mu^v}\frac{(p_2 - p_1)^2}{(z_2 - z_1)^2}$$

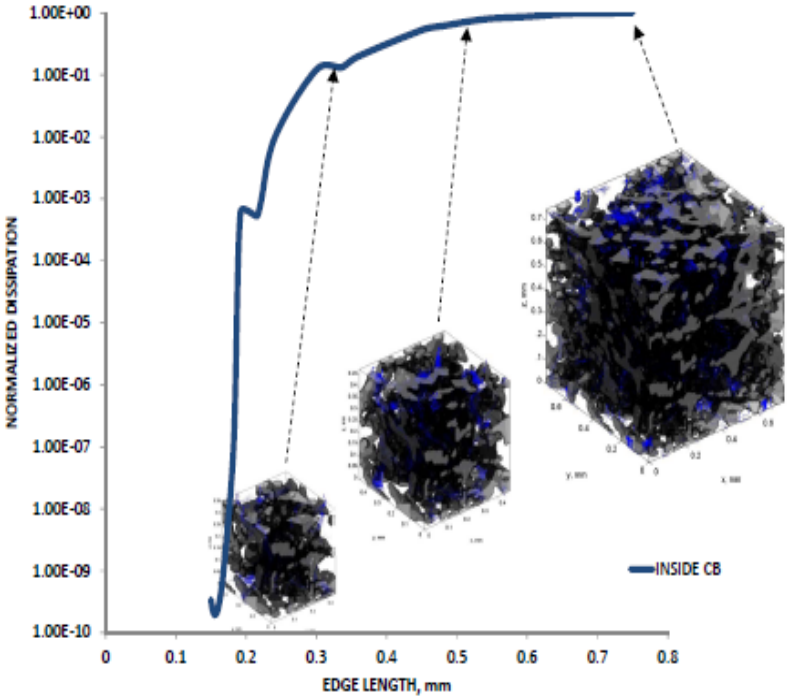

Specimen Type	Compaction Band	Outside Matrix
Volume Averaged Dissipation Rate, J/sec per $1m^3$	71.1	398.8
Dissipation Rate obtained from B.C. , J/sec per $1m^3$	69.8	383.3
Difference, J/sec	1.3	15.6
Homogenization Error e^{hom}	1.9 %	4.1 %

Obtain Pore Volume Binary Images from DEM Assemblies

Algorithm 1 Seed-fill (node, void-flag, solid-flag)

```
if the current node is not a void then
    return
else
    search the spherical particle closest to the current node
    Compute Euclidean distance between current node and the centroid of the closest spherical particle
    if Euclidean distance ≠ radius of the closest spherical particle then
        Perform Flood-fill (the west neighbor of the current node, void-flag, solid-flag)
        Perform Flood-fill (the east neighbor of the current node, void-flag, solid-flag)
        Perform Flood-fill (the north neighbor of the current node, void-flag, solid-flag)
        Perform Flood-fill (the south neighbor of the current node, void-flag, solid-flag)
        Perform Flood-fill (the upper neighbor of the current node, void-flag, solid-flag)
        Perform Flood-fill (the lower neighbor of the current node, void-flag, solid-flag)
    end if
end if
```

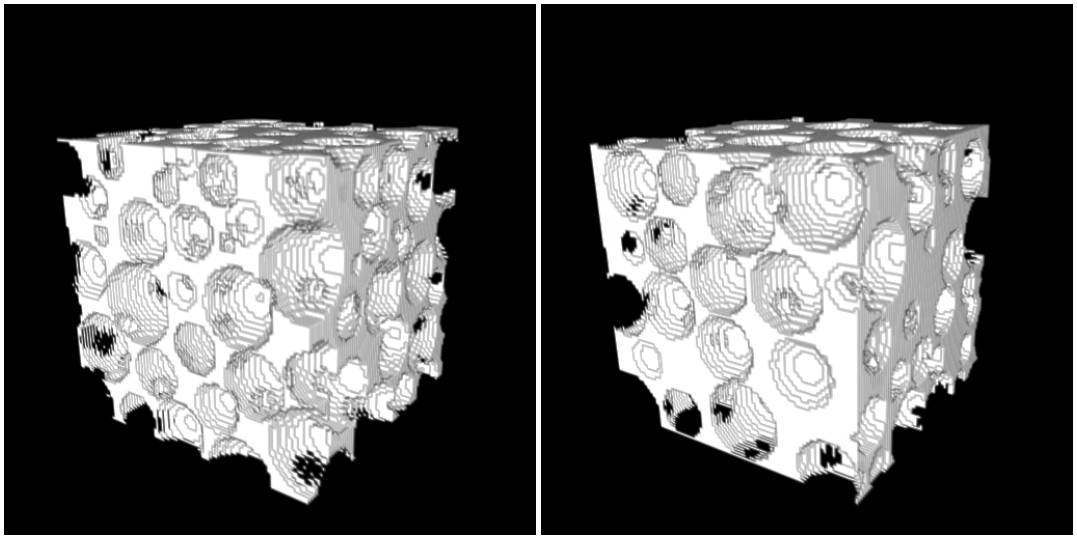

Binary images generated from DEM assemblies

Permeability of Aztec Sandstone Compaction Band Specimen

Sandia National Laboratories

	Porosity	Velocity	Porosity	Effective Permeability
INSIDE CB ϕ = 0.14	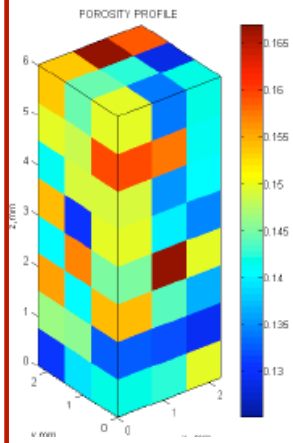	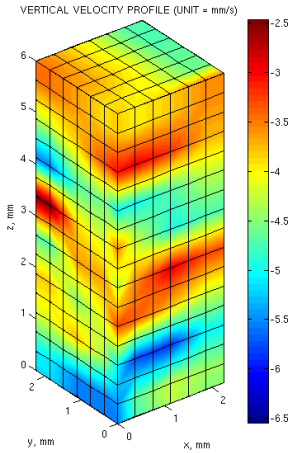	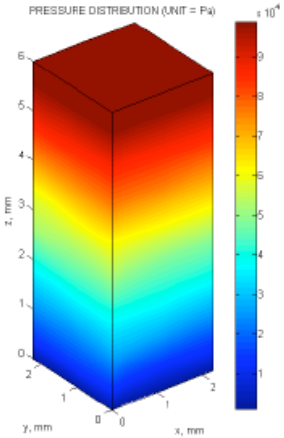	$2.5e\text{-}13m^2$
HOST MATRIX ϕ = 0.21	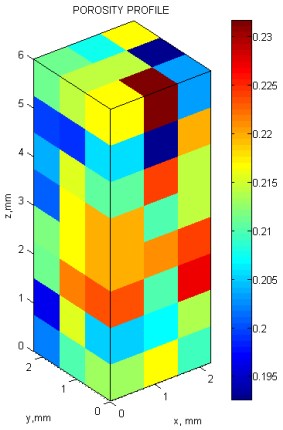	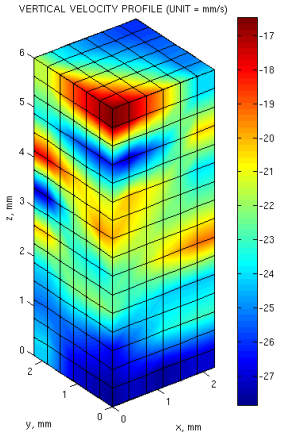	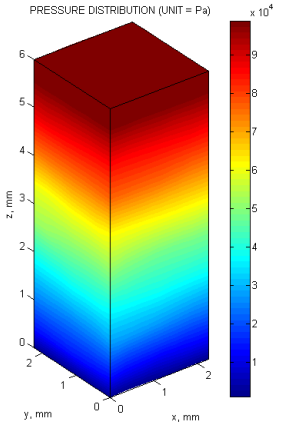	$1.4e\text{-}12m^2$

How to find the shortest path between the lab to Livermore airport?

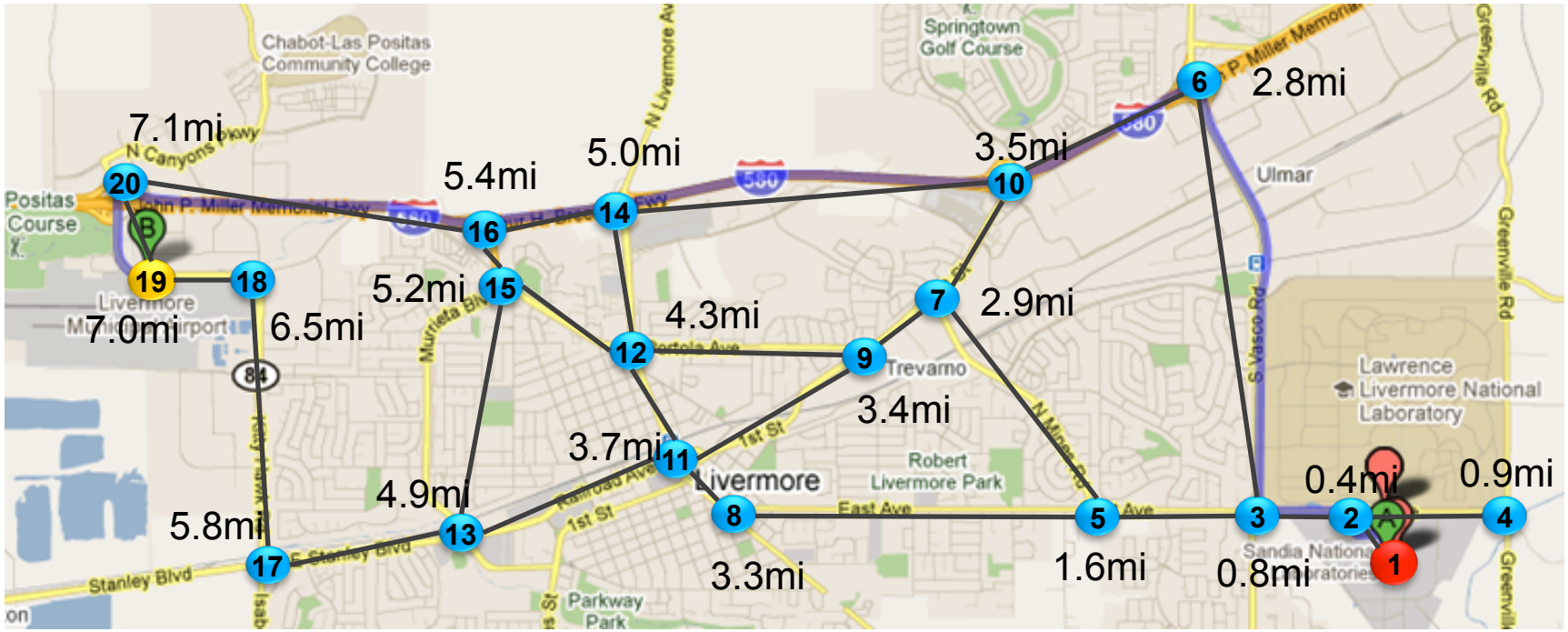

Constitutive relations for solid deformation, flow and heat transport

Sandia National Laboratories

Darcy's Law for deforming porous media

$$\frac{1}{\rho_f}\boldsymbol{W} = \boldsymbol{K}\cdot(-\nabla^{\boldsymbol{X}} p^f + \rho_f \boldsymbol{F}^{\mathrm{T}}\cdot\boldsymbol{G})$$

$$\boldsymbol{Q} = (1/\rho_f)\boldsymbol{W}$$

$$\boldsymbol{K} = J\boldsymbol{F}^{-1}\cdot\boldsymbol{k}\cdot\boldsymbol{F}^{-\mathrm{T}}$$

Fourier's law for deforming porous media

$$Q_\theta = -\boldsymbol{K}_\theta\cdot\nabla^{\boldsymbol{X}}\theta$$

$$\boldsymbol{K}_\theta = J\boldsymbol{F}^{-1}\cdot\boldsymbol{k}_{\boldsymbol{\theta}}\cdot\boldsymbol{F}^{-T}$$

History dependent behavior of solid skeleton

$$\boldsymbol{P}(\boldsymbol{F},\boldsymbol{z},p^f,\theta) = \boldsymbol{P'}(\boldsymbol{F},\boldsymbol{z},\theta) - JBp^f\boldsymbol{F}^{-T}$$

$$\boldsymbol{P}' = \frac{\partial\psi(\boldsymbol{F},\boldsymbol{z},\theta)}{\partial\boldsymbol{F}}$$

$$\psi(\boldsymbol{F},\boldsymbol{z},\theta) = \hat{U}(J) + \hat{W}(\bar{\boldsymbol{b}}^{\boldsymbol{e}}) + \hat{K}(\boldsymbol{z}) + \hat{M}(J,\theta)$$

Hyper-elastic | plastic dissipation | Thermo-mechanical coupling energy

Domain Overlapped Coupling Weak Form

Sandia National Laboratories

Coarse deformation mapping

$$\overline{\boldsymbol{R}}_a[\overline{\boldsymbol{\varphi}}_h, \boldsymbol{\phi}_h] = \int_{\mathcal{B}} \alpha \overline{\boldsymbol{P}} : \operatorname{Grad} N_a \; dV - \beta \overline{\boldsymbol{B}} N_a \; dV + \left(\int_{\mathcal{B}^c} N_a N_b \cdot + \kappa l^2 \operatorname{Grad} N_a : \operatorname{Grad} N_b \; dV \right) \boldsymbol{\phi}_b - \int_{\partial_T \mathcal{B}} \beta \overline{\boldsymbol{T}} \cdot N_a \; dS$$

Fine deformation mapping

$$\boldsymbol{R}'_\alpha[\boldsymbol{\varphi}'_h, \boldsymbol{\phi}_h] = \int_{\mathcal{B}} (1-\alpha) \boldsymbol{P}' : \operatorname{Grad} \lambda_\alpha \; dV - (1-\beta) \boldsymbol{B}' \lambda_\alpha \; dV - \left(\int_{\mathcal{B}^c} \lambda_\alpha N_b + \kappa l^2 \operatorname{Grad} \lambda_\alpha : \operatorname{Grad} N_b \; dV \right) \boldsymbol{\phi}_b - \int_{\partial_T \mathcal{B}} (1-\beta) \boldsymbol{T}' \cdot \lambda_\alpha \; dS$$

Lagrangian Multiplier

$$\boldsymbol{R}^c_a[\overline{\boldsymbol{\varphi}}_h, \boldsymbol{\varphi}'_h] = \left(\int_{\mathcal{B}^c} N_a N_b + \kappa l^2 \operatorname{Grad} N_a : \operatorname{Grad} N_b \; dV \right) \overline{\boldsymbol{\varphi}}_b - \left(\int_{\mathcal{B}^c} N_a \lambda_\beta + \kappa l^2 \operatorname{Grad} N_a : \operatorname{Grad} \lambda_\beta \; dV \right) \boldsymbol{\varphi}'_\beta$$

Optimal Stabilization Parameter Estimation

1D poromechanics governing equation

$$c\frac{\partial^2 \hat{p}}{\partial x^2} = \frac{\partial \hat{p}}{\partial t}, \qquad c = \frac{k}{\mu}\frac{M'H}{H+\nu\beta M'}; M' = \frac{M(K+4G/3)}{K+4G/3+B^2M}$$

Three node stencil (standard Galerkin method)

$$-\hat{p}_{A-1} + 2\hat{p}_A - \hat{p}_{A-1} + \frac{h^2}{6\vartheta c\Delta t}(\hat{p}_{A-1} + 4\hat{p}_A + \hat{p}_{A+1}) = 0$$

Three node stencil (Stabilized Galerkin method)

$$-\hat{p}_{A-1} + 2\hat{p}_A - \hat{p}_{A-1} + \frac{h^2}{12\vartheta c\Delta t}[(2-\gamma)\hat{p}_{A-1} + (8+2\gamma)\hat{p}_A + (2-\gamma)\hat{p}_{A+1}] = 0$$

Growth/decay rate

$$\cosh\frac{h}{(\sqrt{\vartheta c\Delta t})^h} = \frac{(1+h^2/\vartheta c\Delta t)(4+\gamma)/6}{(1-h^2/\vartheta c\Delta t)(2-\gamma)/12}$$

To have real growth/decay rate, we need

$$\gamma > 2 - 12\frac{\vartheta c\Delta t}{h^2} > 0$$

$$\gamma = (2-6\frac{\vartheta c\Delta t}{h^2})\left(\frac{1}{2}+\frac{1}{2}\tanh(2-12\frac{\vartheta c\Delta t}{h^2})\right)$$

Safety factor

Turn off stabilization without introducing switch

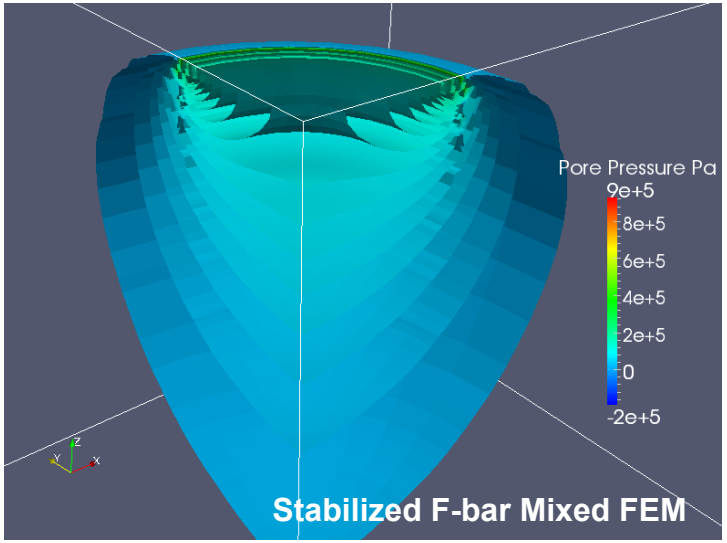

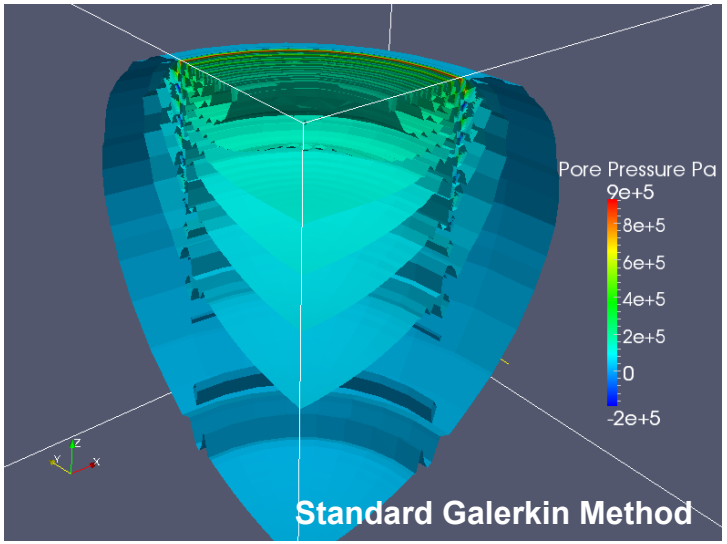

Footing placed on an elastoplastic porous medium

Without Stabilization

In low diffusivity case, the stabilization scheme is able to eliminate spurious oscillation.

With Stabilization

In high diffusivity case, the stabilization scheme does not introduce extra diffusivity that cause error.

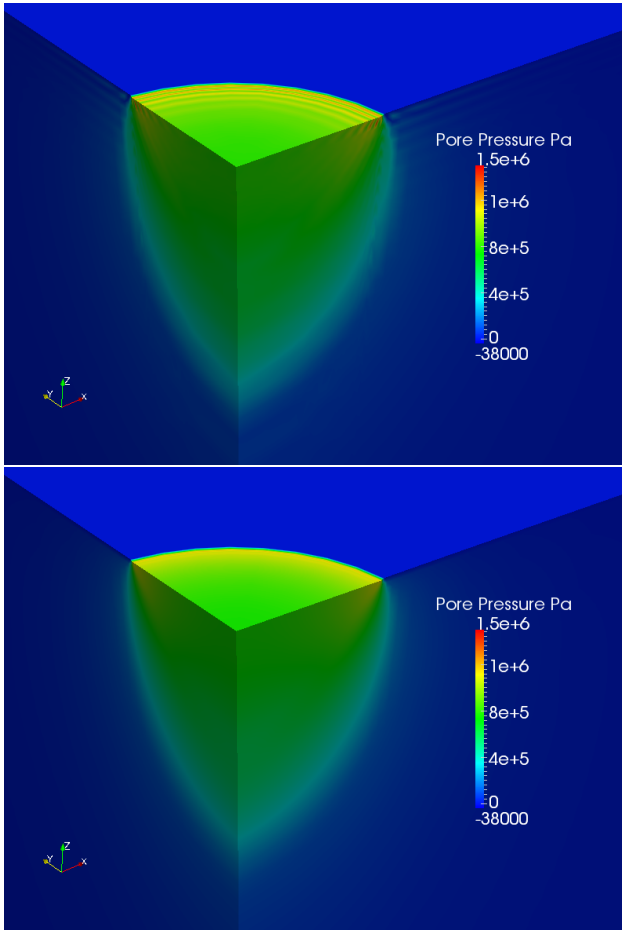

Low diffusivity case

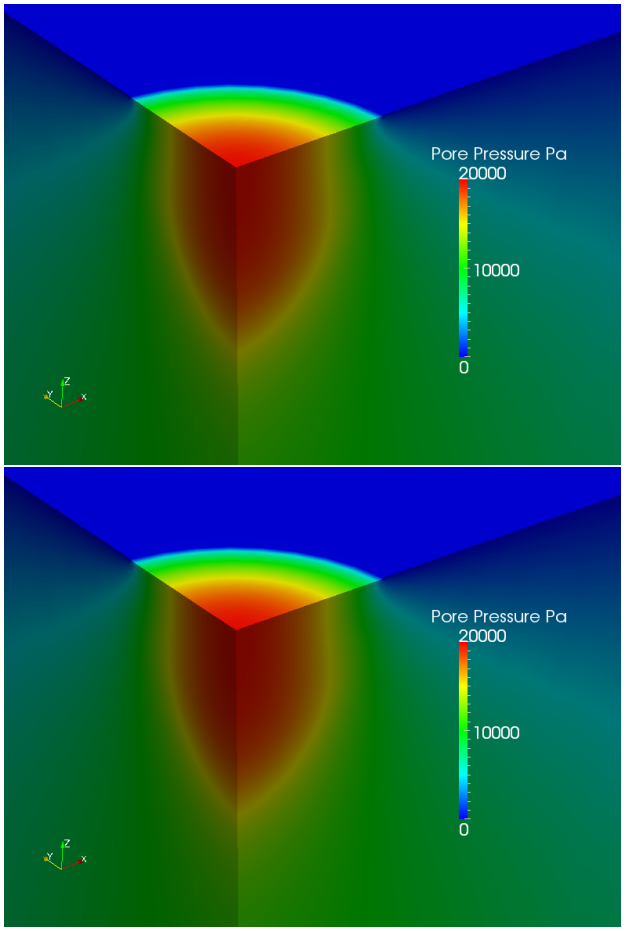

High diffusivity case

From Sun, Ostien, Salinger, International Journal for Numerical and Analytical Methods in Geomechanics, 2013

Application of Level Set Scheme and Graph Theory for geometrical analysis of tomographic images

Sandia National Laboratories

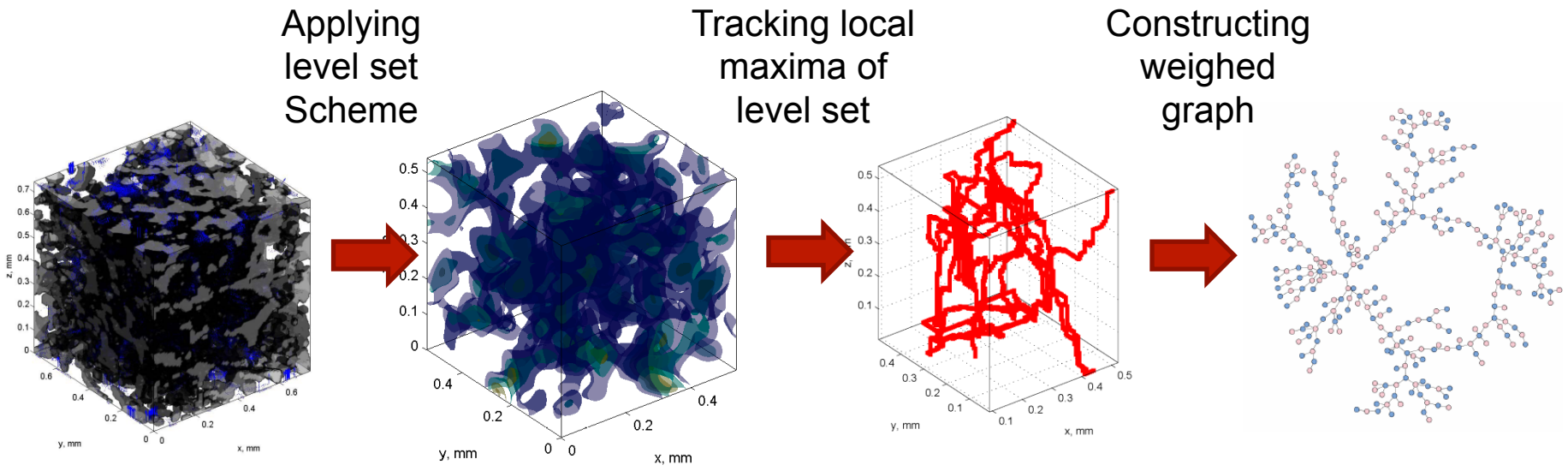

See W.C Sun, J.E. Andrade, J.W. Rudnicki, A multiscale method for characterization of porous microstructures and their impact on macroscopic effective permeability, *International Journal of Numerical Methods in Engineering*, Vol. 88, No.12, 1260-1279, 2011.

Internal Variable Recovery via Lie Algebra

1. Application of Lie Algebra to interpolate internal variables within admissible space

Balance of Linear Momentum

$$D\Phi[\boldsymbol{\varphi}, \bar{\boldsymbol{z}}, \bar{\boldsymbol{y}}](\boldsymbol{\eta}) = \int_B \boldsymbol{P} : \operatorname{Grad} \boldsymbol{\eta} \, dV - \int_B \rho_0 \boldsymbol{B} \cdot \boldsymbol{\eta} \, dV - \int_{\partial_T B} \boldsymbol{T} \cdot \boldsymbol{\eta} \, dS = 0$$

Variational Continuum Projection Operator

$$D\Phi[\boldsymbol{\varphi}, \bar{\boldsymbol{z}}, \bar{\boldsymbol{y}}](\boldsymbol{\zeta}) = \int_B (\bar{\boldsymbol{y}} - \boldsymbol{y}) \cdot \boldsymbol{\zeta} \, dV = 0$$

$$D\Phi[\boldsymbol{\varphi}, \bar{\boldsymbol{z}}, \bar{\boldsymbol{y}}](\boldsymbol{\xi}) = \int_B (\bar{\boldsymbol{z}} - \boldsymbol{z}) \cdot \boldsymbol{\xi} \, dV = 0.$$

2.Application of Lie Algebra to interpolate internal variables within admissible space

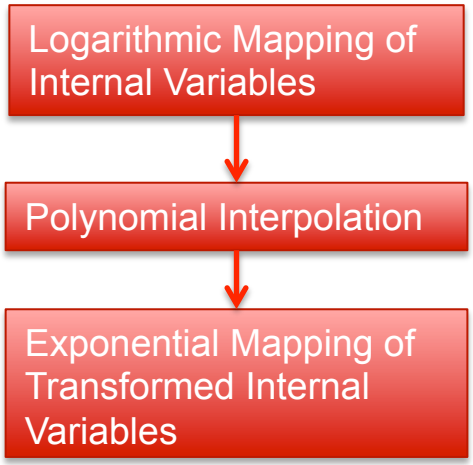

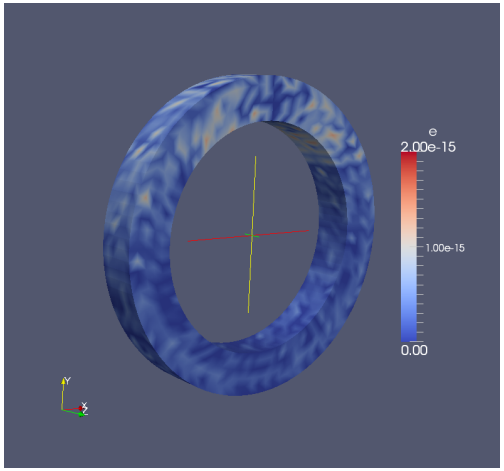

(a)Error of rotation is negligible if logarithmic mapping has been applied

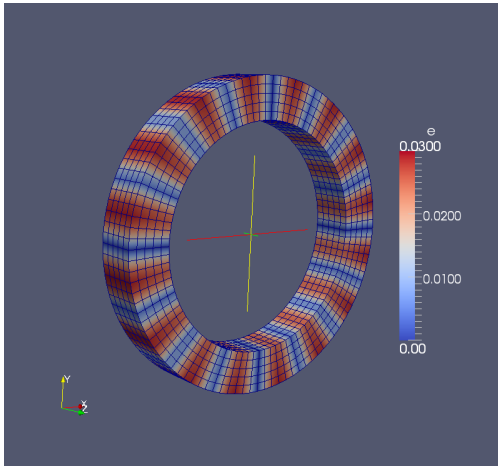

(b)Error of rotation without logarithmic mapping is generated when remeshing

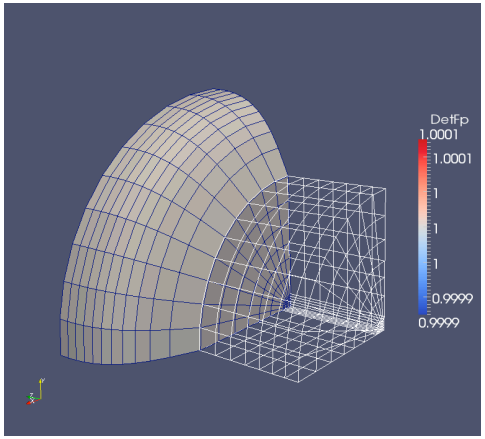

(a) Plastic split of deformation gradient remains isochoric when logarithmic mapping is applied for J2 plasticity model.

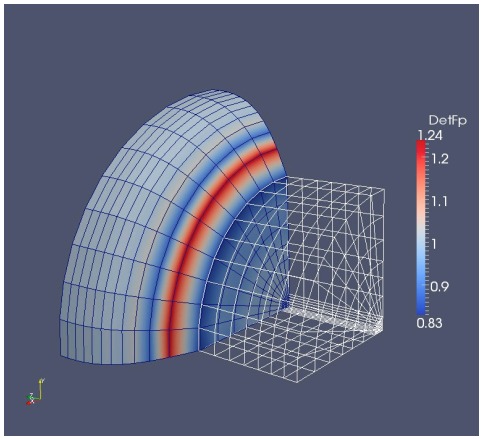

(b) Spurious plastic dilation/contraction generated due to improper linear mapping.

Resolution Issues for Conducting Lattice Boltzmann Simulation on Binary Images

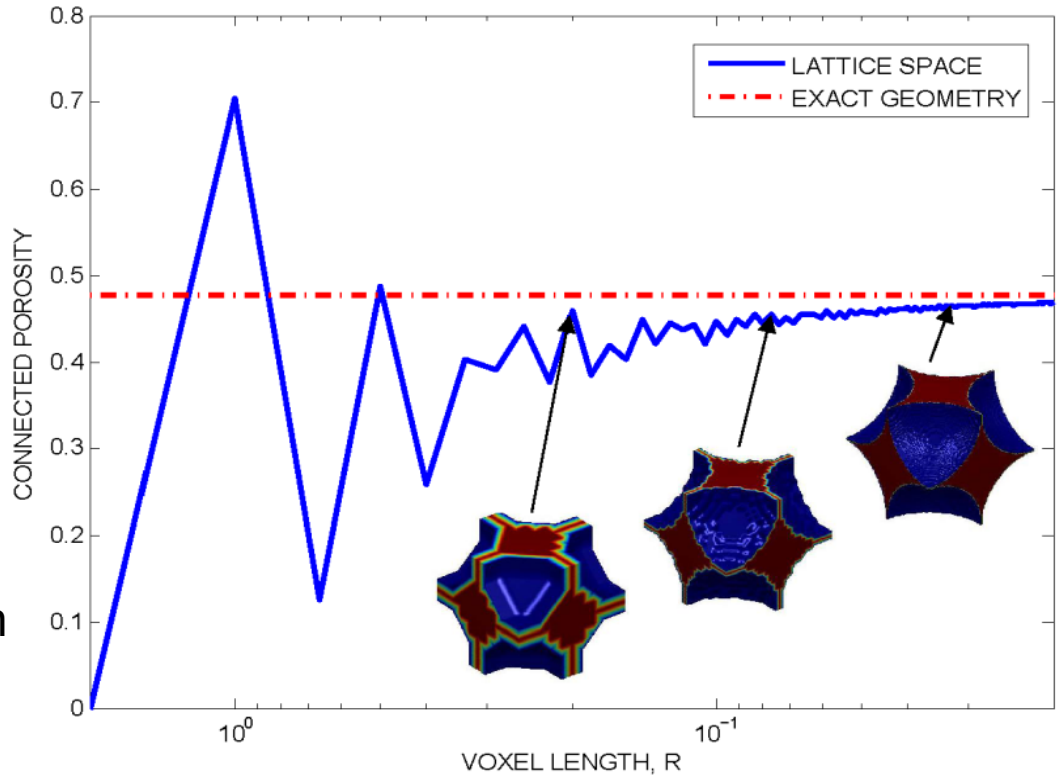

- Low resolution
  - Faster and cheaper computation

- High resolution
  - Higher accuracy
  - Higher cost for computation

Size of Representative Elementary Volume

- Pore- to unit cell up-scaling criterion (Energy Dissipation Rate)

$$D^{micro} = 2\mu^v \epsilon : \epsilon\,; \qquad \epsilon = \frac{1}{2}(\nabla^{\boldsymbol{x}} v + (\nabla^{\boldsymbol{x}} v)^T)$$

$$\frac{1}{\Omega^c}\int_{\Omega^c} D^{micro}\mathrm{d}\Omega^c = \nabla^{\boldsymbol{x}} p \cdot \boldsymbol{k}^{meso} \cdot \nabla^{\boldsymbol{x}} p$$

- Unit Cell- to specimen up-scaling criterion (Hill-Mandel Condition)

$$D^{macro} = \frac{1}{\Omega}\int_{\Omega} \nabla^{\boldsymbol{x}} p \cdot \boldsymbol{v}\ \mathrm{d}\Omega = \frac{1}{\Omega}\int_{\Omega} \nabla^{\boldsymbol{x}} p\ \mathrm{d}\Omega \cdot \frac{1}{\Omega}\int_{\Omega} \boldsymbol{v}\ \mathrm{d}\Omega$$

$$D^{macro} = \frac{1}{\Omega}\int_{\Omega} \frac{1}{\mu^v}\nabla^{\boldsymbol{x}} p \cdot \boldsymbol{k}^{meso} \cdot \nabla^{\boldsymbol{x}} p\ \mathrm{d}\Omega = \frac{k_{zz}^{marco}}{\mu^v}\frac{(p_2 - p_1)^2}{(z_2 - z_1)^2}$$

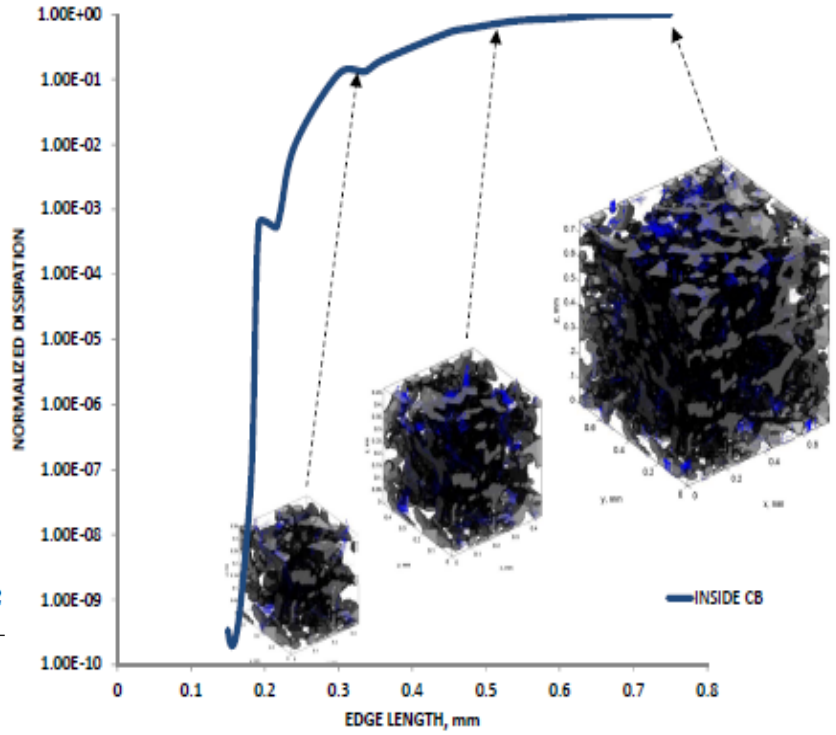

Specimen Type	Compaction Band	Outside Matrix
Volume Averaged Dissipation Rate, J/sec per $1m^3$	71.1	398.8
Dissipation Rate obtained from B.C. , J/sec per $1m^3$	69.8	383.3
Difference, J/sec	1.3	15.6
Homogenization Error e^{hom}	1.9 %	4.1 %

Implementation of Total Lagrangian Poro-plasticity Problem

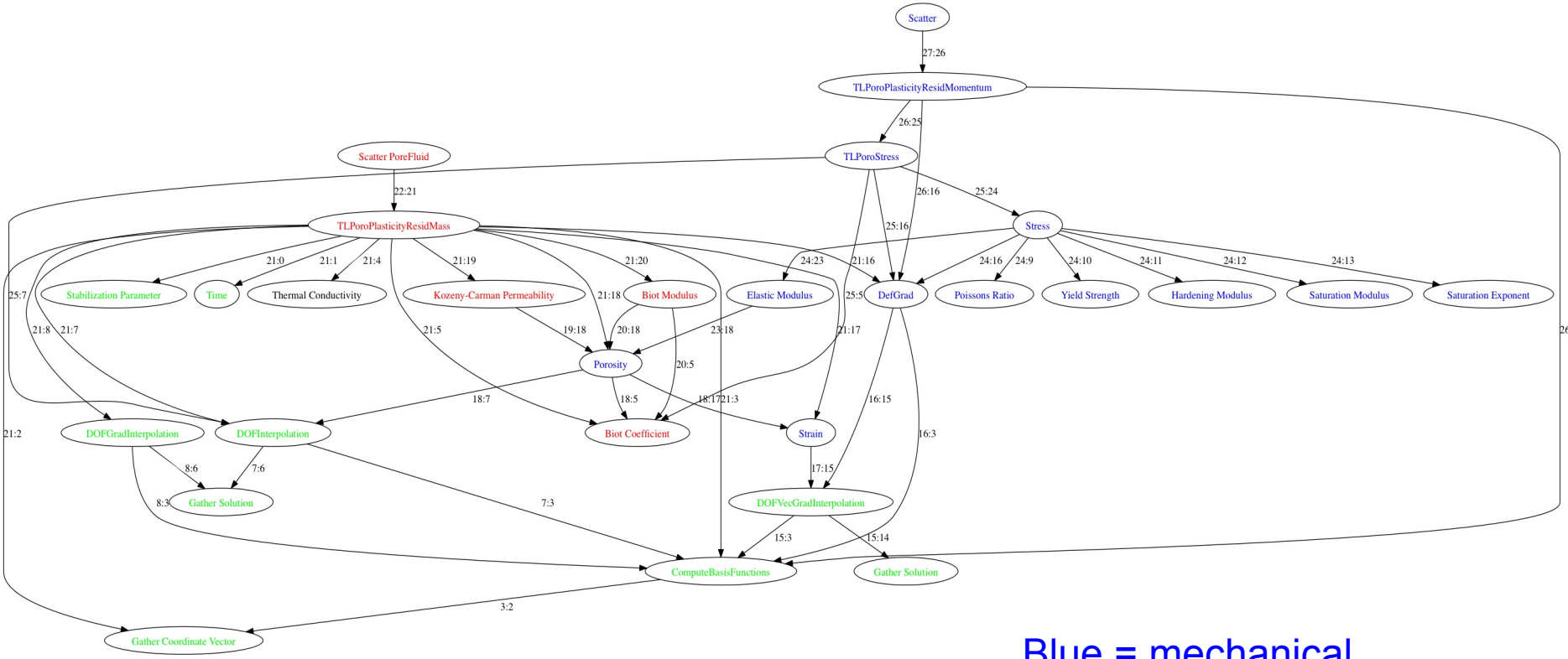

Blue = mechanical

Red = pore-fluid diffusion

Purple = coupled terms

Green = General FEM

- Gather coordinates, displacement and pore-pressure fields
- Interpolate fields and gradients to integration points
- Chain together Evaluators to compute momentum and mass Residuals of the solid and pore-fluid constituents
- Apply LBB stabilizer
- Scatter back to the global system of equations

Sandia National Laboratories

Hydrogen Transport

Stabilized hydrogen diffusion-deformation K-field problem for low diffusive materials

Sandia National Laboratories

Balance of Linear Momentum

$$\nabla^{\boldsymbol{X}} \cdot \boldsymbol{P}(\boldsymbol{F}, \overline{\boldsymbol{z}}, C_T) = \boldsymbol{0}$$

Concentration Sensitive Yield Function

$$f(\boldsymbol{\tau}, \overline{\boldsymbol{z}}, C_T) = ||\mathrm{dev}[\boldsymbol{\tau}]|| - \sqrt{\frac{2}{3}}[\sigma_Y(C_T) + K\alpha \leq 0$$

Hydrogen Transport Theorem

$$D^* \dot{C}_L - \nabla^{\boldsymbol{X}} \cdot \boldsymbol{D_L} \nabla^{\boldsymbol{X}} C_L + \nabla^{\boldsymbol{X}} \cdot \frac{V_H}{RT} C_L \boldsymbol{D_L} \nabla^{\boldsymbol{X}} S_H + \theta_T \frac{dN_T}{d\epsilon_p} \dot{\epsilon}_p = 0$$

L2 Projection of Hydrostatic Stress

$$\int_{\mathcal{B}} N_a (\sigma_h - N_b \sigma_b) \, dV = 0$$

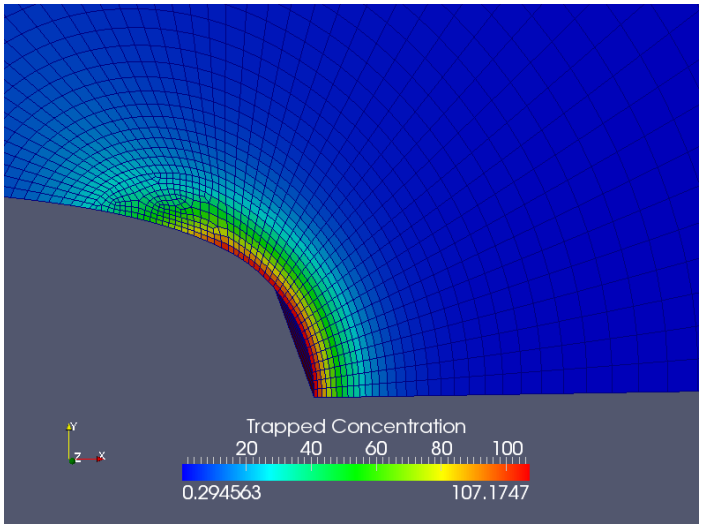

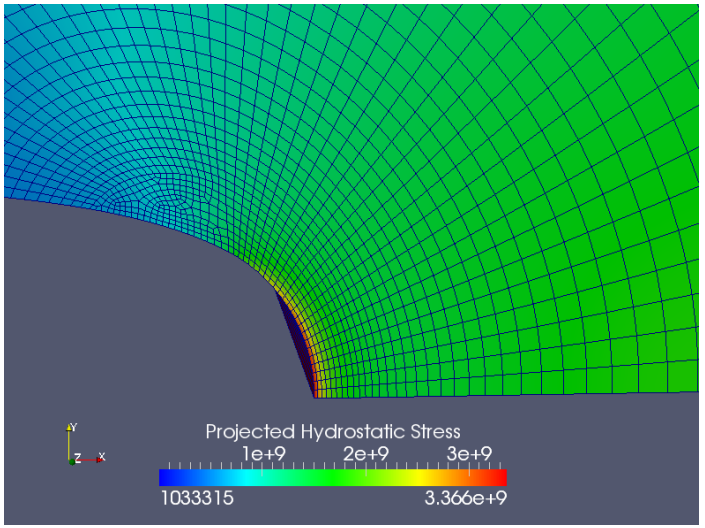

Implicit Time Integration of Fully Coupled Scheme

Backward Euler Scheme

$$\begin{bmatrix} \mathbf{0} & \mathbf{0} \\ \boldsymbol{M_{c_L u}} & \boldsymbol{K^{tran}_{c_L c_L}} \end{bmatrix} \begin{bmatrix} \dot{\boldsymbol{u}} \\ \dot{\boldsymbol{c}}_{\boldsymbol{L}} \end{bmatrix} + \begin{bmatrix} \boldsymbol{K_{uu}} & \boldsymbol{B_{uc_L}} \\ \mathbf{0} & \boldsymbol{K^{st}_{c_L c_L}} \end{bmatrix} \begin{bmatrix} \boldsymbol{u} \\ \boldsymbol{c}_L \end{bmatrix} = \begin{bmatrix} \boldsymbol{F^{ext}_{u}} \\ \boldsymbol{F^{ext}_{c_L}} \end{bmatrix}$$

$$\begin{bmatrix} \boldsymbol{K_{uu}} & \boldsymbol{B_{uc_L}} \\ \boldsymbol{M_{c_L u}} & \boldsymbol{K^{st}_{c_L c_L}} \delta t + \boldsymbol{K^{tran}_{c_L c_L}} \end{bmatrix} \begin{bmatrix} \boldsymbol{u_{n+1}} \\ \boldsymbol{c_{Ln+1}} \end{bmatrix} = \begin{bmatrix} \boldsymbol{F^{ext}_{u}} \\ \boldsymbol{F^{ext}_{c_L}} + \boldsymbol{M_{c_L u}} \boldsymbol{u_n} + \boldsymbol{K^{tran}_{c_L c_L}} \boldsymbol{c_{Ln}} \end{bmatrix}$$

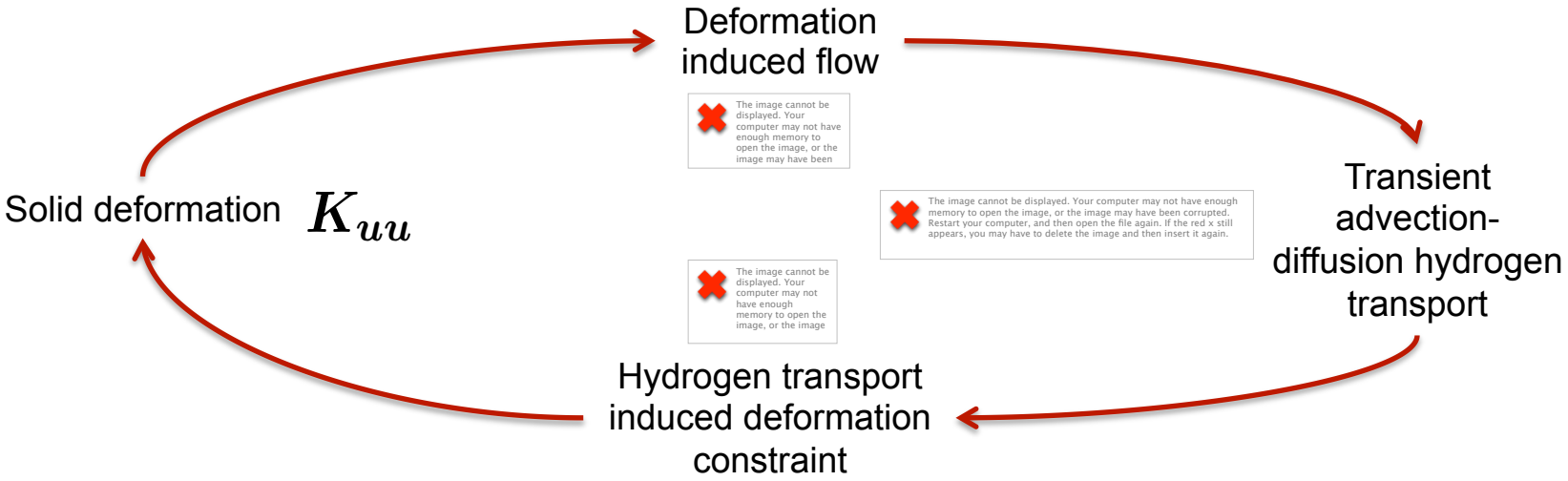

Physical interpretation of the matrix form

Challenges on Implementation of Hydrogen Transport Problem

Sandia National Laboratories

1. Numerical instability may occur if (1) time step is too small and/or (2) diffusivity is too small (i.e. stainless steel) (Harari, 2004) and (3) boundary layer due to the advection term is thinner than the side length of the finite element (Belytschko, Liu, Moran, 2012).

2. Hydrogen transport problem is highly nonlinear, thus require a consistent linearization to implicitly solve for solutions (i.e., NUMEROUS manual, mechanical derivations EACH time the problem is amended).

3. Volmetric Locking, which may occur under perfectly plastic response / isochoric deformation..etc.

Example

Say we want to find the linearized D* (i.e., the first order
term in the Taylor expansion). D* depends on the trapped solvent, temperature, lattice concentration—but trapped solvent also depends on equivalent plastic strain and hence, displacement, yield stress…etc.

How do we derive consistent linearization with respect to all the dependent variables ?

Notice that we need to restart the entire process if we make any changes….

$$D^* - \textit{effective diffusion constant}$$

$$D^* = \frac{N_T N_L}{K_T C_L^2}\left[\frac{1}{(1+\frac{N_L}{K_T C_L})^2}\right]$$

$$C_T = \frac{N_T}{1+\frac{N_L}{K_T C_L}}$$

$$\theta_T = \frac{1}{1+\frac{N_L}{K_T C_L}}$$

$$C_T = \theta_T N_T$$

$$D_L = D_0 e^{-Q/RT}$$

$$N_L = N_A/V_M$$

$$K_T = e^{W_B/RT}$$

$$N_T = 10^{(A-Be^{-C\epsilon_p})}$$

$$\sigma_e = \sigma_0 + H\epsilon_p^m$$

$D_0 = 2.0 \times 10^{-6}\ m^2/s - \textit{pre-exponential factor}$
$Q = 6900 J/mol - \textit{diffusion activation enthalpy}$
$R = 8.314\ J/(molK) - \textit{ideal gas constant}$
$T = 300\ K - \textit{room temperature}$
$D_L = 1.27 \times 10^{-8}\ m^2/s\ (300K) - \textit{diffusion coefficient}$
$N_A = 6.0232 \times 10^{23}\ atoms/mol - \textit{Avogadro's number}$
$V_M = 7.166 \times 10^{-6}\ m^3/mol - \textit{molar volume of Fe}$
$N_L = 1.40 \times 10^5\ \textit{solvent lattice}\ mol/m^3$
$W_B = 60 \times 10^3\ J/mol - \textit{trap binding energy}$
$K_T = 2.801 \times 10^{10} - \textit{equilibrium constant}$
$V_H = 2.0 \times 10^{-6}\ m^3/mol\ (\sim 300K) - \textit{partial molar volume}$
$\Delta H_s = 28.6 \times 10^3\ J/mol - \textit{enthalpy of solution}$
$p_{H_2} = 1\ atm - \textit{hydrogen pressure}$
$C_{L,0} = 2.0 \times 10^{26} e^{-\Delta H_s/RT}\sqrt{p_{H_2}}\ atoms/m^3$
$C_{L,0} = 3.47 \times 10^{-3}\ mol/m^3 - \textit{initial concentration}$
$N_T = 10^{(23.3-2.33e^{-4.0\epsilon_p})}/N_A - \textit{trapped solvent}\ mol/m^3$
$N_{T,0} = 1.549 \times 10^{-3} - \textit{trapped solvent}\ mol/m^3$
$\theta_{T,0} = 0.9986$
$C_{T,0} = 1.547 \times 10^{-3}\ mol/m^3 - \textit{initial concentration}$
$C_{total,0} = C_{L,0} + C_{T,0} = 5.017 \times 10^{-3}\ mol/m^3$

$$\frac{\partial N_T}{\partial \epsilon_p} = 10^{(A-Be^{-C\epsilon_p})} ln(10) BCe^{-C\epsilon_p}/N_A - \textit{trapped solvent}\ mol/m^3$$

Implementation of Hydrogen Diffusion-Mechanics Problem with automatic differentiation

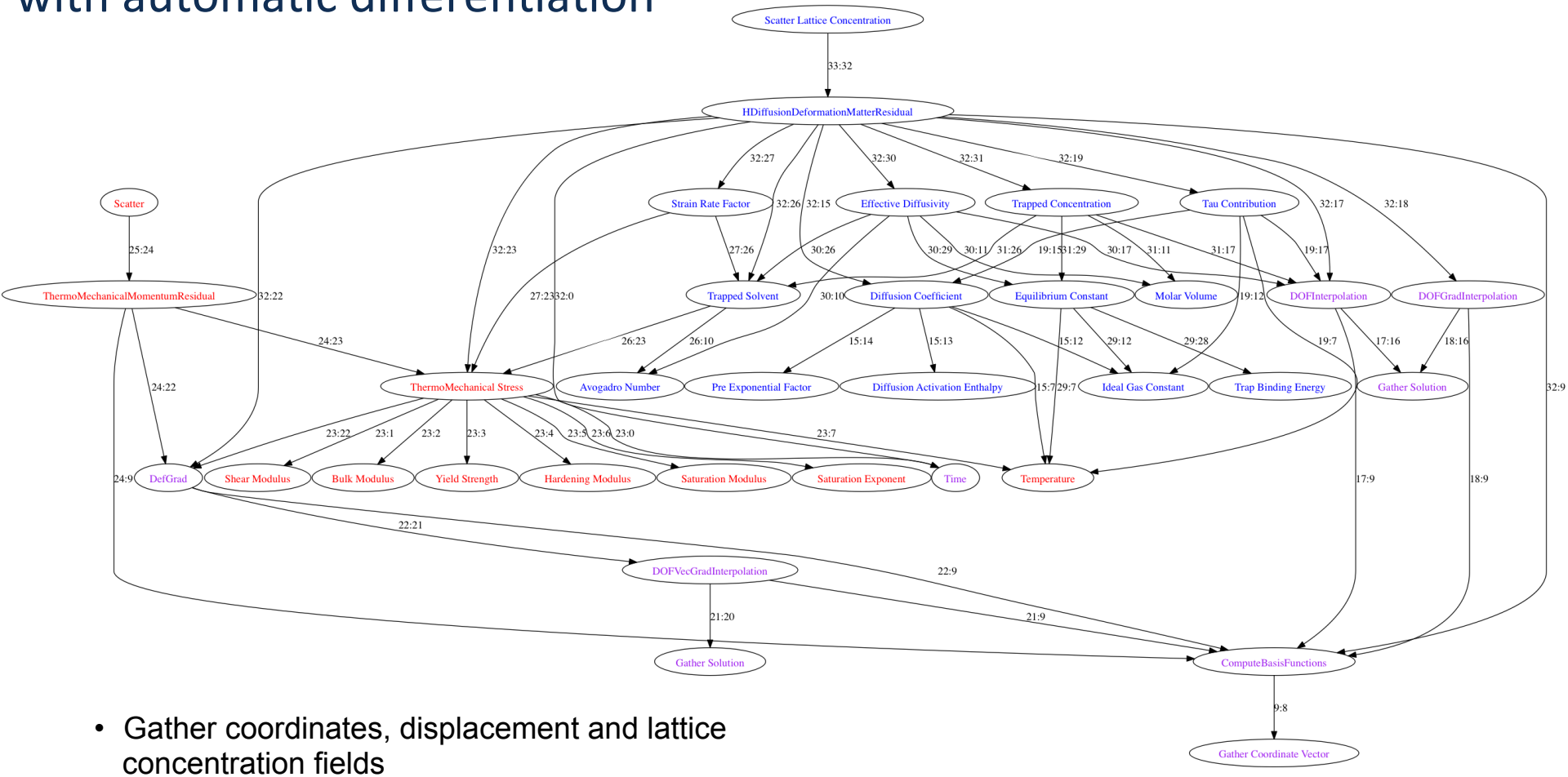

- Gather coordinates, displacement and lattice concentration fields
- Interpolate fields and gradients to integration points
- Chain together Evaluators to compute Momentum and Conservation of Hydrogen Residuals
- Scatter back to the global system of equations

Blue = Hydrogen Transport

Red = Solid Mechanics (J2 Plasticity)

Purple = coupled terms

Combined F-bar formulation

Isochoric-volumetric split

$$\boldsymbol{F} = \boldsymbol{F}_{\mathrm{vol}} \cdot \boldsymbol{F}_{\mathrm{iso}}$$

Replacing volumetric split with assumed term

$$\overline{\boldsymbol{F}} = \bar{J}^{1/3}\boldsymbol{F}_{\mathrm{iso}} = \bar{J}^{1/3}J^{-1/3}\boldsymbol{F}$$

Classical Combined F-bar approach

$$\widetilde{\boldsymbol{F}} = \alpha\boldsymbol{F} - (1-\alpha)\overline{\boldsymbol{F}}.$$

Current Approach via Lie algebra

$$J = J^e J^p J^C \quad ; \quad J^C = 1 + \lambda(C - C_o)$$

$$\widetilde{J}(X) = \exp\left(\frac{1-\alpha}{\mathrm{V}_{\mathcal{B}^e}}\int_{\mathcal{B}^e} \log J(X)\,\mathrm{dV} + \alpha \log J(X)\right)$$

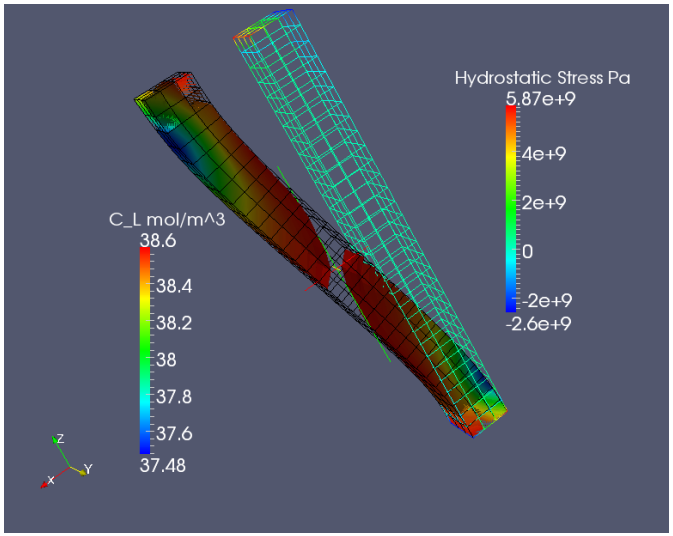

Concentration prediction affected by locking

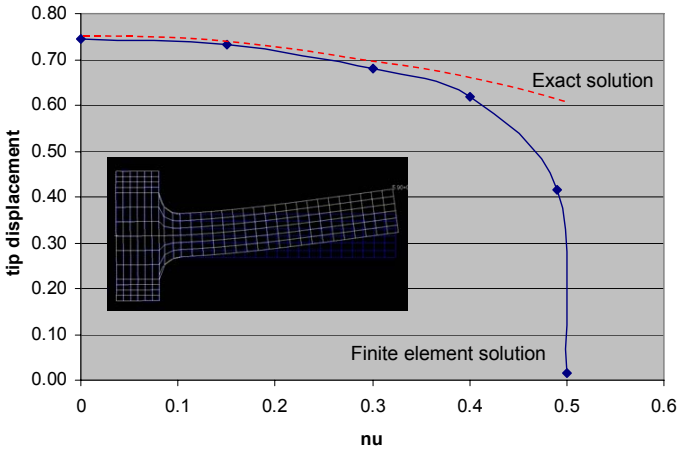

Volumetric Locking

Stabilization at small time limit

Hydrogen Transport Theorem

$$D^*\dot{C}_L - \nabla^{\boldsymbol{X}} \cdot \boldsymbol{D_L} \nabla^{\boldsymbol{X}} C_L + \nabla^{\boldsymbol{X}} \cdot \frac{V_H}{RT} C_L \boldsymbol{D_L} \nabla^{\boldsymbol{X}} S_H + \theta_T \frac{dN_T}{d\epsilon_p} \dot{\epsilon}_p = 0$$

transient term

Hydrogen diffusion term

Advection coupling term

Plastic strain nonlinear coupling term

- Spurious oscillations may occur when
  - *D** is large, which means local rate of change dominates
  - The mesh size h is large (relative to the advection and diffusion length scale)
  - The time step is small (relative to the advection and diffusion time scale).
  - Notice that Peclet number measures whether advection of diffusion is more important, but does not tell much about the transient term!

- Examples of stabilization scheme
  - Petrov-Galerkin/streamline upwind method (Hughes, 1978, Johnson, 1984)
  - Space-time finite incremental calculus method (Onate and Manzan 2000)
  - SUPG with adaptive stabilization parameters (Tezduyar 2003)
  - Spurious oscillations at layers diminishing method (Volker and Schmeyer, 2008).
  - Artificial diffusivity (Onate and Manzan, 2000).

Stabilization for hydrogen convection-diffusion problem

- For transient problem, stability criteria must be satisfied for the pair of time step and element size *h* used in simulations. γ is the parameter for backward Euler time integrator (Harari, 2004).

$$\frac{h^2 D^*}{6\gamma D_L \Delta t} < 1$$

- Meanwhile, stability of the steady solution can be predicted by the Peclet number. If Pe is less than 1 and D^*/D_L is reasonably close to h^2/dt

$$Pe = \frac{V_H}{RT} |\nabla^{\boldsymbol{X}} S_H| h < 1$$

- add stabilization term to penalize the deficiency

$$R_{stab} = \int_\Omega [\tau(\eta^h - \frac{1}{V_\Omega}\int_\Omega \eta^h d\Omega)(\dot{C}_L^h - \frac{1}{V_\Omega}\int_\Omega \dot{C}_L^h d\Omega)]\, d\Omega$$

$$R_{stab} = \int_\Omega \tau \nabla^{\boldsymbol{X}} \eta^h \nabla^{\boldsymbol{X}} \dot{C}_L^h \, d\Omega$$

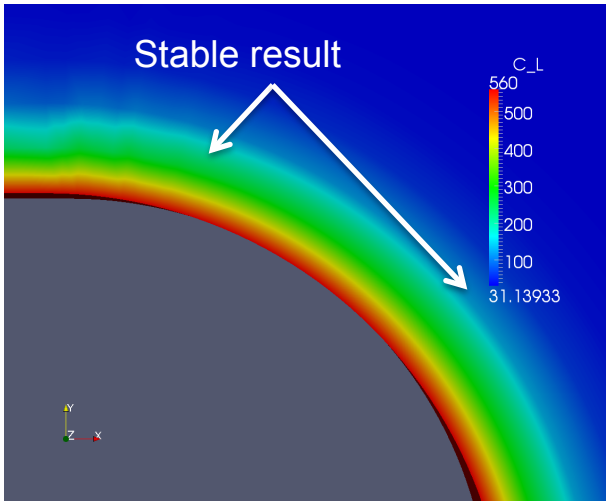

Stabilized Implicit Gakerlin Formulation

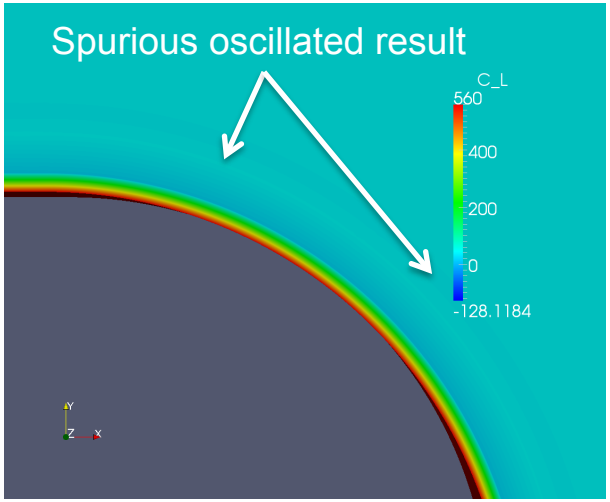

Standard Implicit Galerkin Formulation

Conclusion and Future Perspective

Sandia National Laboratories

- We have implemented a fully implicit hydrogen transport model in the Laboratory of Computational Mechanics package with the following desirable features
  - Capacity to conduct fully coupled, fully implicit simulations with stabilization scheme.
  - Automatic differentiation, which makes it fast and easy to make amendment to existing model and eliminate chance of making error in derivation
  - Stabilization scheme available to handle material with extremely low diffusivity, thin boundary layer…etc.
  - A L2 projection scheme to obtain a C^0-continuous stress gradient term that enables the advection term to be correctly modeled without introducing errors during the extrapolation process.
  - Localization element is currently developing for modeling boundary/ lattice diffusion and fracture.